

**Bioengineering Adeno-Associated Viral Vectors for  
Cardiac-Targeted Gene Therapy Applications**

---

A Dissertation

Presented to the Faculty of  
The School of Engineering and Applied Science  
University of Virginia

---

In Partial Fulfillment  
Of the Requirements for the Degree  
Doctor of Philosophy in Biomedical Engineering

Bryan Andrew Piras  
August 2013

## Approval Sheet

This dissertation is submitted in partial fulfillment of the requirements for the degree of  
Doctor of Philosophy in Biomedical Engineering

  
\_\_\_\_\_  
Author

This dissertation has been read and approved by the Examining Committee

\_\_\_\_\_  
Brent A. French, PhD  
Dissertation Advisor


\_\_\_\_\_  
Jeffrey J. Saucerman, PhD  
Committee Chair

\_\_\_\_\_  
Shayn M. Peirce-Cottler, PhD

\_\_\_\_\_  
Frederick H. Epstein, PhD

\_\_\_\_\_  
Zequan Yang, MD, PhD

Accepted for the School of Engineering and Applied Science:

  
\_\_\_\_\_  
Dean, School of Engineering and Applied Science

August 2013

## Acknowledgements

I'm pretty sure that I could write several thousand additional words to add to this dissertation composed solely of the gratitude I have to a great many people. But in the interests of brevity and getting to the Fun Stuff, I'll see what I can fit into slightly less space.

First is my advisor Dr. Brent French, who has a brilliant mind for experimental design and grant and manuscript writing and from whom I have learned a great deal about both over these past, well, there's no reason to say quite how many years. Thanks for helping me to become a decent (I hope) scientist. The rest of my committee has also been extremely helpful throughout the duration of my graduate schooling. Dr. Jeff Saucerman, Dr. Shayn Peirce-Cottler, Dr. Fred Epstein and Dr. Zequan Yang have comprised what I would consider to be a pretty ideal committee and whose advice and support I have very greatly appreciated. I would also like to thank former committee member Dr. Mike Lawrence, who provided some much needed advice but also a *really* hard comprehensive exam question.

A wide cast of characters has trafficked in and out of the French lab over the last few years and of these the largest thanks is owed to Dr. Prasad Konkalmatt, who taught me most of what I know about the fine art of AAV production, which factors rather heavily into this document. My experiments also would have been impossible without the expert surgical skills of Dr. Yaqin (Carolyn) Xu and Dr. Yikui (Jarod) Tian, both of whom are somehow able to tie a suture around a nearly impossible-to-see artery in a mouse heart that quivers at several hundred beats per minute and, by the way, they get the mice to live afterwards. Without Jarod in particular I would

probably still be figuring out how to finish my experiments. Additional thanks go to Dr. Robert Smith, Dr. Reid Harris, Richard Guyer and Dan O'Connor, great friends and ridiculously, unfairly smart guys who I have been lucky to know and work with. More thanks are due to Dr. Ron Beyers, Dr. Feng Wang, Dr. Arbin Katwal, Sarah Hansen, and Nathan Thomas, who have variously provided encouragement, advice, help with experiments, and help with sanity.

Some fellow graduate students and lab collaborators have provided assistance that has found its way directly into this dissertation. Karen Ryall in the Saucerman lab helped me to acquire mosaic fluorescent micrographs and has been a great friend. Dr. Siva Dasa and Marc Seaman in the Kelly lab helped with immunofluorescence, an area I was not particularly familiar with before taking on the GFP cells in Chapter 4. Dan Lin in the Hossack lab lent his expertise with mouse tail vein injections. And Kyle Martin in the Peirce-Cottler lab helped me acquire some confocal images that I think look pretty cool.

A last round of thanks go to Amy, Cynthia, Molly and Rachel, friends who are/were fellow grad students and provided lots of support. Finally, there are, believe it or not, some people I know who don't do science and three in particular have been pretty important to me. Jocelyn has made life in Charlottesville mean much more than whether my experiments worked and has provided endless encouragement. And at last, my parents, Julie and Guy, who for some baffling reason encouraged me to go to graduate school and, when the idea stuck, spent the next however-many-years complaining that I wasn't around anymore. This is for them.



## Table of Contents

<b>Acknowledgements</b>	<b>i</b>
<b>Abstract</b>	<b>iv</b>
<b>List of Figures</b>	<b>vi</b>
<b>List of Abbreviations</b>	<b>viii</b>
<b>CHAPTER 1 Dissertation Introduction and Specific Aims</b>	<b>1</b>
<b>CHAPTER 2 Systemic Delivery of shRNA by Single-Stranded and Double-Stranded AAV9 Provides Highly Efficient Knockdown of Ubiquitously Expressed GFP in Mouse Heart, But Not Liver</b>	<b>8</b>
Introduction	9
Materials and Methods	10
Results	17
Discussion	33
<b>CHAPTER 3 Myocardial Injury Independent of Ischemia/Reperfusion is Sufficient to Alter Viral Distribution and Transgene Expression and Simulates the Ischemic Induction of AAV9 Independent of the Compound Injected</b>	<b>39</b>
Introduction	40
Materials and Methods	42
Results	47
Discussion	59
<b>CHAPTER 4 AAV-Mediated Delivery of a Modified Periostin Promoter Driving Cre Recombinase Activates Gene Expression in Cells that Express Markers for Hematopoietic Stem Cells in the Infarct Borderzone After Reperfused Myocardial Infarction</b>	<b>65</b>
Introduction	66
Materials and Methods	68
Results	76
Discussion	96
<b>CHAPTER 5 Dissertation Conclusions and Future Directions</b>	<b>103</b>
<b>References</b>	<b>109</b>

## **Abstract**

Recombinant adeno-associated virus (AAV) is one of the leading vectors being tested as a gene delivery vehicle for the treatment of many diseases, both in preclinical studies and clinical trials. AAV vectors deliver genes to various tissues following systemic injection and provide robust and long-term gene expression, often without evoking detectable immune responses. While many advances have been made in AAV-mediated cardiac gene therapy, a variety of challenges remain, three of which we investigated. First, although cardiac-specific transgene expression has been demonstrated, gene knockdown has yet to be achieved selectively in the heart. Second, because it has a lag phase before reaching maximal expression, AAV is delivered prior to myocardial infarction (MI) in most preclinical studies of heart failure, but would be more valuable in the clinical setting if it could be administered post-MI. Third, fibroblasts account for more than half of the cells in the heart and would be a viable target for many cardiac-directed therapies, but so far have not been effectively targeted by AAV.

We proposed several lines of investigation designed to address these challenges by bioengineering AAV vectors for cardiac-targeted gene therapy. First, to assess the potential for cardiac-selective gene knockdown, we developed an AAV9 vector to deliver short hairpin RNA against GFP to inhibit gene expression in transgenic ubc-GFP mice. We then tested the hypothesis that single-stranded AAV9, but not double-stranded AAV9, could provide cardiac-selective knockdown due to inefficient conversion of single-stranded AAV genomes into double-stranded DNA in the liver. Second, our lab has demonstrated that AAV9 provides robust and

accelerated expression in cardiomyocytes after ischemia and reperfusion, but the mechanisms behind this ischemic induction effect are unknown. We attempted to elucidate these mechanisms, which we hypothesized were related to vascular permeability and AAV9 receptor availability. Finally, we developed an AAV expression cassette with the aim of targeting expression to cardiac fibroblasts and set out to determine the best serotype and time-point after myocardial infarction for targeting gene therapy to cardiac fibroblasts.

In the first aim, to provide cardiac-selective knockdown, we were successful in restricting knockdown primarily to cardiac tissue, with slight mRNA knockdown but no protein reduction in liver and skeletal muscle. However, our hypothesis regarding low liver knockdown – inefficient conversion of single-stranded AAV genomes into double-stranded DNA in the liver – was not supported by the data, with cardiac and liver knockdown being comparable between single- and double-stranded AAV. Results from the second aim, to elucidate the mechanisms behind ischemic induction of AAV9, were less clear due to unanticipated experimental confounds. Injection of several compounds to the myocardium revealed that tissue injury likely leads to an increase in AAV transduction primarily through post-entry cellular processing of AAV rather than through increased viral uptake by the cells, as hypothesized. Finally, our attempts to transduce cardiac fibroblasts with AAV instead led to gene expression in cells that express markers for hematopoietic stem cells but not fibroblasts. We obtained higher expression in these cells with AAV9 than with AAV1 or AAV6, and found increased expression when mice were injected 2 days post-myocardial infarction compared to mice injected at reperfusion.

## List of Figures

### CHAPTER 1 Dissertation Introduction and Specific Aims

1.1	AAV shRNA expression cassettes	3
-----	--------------------------------	---

### CHAPTER 2 Systemic Delivery of shRNA by Single-Stranded and Double-Stranded AAV9 Provides Highly Efficient Knockdown of Ubiquitously Expressed GFP in Mouse Heart, But Not Liver

2.1	AAV shRNA expression cassettes	12
2.2	Efficient shRNA-mediated knockdown of GFP in vitro	18
2.3	shRNA-mediated knockdown in the heart is dose-dependent	19
2.4	Luciferase provides an independent confirmation of gene expression when placed downstream of a knockdown cassette	21
2.5	Fluorescent sections from heart and liver show highly efficient cardiac knockdown and no liver knockdown	22
2.6	H&E staining shows no histological evidence of liver damage	24
2.7	Vector genomes and GFP mRNA in heart and liver	25
2.8	GFP protein in heart and liver	26
2.9	Fluorescent sections show no difference in knockdown between ssAAV and dsAAV	29
2.10	H&E staining shows no histological evidence of liver damage after treatment with ssAAV or dsAAV	30
2.11	Vector genomes and GFP mRNA after treatment with ssAAV and dsAAV	31
2.12	GFP protein after treatment with ssAAV and dsAAV	32

### CHAPTER 3 Myocardial Injury Independent of Ischemia/Reperfusion is Sufficient to Alter Viral Distribution and Transgene Expression and Simulates the Ischemic Induction of AAV9 Independent of the Compound Injected

3.1	AAV luciferase expression cassettes and experiment timeline	43
3.2	A pilot study with NHP shows increased expression compared to PBS-injected mice	49
3.3	miR122 target sites increase cardiac specificity from the cTnT promoter	51
3.4	Neuraminidase increases binding of ECL and decreases binding of MAL 20 minutes after intramyocardial injection	52
3.5	Intramyocardial injection increases luciferase expression independent of the injected compound	54
3.6	Injected myocardium contains more viral genomes and greater luciferase activity than uninjected myocardium	56
3.7	Intramyocardial injection of histamine/papaverine does not increase Evans Blue extravasation into the injected region	58

## **CHAPTER 4 AAV-Mediated Delivery of a Modified Periostin Promoter Driving Cre Recombinase Activates Gene Expression in Cells that Express Markers for Hematopoietic Stem Cells in the Infarct Borderzone After Reperfused Myocardial Infarction**

4.1	AAV expression cassettes containing a modified periostin promoter and experimental design	69
4.2	Transgenic mouse strains expressing a green fluorescent protein or luciferase upon Cre-mediated recombination	72
4.3	In vitro expression of GFP from the periostin promoter	77
4.4	Expression in Flox-GFP mice treated with AAV in the absence of myocardial infarction and after MI	79
4.5	Flox-Luc mice treated with AAV1 and AAV6 packaged with pAPiCre and AAV9 packaged with pAPiCre-miR122	81
4.6	AAV9 packaged with pAPiCre-miR122 provides greater expression than AAV6 when injected two days post-MI	83
4.7	Flox-GFP mice contain more GFP-positive cells after treatment with AAV9 than with AAV6	85
4.8	Confocal z-stacks of GFP-positive cells from mice treated with AAV9	86
4.9	Mice treated with AAV9 two days after reperfused MI show higher luciferase expression than mice that receive AAV at reperfusion	87
4.10	Flox-GFP cardiac sections treated with antibodies targeting smooth muscle and fibroblasts	89
4.11	Flox-GFP cardiac sections treated with antibodies targeting fibroblasts and collagen	90
4.12	Flox-GFP cardiac sections treated with antibodies targeting CD34, CD45 and CD68	91
4.13	Flox-GFP cardiac sections treated with an antibody targeting VEGF receptor 2	93
4.14	Flox-GFP cardiac sections treated with antibodies targeting endothelial, inflammatory and progenitor cells	94
4.15	Flox-GFP cardiac sections treated with markers of proliferation, cardiac stem cells and cardiomyocytes	95
T4.1	Primary antibodies used to identify GFP-positive cells 9 days post-MI after treatment with AAV6 packaged with pAPiCre or AAV9 packaged with pAPiCre-miR122	75

## List of Abbreviations

AAV	adeno-associated virus
ssAAV	single-stranded AAV
dsAAV	double-stranded AAV
MI	myocardial infarction
ITRs	inverted terminal repeats
shRNA	short hairpin RNA
shGFP	shRNA targeting GFP
shControl	control shRNA targeting an off-target gene
RNAi	RNA interference
GFP	green fluorescent protein
ubc-GFP	transgenic mice expressing GFP from the human ubiquitin C promoter
cTnT	cardiac troponin T promoter
vg	viral genomes
gDNA	genomic DNA
H&E	hematoxylin and eosin
qPCR	quantitative PCR
RT-PCR	reverse transcriptase PCR
GA	gastrocnemius
bp	base pair
MRN	Mre11/Rad50/Nbs1 heterotrimeric protein complex
LV	left ventricle/ventricular
IM	intramyocardial
miR122	microRNA 122
IV	intravenous
H&P	histamine and papaverine
NAD	neuraminidase
NHP	neuraminidase, histamine and papaverine
MAL	Maackia amurensis lectin
ECL	Erythrina cristagalli lectin
Dox	doxorubicin
CMV	cytomegalovirus
CAG	CMV-enhanced chicken beta-actin promoter
Flox-GFP	B6.Cg-Gt(ROSA)26Sor <sup>tm6(CAG-ZsGreen1)Hze</sup> /J mice express a GFP
Flox-Luc	FVB.129S6(B6)-Gt(ROSA)26Sor <sup>tm1(Luc)Kael</sup> /J mice express luciferase
DDR2	discoidin domain receptor 2
SM-MHC	smooth-muscle myosin heavy chain
VEGFR-2	vascular endothelial growth factor receptor 2
BMDC	bone-marrow derived cell
HSC	hematopoietic stem cell
ChIP	chromatin immunoprecipitation

## **CHAPTER 1**

Dissertation Introduction and Specific Aims

Eukaryotic viruses such as recombinant adenovirus and adeno-associated virus (AAV) are two of the primary vectors being tested as gene delivery vehicles for the treatment of various diseases, both in preclinical studies and clinical trials. While adenoviral vectors provide rapid gene expression after delivery, they also cause dose-dependent, potentially severe immunological complications in the recipient host leading to short-lived transgene expression.<sup>1</sup> In contrast, AAV vectors provide robust, long-term gene expression, usually without evoking a detectable immune response, and are capable of delivering genes to a variety of tissues following systemic intravenous injection.<sup>2-4</sup>

The AAV genome is comprised of short, single-stranded DNA characterized by identical 145 base pair inverted terminal repeat (ITR) sequences, one at each end of the genome.<sup>5</sup> ITRs are essential for replication, packaging, and integration of the viral genome and are the only genetic elements required for the packaging of AAV vectors.<sup>6,7</sup> In addition to the two ITR sequences, wild-type AAV consists of a replication gene and a capsid gene, the sequence of which differs slightly between AAV serotypes, affecting tissue tropism and transduction efficiency. Generation of recombinant AAV involves inserting an expression cassette, generally a transcriptional promoter and a gene of interest, between the two ITRs in place of the replication and capsid genes.<sup>8</sup> A wild-type and generic recombinant AAV genome are shown in Figure 1.1. While wild-type AAV requires adenovirus to aid in replication (hence the name adeno-associated), helper plasmids driving expression of the necessary adenoviral genes, as well as the AAV replication and capsid genes,



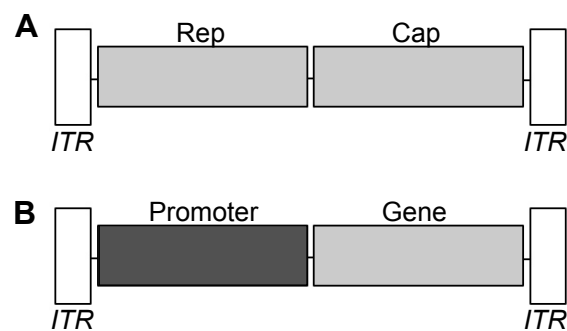


**Figure 1.1. Wild-type and recombinant AAV vectors.** (A) Wild-type AAV vectors consist of replication (Rep) and capsid (Cap) genes between two identical inverted terminal repeat (ITR) sequences. (B) Recombinant AAV vectors require the ITR sequences and generally contain a promoter driving the expression of a gene of interest, in addition to other regulatory elements (not shown).

have been employed in laboratories for over a decade, eliminating the need for adenovirus in the packaging of replication-deficient recombinant AAV.<sup>9</sup>

A wide variety of AAV serotypes have been isolated from multiple species.<sup>10</sup> While different serotypes contain slightly different ITR sequences, they can be “pseudotyped” – ITRs from one serotype of AAV can be packaged into the capsid of another. For example, an expression cassette flanked by AAV2 ITRs can be packaged into an AAV9 capsid. AAV2 is the most widely studied serotype for direct gene transfer, but it has a low transduction rate and a long lag phase (6 weeks in the heart) prior to reaching maximal gene expression compared to more recently discovered serotypes.<sup>11,12</sup> As a result, these newer serotypes are now being examined for their ability to more efficiently transduce tissues and quickly reach maximal, steady-state expression levels. In particular, AAV9 provides robust expression in cardiomyocytes, with 358-fold higher luciferase reporter gene expression than AAV2 when injected intravenously into 7 day old mice.<sup>13</sup> In addition, the lag phase for AAV9 is significantly shorter than for AAV2, with expression approaching a steady plateau phase within 3 weeks post-injection in neonatal and adult mice.<sup>13</sup>

AAV-based gene therapy has seen a great deal of progress in the last two decades, from the first Phase I clinical trial conducted in cystic fibrosis patients in 1996,<sup>14</sup> to the first approval of an AAV-based therapy by the European Commission to treat lipoprotein lipase deficiency in 2012.<sup>15</sup> The discovery of new serotypes in particular has increased the potential for new therapies, especially those directed towards the heart. Despite many advances, however, a variety of challenges remain

with AAV-mediated cardiac gene therapy, three of which comprise the subject of this dissertation. First, although cardiac-specific transgene expression has been demonstrated, reducing the possibility of undesired off-target effects in other tissues, gene knockdown has yet to be confined selectively to the heart. Second, AAV-mediated treatment to reduce heart failure after myocardial infarction (MI) would be most useful in a clinical setting if it could be delivered at the time of reperfusion. Our lab has demonstrated that AAV9 provides robust and accelerated transduction to cardiomyocytes after reperfused MI, but the mechanisms behind this ischemic induction effect are unknown.<sup>16</sup> Third, while AAV9 in particular is extremely effective at transducing cardiomyocytes, it has not proven effective for targeting cardiac fibroblasts, which account for more than half of the cells in the heart.<sup>17</sup> Cardiac fibroblasts are integral to the post-MI wound healing process and would be a viable target for many cardiac-directed therapies.

For this dissertation, we proposed several lines of investigation designed to address these cardiac-oriented challenges by bioengineering AAV vectors for cardiac-targeted gene therapy as summarized in the following specific aims:

**Aim 1: Develop an AAV9 vector to deliver short hairpin RNA (shRNA) against GFP to inhibit gene expression in transgenic ubc-GFP mice, and test the hypothesis that single-stranded AAV9 provides cardiac-selective knockdown.** While AAV9-mediated shRNA delivery has been reported previously,<sup>18-20</sup> few if any studies have looked at the effects of systemic delivery on multiple tissues. Three sub-aims were proposed: a) develop and test in vitro an shRNA targeting GFP (shGFP) under control of the mouse U6 promoter; b) use AAV9

to deliver the expression cassette in ubc-GFP mice and assess transduction and knockdown efficiency in heart and liver tissues by analyzing vector genomic DNA content and GFP mRNA and protein levels; and c) repeat sub-aim b using a double-stranded AAV9 to test the hypothesis that it provides greater expression than single-stranded AAV in liver but not in heart and therefore, when using single-stranded AAV, cardiac-selective knockdown may be attainable even with a non-tissue specific U6 promoter.

**Aim 2: Elucidate the mechanisms behind ischemic induction of AAV9.**

Our lab has demonstrated that AAV9 provides robust and accelerated transduction to cardiomyocytes after ischemia and reperfusion, but the mechanisms behind this ischemic induction effect are unknown.<sup>16</sup> Inflammatory factors released during ischemia increase vascular permeability, which should increase the efflux of AAV from the bloodstream into tissues. Additionally, evidence suggests that AAV9 binds to N-linked glycans with terminal galactosyl residues.<sup>21</sup> These are sialylated under normal conditions, but may become desialylated to reveal AAV9 receptors under conditions of ischemia. We proposed to test the hypothesis that both an increase in vascular permeability (achieved using histamine and papaverine) and the removal of the sialic acid on the AAV9 receptor (by using the enzyme neuraminidase) will recapitulate the increase in transduction of AAV9 our lab has documented in ischemic tissue.

**Aim 3: Develop an AAV expression cassette for fibroblast gene expression and determine the best serotype and time-point for therapy to cardiac fibroblasts.** While AAV9 is effective at targeting cardiomyocytes, it has not

been demonstrated to be effective for fibroblast transduction. However, there is evidence to suggest that AAV1 and 6 may efficiently transduce fibroblasts.<sup>22,23</sup> Furthermore, the activity of the periostin promoter has been shown to be strong in fibroblasts.<sup>24</sup> Therefore, I proposed two sub-aims to be completed: a) develop an AAV expression cassette containing the periostin promoter for fibroblast expression; and b) compare AAV1, -6 and -9-mediated transduction in vivo to determine the most effective serotype and time point with which to transduce cardiac fibroblasts after myocardial infarction.

The following three chapters are organized according to the above aims, and present the hypotheses surrounding each in greater detail, as well as detailed methods, results, and discussion for each of the proposed experiments.

## **CHAPTER 2**

Systemic Delivery of shRNA by Single-Stranded and Double-Stranded AAV9  
Provides Highly Efficient Knockdown of Ubiquitously Expressed GFP in Mouse  
Heart, But Not Liver

## Introduction

RNA interference (RNAi) is a powerful technique that provides for the suppression of target genes without the need for homologous recombination or knockout mice. While the knockdown of a gene using RNAi is never complete compared to knockout mice, it is inexpensive and much faster for evaluating the effect of gene knockdown. In addition, AAV delivery of RNAi provides temporal control over gene knockdown and is less subject to compensatory mechanisms that may develop over generations of selection in knockout mice. The application of RNAi technology can take many forms, but it is typically implemented within a cell in the form of a 60-70 base-pair short hairpin RNA (shRNA), which is processed into an approximately 20 base-pair short-interfering RNA through the endogenous microRNA pathway.<sup>25</sup> RNA interference technology is an intense area of research for the development of new therapies, and a number of studies have previously demonstrated the utility of AAV for delivering shRNA in vivo, including to heart and liver tissues.<sup>26-29</sup>

While AAV9-mediated cardiac-specific transgene overexpression has been demonstrated,<sup>13</sup> cardiac-specific knockdown has not. Because most RNA polymerase II promoters, required for tissue-specificity, are not ideal for short transcripts such as shRNA, strictly cardiac-specific shRNA expression is quite challenging. Giering et al.<sup>30</sup> have demonstrated liver-specific RNA polymerase II promoter-driven expression of shRNA, but our attempts to use a cardiac-specific promoter have not provided robust enough expression in cardiomyocytes for gene knockdown. However, the AAV9 capsid has been shown to be more cardiac-selective

than other serotypes, though knockdown expression profiles across multiple tissues after systemic delivery of AAV9 carrying shRNA have not, to our knowledge, been reported. Here, we describe a knockdown system targeting enhanced green fluorescent protein (GFP) in transgenic mice that express GFP under control of the human ubiquitin-C promoter (ubc-GFP).<sup>31</sup> We then analyzed vector distribution and GFP expression throughout the heart and liver and found that, while AAV9 provided highly efficient knockdown in the heart as measured by mRNA and protein analysis, there was no knockdown in the liver despite the presence of 3.7-fold more viral genomes. To determine whether this cardiac-selective knockdown was a result of using single-stranded AAV (ssAAV) genomes, we performed an additional experiment comparing knockdown between single- and double-stranded AAV (dsAAV), which obviates the need for cellular conversion from single- to double-stranded DNA.<sup>32</sup> These studies showed that single-stranded vectors provided equal or greater knockdown in cardiac and liver tissues than double-stranded vectors.

## **Materials and Methods**

**Plasmid Design and In Vitro Validation:** A knockdown cassette was designed by using PCR to amplify the U6 promoter from mouse genomic DNA and inserting it into a vector containing AAV2 ITRs. A short hairpin RNA containing a target sequence for GFP (shGFP) described by Tiscornia et al.<sup>33</sup> was synthesized and inserted downstream of the U6 promoter. This plasmid, “pAUSiG,” was later modified by inserting a reporter cassette containing firefly luciferase driven by the cardiac troponin T (cTnT) promoter downstream of the U6-shGFP cassette to



generate the plasmid “pAUSiGTL.” A control plasmid was made by replacing the shRNA targeting GFP with an shRNA against an off-target gene.

Plasmids were further modified for the experiment comparing single- to double-stranded AAV. The double stranded vector, pAscUSiG, was created by digesting pAUSiG with XbaI and BamHI and cloning the U6-shGFP cassette into pAAVsc-CMV-PIGFP, a plasmid containing a mutated 5' ITR that allows for double-stranded packaging, obtained from the University of Pennsylvania Vector Core.<sup>34</sup> An ideal single-stranded control vector containing the U6-shGFP expression cassette would not be different from the double-stranded vector aside from the ITR. However, to avoid the possibility that the short (1200 bp) expression cassette in pAUSiG could be converted to double-stranded AAV on a limited but potentially significant basis, the cassette was extended to approximately 2800 bp, which exceeds the packaging capability of a dsAAV genome. The new plasmid, pAUSiGrLuc, was made by PCR amplifying luciferase from pAUSiGTL and blunt end ligating it into the AccI site in pAUSiG. A bacterial colony with luciferase inserted in reverse (rLuc) was selected to further guarantee against luciferase expression. All plasmid constructs are shown in Figure 2.1A-E.

pAUSiG and pAUSiGTL were tested in vitro by cotransfection of the AAV-293 cell line (Agilent Technologies Inc., Clara, CA) via the calcium phosphate method with a plasmid expressing GFP from the cTnT promoter (cTnT-GFP).<sup>35</sup> Control cells were transfected with cTnT-GFP and a plasmid expressing an off-target shRNA. Three days after transfection, cells were trypsinized and collected for RNA and protein isolation. RNA was isolated with the RNeasy Mini Kit (Qiagen, Inc., Valencia,

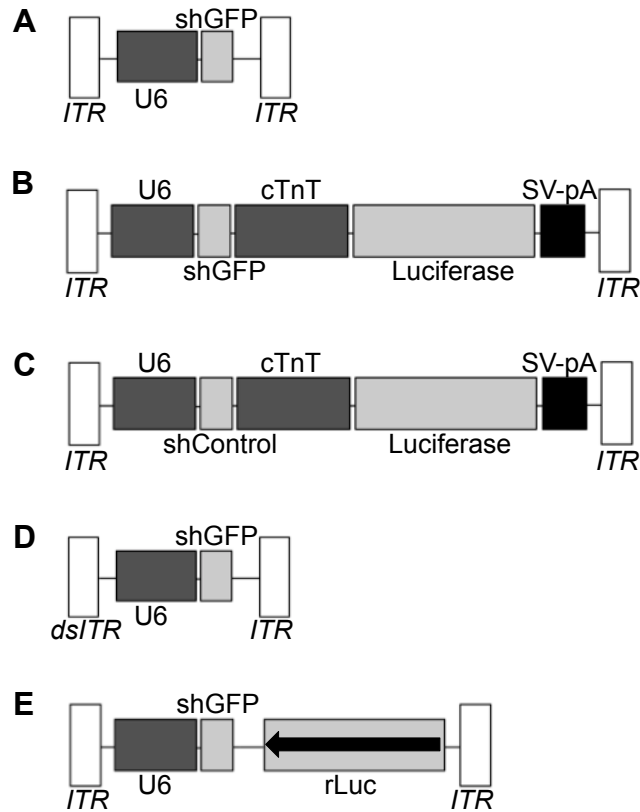


**Figure 2.1. AAV shRNA expression cassettes.** (A) pAUSiG vector carrying the mouse U6 promoter driving an shRNA against GFP (shGFP) between the two AAV2 ITRs. (B) pAUSiGTL vector (derived from pAUSiG) carrying the cardiac troponin T promoter driving the firefly luciferase reporter with an SV40 polyadenylation signal. (C) A modified version of pAUSiGTL with the shGFP sequence replaced with an shRNA sequence against an off-target gene (shControl). (D) pAscUSiG vector created by inserting the U6-shGFP cassette from pAUSiG into a vector containing the mutated 5' ITR for double-stranded genome packaging. (E) pAUSiGrLuc vector made by inserting luciferase in reverse orientation into an *AccI* site on pAUSiG.

CA) and reverse transcribed with SuperScript II Reverse Transcriptase (Invitrogen, Carlsbad, CA) for analysis using the Bio-Rad CFX96 Real-Time PCR Detection System (Bio-Rad Laboratories, Hercules, CA). Quantitative PCR was used to assess relative amounts of GFP mRNA present in transfected cells using the comparative  $C_T$  method, with expression normalized by GAPDH. Western analysis was used to evaluate GFP protein content by homogenizing cells in buffer containing 50 mM Tris-HCl, 2 mM each of EDTA and EGTA, 0.3% Triton-X 100, and a protease inhibitor cocktail (78425, Thermo Scientific, Rockford, IL). Total protein was quantified with the Bio-Rad DC Protein Assay, and blots were probed with goat anti-GFP (BA-0702, Vector Laboratories, Inc., Burlingame, CA) at a 1:3000 dilution prior to the application of a biotinylated secondary antibody with a chemiluminescent substrate for quantification.

**AAV Vector Production:** Vector genomes with AAV2 ITR sequences were cross-packaged into AAV9 capsids via triple transfection of AAV-293 cells, then purified by ammonium sulfate fractionation and iodixanol gradient centrifugation. Titers of the AAV vectors [viral genomes (vg)/ml] were determined by qPCR. The following primers were used for amplifying the mouse U6 promoter: 5'-TCGCACAGACTTGTGGGAGAA-3' (forward) and 5'-CGCACATTAAGCCTCTATAGTTACTAGG-3' (reverse). Known copy numbers ( $10^5$ - $10^9$ ) of plasmids carrying the corresponding expression cassettes were used to construct standard curves for quantification.

**Animal Procedures:** The animal protocol used in this study was approved by the University of Virginia Institutional Animal Care and Use Committee (Protocol

Number: 2802) and strictly conformed to the “Guide for the Care and Use of Laboratory Animals” (NIH Publication 85-23, revised 1985). ubc-GFP mice were maintained on a 12/12 hour light/dark cycle at 24°C and 60% humidity.

**Vector Administration:** To deliver virus, 8-10 day old ubc-GFP mice were anesthetized with 1-1.2% isoflurane in oxygen while a needle was inserted through the thoracic wall into the left ventricular chamber, after which viral solution (50-110  $\mu$ L containing  $4.5 \times 10^9$  to  $4.5 \times 10^{10}$  vg/g body weight for the dose ranging study,  $1.1 \times 10^{11}$  vg/g for the study with pAUSiGTL, or  $8 \times 10^{10}$  vg/g for the study comparing single- to double-stranded AAV) was slowly injected.

**Bioluminescence Imaging:** Luciferase expression was assessed in live mice using an in vivo bioluminescence imaging system (IVIS 100, Caliper Life Sciences, Hopkinton, MA) as described previously.<sup>11,36,16</sup> Briefly, mice were anesthetized with isoflurane and injected with 150  $\mu$ L of 30 mg/mL D-luciferin (Gold Biotechnologies, Inc., St. Louis, MO) intraperitoneally. Images were collected 10-15 minutes after substrate injection.

**Fluorescence Microscopy:** For fluorescence microscopy, heart and liver tissues were excised and fixed for one hour at room temperature in 4% PFA, rinsed in PBS, and incubated overnight at 4°C in 30% sucrose in PBS before embedding in OCT. Six micron cryosections were cut from each tissue and analyzed with an Olympus BX-41 Microscope (Olympus America, Inc., Center Valley, PA) with a Retiga-2000R camera (QImaging, Surrey, BC). Further imaging was performed with an Olympus IX81 inverted microscope with 10 $\times$  UPlanFLN 0.30 NA objective, Orca-AG CCD camera

(Hamamatsu, Bridgewater, NJ), automated stage (Prior Scientific, Rockland, MA), and IPLab software (Scanalytics, Fairfax, VA).

**Histology:** Liver tissue prepared for fluorescence microscopy was also assessed for potential damage caused by expression of shRNA. Six micron liver sections were stained with hematoxylin and eosin and photographed using an Olympus BX-51 high magnification microscope with attached Olympus DP70 digital camera.

**Determination of AAV Vector Genome Copy Number:** Total genomic DNA was isolated from mouse hearts with the Qiagen AllPrep DNA/RNA system (Qiagen Inc., Valencia, CA). AAV vector genome copy numbers were determined by qPCR using the Bio-Rad iTaq Universal SYBR Green Supermix PCR kit (Bio-Rad Laboratories, Hercules, CA) and a Bio-Rad CFX Connect real-time system. The following primers were used to amplify luciferase for all ssAAV treated mice, including the shGFP and shControl groups: 5'-AAGATTCAAAGTGCCTGCTGGTG-3' (forward) and 5'-TTGCCTGATACCTGGCAGATGGAA-3' (reverse). For the dsAAV treated group, the following primers were used to amplify a portion of the expression cassette downstream of the mutated ITR, including part of the U6 promoter: 5'-GTAGCCATGCTCTAGGAAGATCAA-3' (forward) and 5'-AGTAGCCGAGCTTCTCCCAC-3' (reverse). Known copy numbers ( $10^2$ – $10^7$ ) of plasmids containing luciferase or the dsAAV expression cassette were used to construct the standard curve. Results are expressed as the number of vector copy numbers per  $\mu\text{g}$  of genomic DNA.

**mRNA Analysis:** After hearts and livers were harvested, one-third of each was frozen in RNAlater (Qiagen Inc.) for storage. Tissues were subsequently processed with the Qiagen AllPrep DNA/RNA system, after which mRNA was converted to

cDNA using the Bio-Rad iScript cDNA Synthesis Kit before qPCR analysis with the Bio-Rad iTaQ Universal SYBR Green Supermix. The following primers were used for amplifying GFP: 5'-TGACCCTGAAGTTCATCTGCACCA-3' (forward) and 5'-TCTTGTAGTTGCCGTCGTCCTTGA-3' (reverse); and, for normalization, GAPDH: 5'-TCAACAGCAACTCCCACTCTTCCA-3' (forward) and 5'-ACCCTGTTGCTGTAGCCGTATTCA-3' (reverse).

**Western Analysis:** Immunoblots were used to evaluate GFP content in heart and liver (and skeletal muscle for the single- versus double-stranded [ss/ds] experiment) by homogenizing tissues in buffer containing 50 mM Tris-HCl, 2 mM each of EDTA and EGTA, 0.3% Triton-X 100, and a protease inhibitor cocktail. Protein was quantified with the Bio-Rad DC Protein Assay, and goat anti-GFP (BA-0702, Vector Laboratories, Inc., Burlingame, CA) was applied at a 1:3000 dilution prior to incubation with a fluorescent secondary antibody and detection with the Odyssey Imaging System (LI-COR Biosciences, Lincoln, NE). Signals from an anti-actin antibody (A2103, Sigma-Aldrich, St. Louis, MO) or anti-GAPDH antibody (600-401-A33; Rockland Immunochemicals Inc., Gilbertsville, PA, USA) were used as loading controls.

**Statistical Analysis:** Data are expressed as mean  $\pm$  SEM where appropriate. Results from the dose-dependent study were analyzed by the nonparametric Kruskal-Wallis test. The mRNA and protein analysis from the ss/ds experiment was compared by one-way ANOVA and the Tukey method was used to assess significance. All other comparisons were analyzed with Student's t-test.  $P < 0.05$  was considered significant in all comparisons.

## Results

**Efficient In Vitro Knockdown of GFP:** The shGFP expression cassette was tested in vitro by cotransfection via the calcium phosphate method with a plasmid expressing GFP from the cTnT promoter. Control cells were transfected with cTnT-GFP and a plasmid expressing an off-target shRNA. Efficient knockdown of GFP was achieved 3 days after cotransfection (Fig 2.2A-B). Results from qPCR indicated a 61% reduction in GFP transcript (Fig. 2.2C,  $n=3/\text{group}$ ,  $p<0.01$  vs. control), while Western blot analysis revealed a 90% reduction of GFP protein compared to the off-target shRNA control (Fig. 2.2D,  $n=3/\text{group}$ ,  $p<0.001$ ).

**shRNA-Mediated Knockdown in Heart is Dose-Dependent:** To test the effect of dose on GFP knockdown, 3 different doses of the pAUSiG vector packaged in AAV9 were administered to ubc-GFP mice:  $4.5\times 10^9$  vg/g ( $n=3$ ),  $2.25\times 10^{10}$  vg/g ( $n=3$ ), and  $4.5\times 10^{10}$  vg/g ( $n=2$ ). Control mice ( $n=2$ ) were left uninjected. Seven to eight weeks after injection, mice were euthanized and their hearts were collected for fluorescence microscopy and mRNA analysis. Figure 2.3A-D shows fluorescence micrographs of hearts from control mice (A) and mice that received  $4.5\times 10^9$  vg/g (B),  $2.25\times 10^{10}$  vg/g (C) and  $4.5\times 10^{10}$  vg/g (D), demonstrating a decrease in fluorescent cells with increasing dose of AAV9. These results were confirmed with qPCR analysis of mRNA, which demonstrated a 55% reduction in mRNA with the medium dose of  $2.25\times 10^{10}$  vg/g and an 82% reduction in transcript with  $4.5\times 10^{10}$  vg/g compared to the control group (Fig. 2.3E,  $p=0.052$ ).

**Luciferase Provides an Independent Confirmation of Gene Expression When Placed Downstream of a Knockdown Cassette:** For the initial study to assess GFP

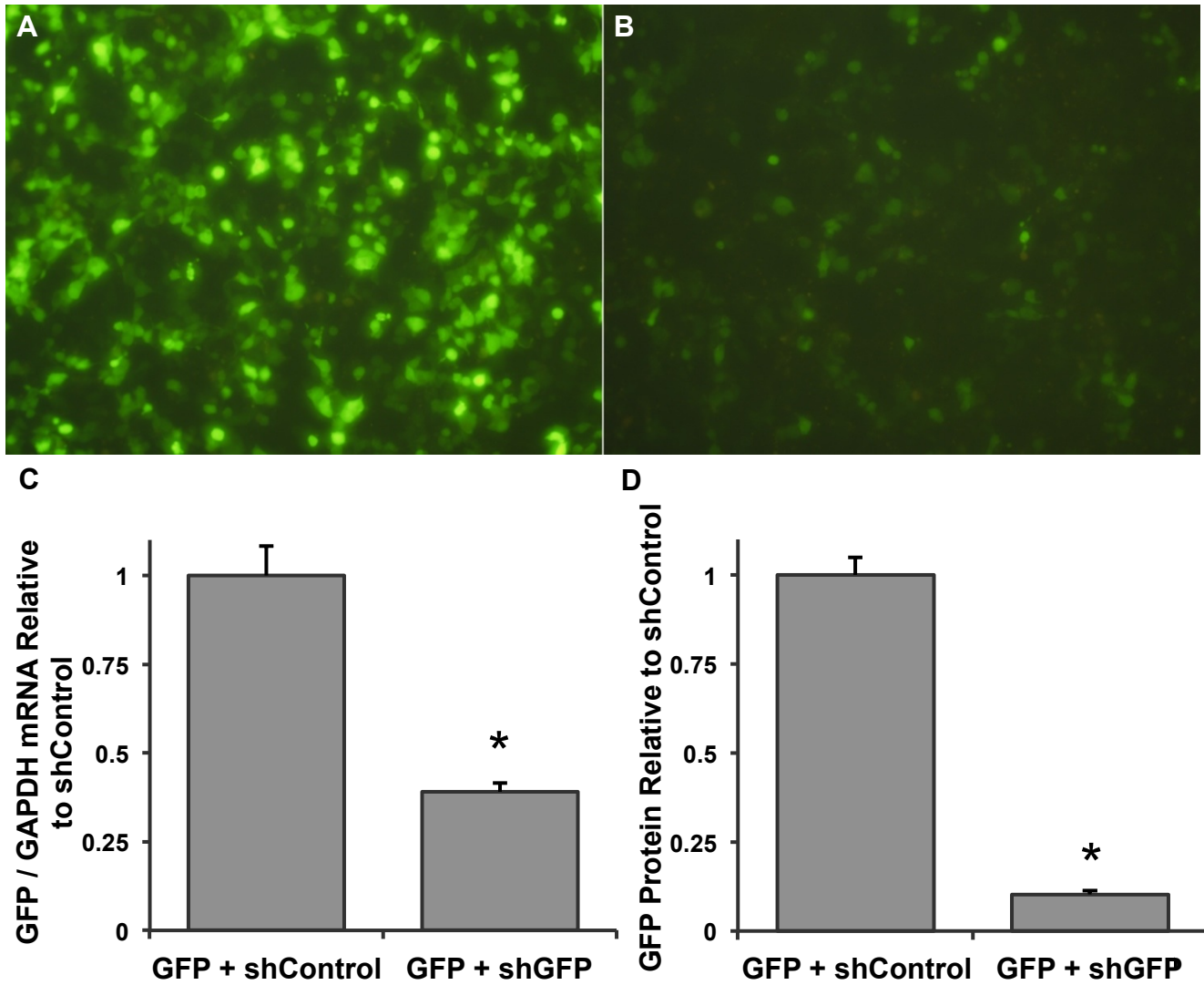


**Figure 2.2. Efficient shRNA-mediated knockdown of GFP in vitro.** (A) AAV-293 cells dual-transfected with a plasmid expressing GFP from the cardiac troponin T promoter and a plasmid expressing a negative control shRNA from the mouse U6 promoter (shControl). (B) Cells transfected similarly but with the pAUSiGTL plasmid expressing shGFP. Cells were imaged 3 days post-transfection. (C) GFP mRNA from transfected cells harvested 3 days post-transfection. GAPDH was used to normalize GFP expression, which was found to be reduced by 61% compared to the shControl group (n=3/group,  $p<0.01$ ). (D) GFP protein expressed relative to shControl showed a 91% reduction in the shGFP group (n=3/group,  $p<0.001$ ).



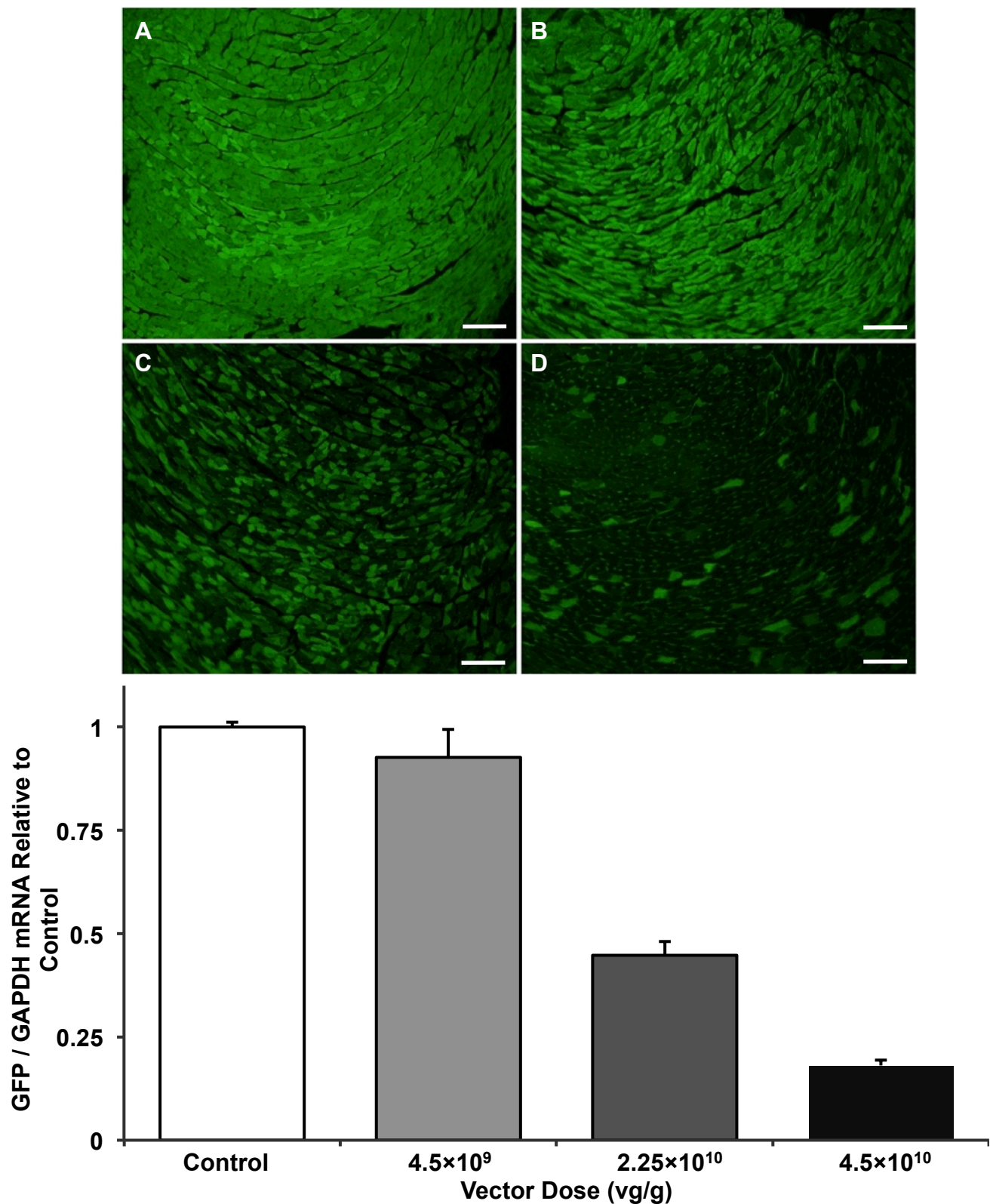


**Figure 2.3. shRNA-mediated knockdown in the heart is dose-dependent.** Fluorescent tissue sections showing GFP expression in ubc-GFP mice 7 weeks after: (A) being treated as uninjected controls (n=2) or (B)-(D) injection with  $4.5 \times 10^9$  (n=3),  $2.25 \times 10^{10}$  (n=3), or  $4.5 \times 10^{10}$  (n=2) viral genomes per gram, respectively. Scale bars are equal to 50 microns. (E) GFP mRNA from harvested cardiac tissue, normalized by GAPDH and expressed relative to the uninjected control group. qPCR analysis of mRNA demonstrated a 55% reduction in GFP mRNA with the medium dose of  $2.25 \times 10^{10}$  vg/g and an 82% reduction in transcript with the high dose of  $4.5 \times 10^{10}$  vg/g compared to the control group (p=0.052 by Kruskal-Wallis analysis).

knockdown in heart and liver tissues, the pAUSiGTL vector was packaged into AAV9 to provide an independent confirmation of gene transfer via the luciferase reporter gene. Seven mice were injected with  $1.1 \times 10^{11}$  vg/g AAV9-pAUSiGTL, while an additional 7 mice were injected with  $1.1 \times 10^{11}$  vg/g of a similar vector containing an off-target shRNA as a control (shControl). Mice imaged 7 weeks after injection demonstrated cardiac-restricted expression of luciferase from the cardiac-specific cTnT promoter (Fig. 2.4). These results provided confirmation of viral delivery and gene expression in live mice prior to tissue-level analysis of gene knockdown.

**Highly Efficient Knockdown of GFP in Heart but Not Liver:** After imaging, mice were euthanized and their hearts and livers were collected for analysis by fluorescence microscopy, as well as for analysis of AAV genomes, GFP mRNA and GFP protein. Six micron cryosections of heart and liver tissue revealed a large difference between the number of fluorescing cardiomyocytes treated with shControl and shGFP (Fig. 2.5A&C and B&D, respectively), while there was no appreciable difference in fluorescence between groups in the liver (Fig. 2.5E&G and F&H). While shControl-treated ubc-GFP mouse hearts were nearly homogenous in fluorescence, the majority of cardiomyocytes in shGFP-treated mice did not exhibit fluorescence levels above background. Liver sections from both groups appeared slightly less homogenous, with no apparent difference between treatment groups. Liver sections were also stained with hematoxylin and eosin to detect potential liver tissue damage due to shRNA production as reported previously.<sup>29</sup> Representative H&E stained liver sections after treatment with a control AAV not expressing shRNA

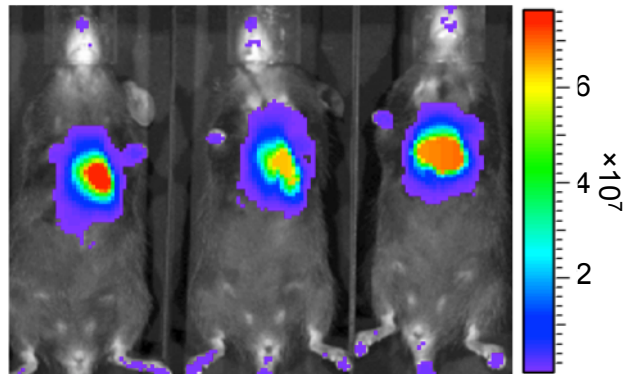


**Figure 2.4. Luciferase provides an independent confirmation of gene expression when placed downstream of a knockdown cassette.** Further experiments used the pAUSiGTL vector packaged in AAV9 to provide an independent indicator of gene expression with the luciferase reporter. Mice imaged by bioluminescence 7 weeks after injection had cardiac restricted expression of luciferase as a result of the cardiac-specific cTnT promoter. These results provided confirmation of viral delivery and expression in live mice prior to tissue-level analysis of gene knockdown.

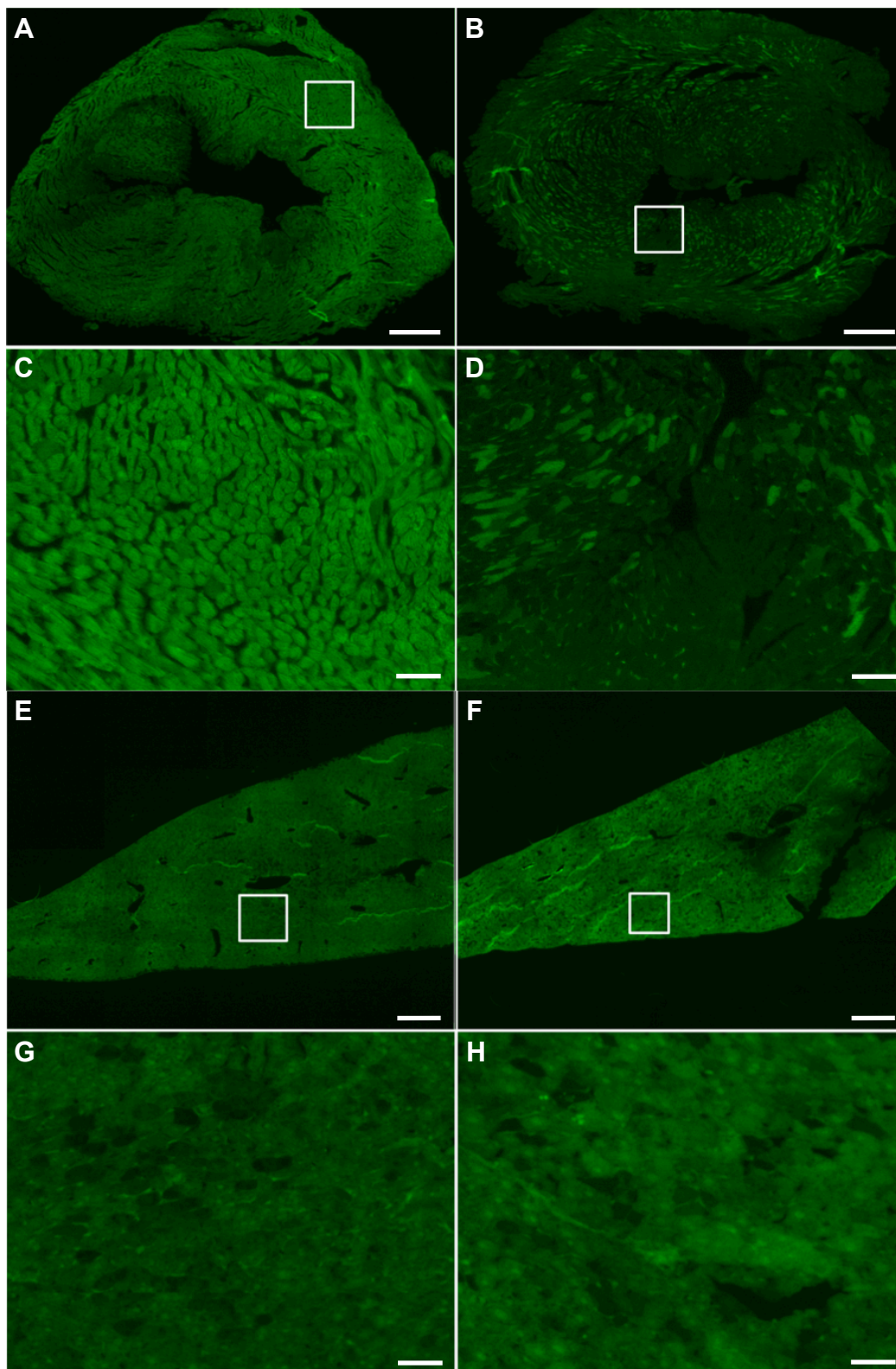


**Figure 2.5. Fluorescent sections from heart and liver show highly efficient cardiac knockdown and no liver knockdown.** Mice were injected with AAV9 capsids containing the single-stranded pAUSiGTL vector expressing shGFP or AAV9 containing an off-target shRNA. Tissues were harvested 7 weeks after injection. (A) and (E) show heart and liver, respectively, treated with the off-target shRNA (scale bars = 500  $\mu$ m), while (C) and (G) show the same sections magnified in the area of the white boxes (scale bars = 50  $\mu$ m). (B) and (F) show heart and liver, respectively, treated with shGFP (scale bars = 500  $\mu$ m), while (D) and (H) show the same sections magnified in the area of the white box (scale bars = 50  $\mu$ m).

(Fig. 2.6A), shControl AAV (Fig. 2.6B) and shGFP AAV (Fig. 2.6C) showed no histological evidence of damage.

To assess the distribution of viral genomes between tissues, genomic DNA (gDNA) was isolated from heart and liver and analyzed by qPCR to determine mean vector copy numbers per microgram of gDNA. Figure 2.7A shows that liver had approximately 3.7-fold more vector genomes than the heart ( $1.47 \times 10^6$  copies/ $\mu$ g gDNA versus  $3.97 \times 10^5$  copies/ $\mu$ g gDNA, respectively;  $n=6$ /group,  $p<0.001$ ). In addition to gDNA, mRNA was also isolated from heart and liver. After conversion to cDNA, qPCR was performed to assess GFP transcript levels normalized by GAPDH transcripts in each tissue. Figure 2.7B shows the expression of GFP/GAPDH mRNA relative to the shControl group for heart and liver. The shGFP group in heart showed a 77% reduction in GFP mRNA compared to the shControl group ( $n=7$ /group,  $p<0.0001$ ). While the shGFP group showed a trend towards decreased GFP mRNA in liver, it was not significant ( $n=7$ /group,  $p=0.38$ ). These results show that despite increased prevalence of viral genomes in the liver, greater knockdown of GFP was achieved in the heart.

Finally, Western blot analysis was performed on protein isolated from heart and liver (Fig. 2.8). Actin-normalized GFP expression was reduced by 71% in the shGFP-treated group compared to the shControl group in heart ( $n=4$ /group;  $p<0.0001$ ), but there was no difference in GFP expression between groups in the liver. These results corroborate the data from fluorescence microscopy of tissue sections and mRNA analysis, demonstrating that knockdown of GFP in the heart is highly efficient with no significant reduction of GFP expression in the liver.



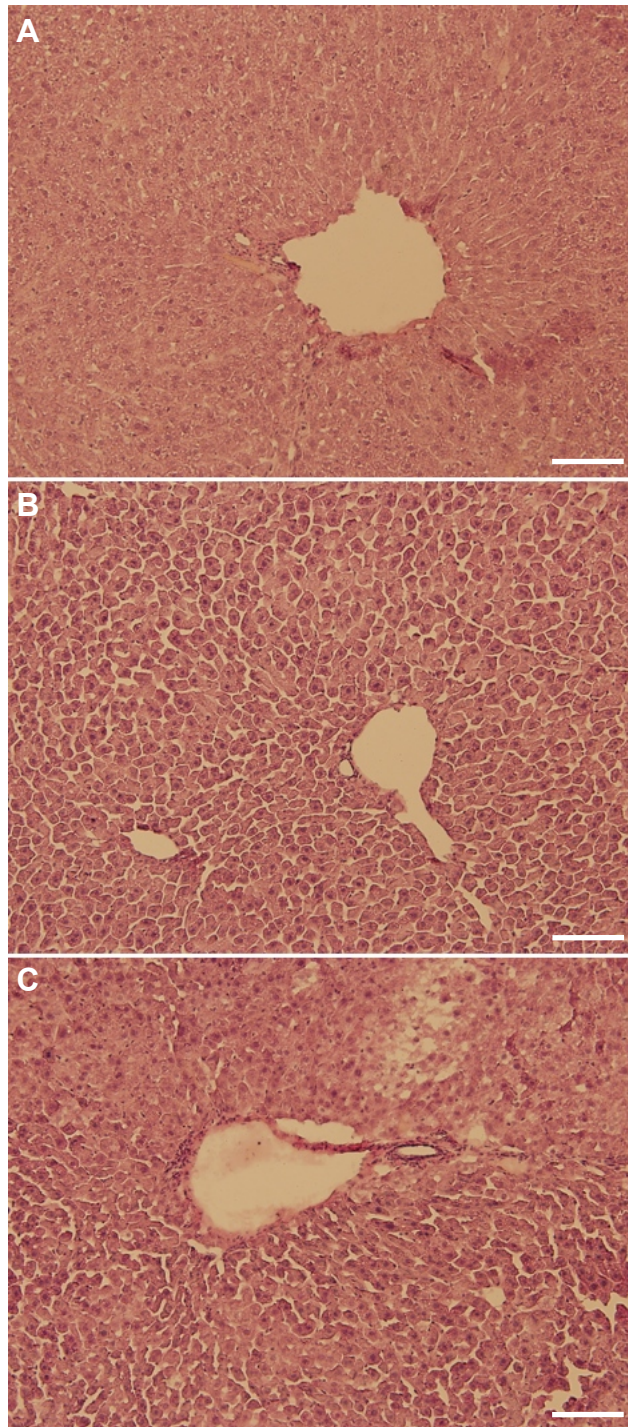


**Figure 2.6. H&E staining shows no histological evidence of liver damage.** Liver sections photographed after staining with hematoxylin and eosin show no signs of liver damage when comparing: (A) liver treated with a control AAV not expressing shRNA to (B) shControl and (C) shGFP treated liver. Scale bars are equal to 100  $\mu\text{m}$ .

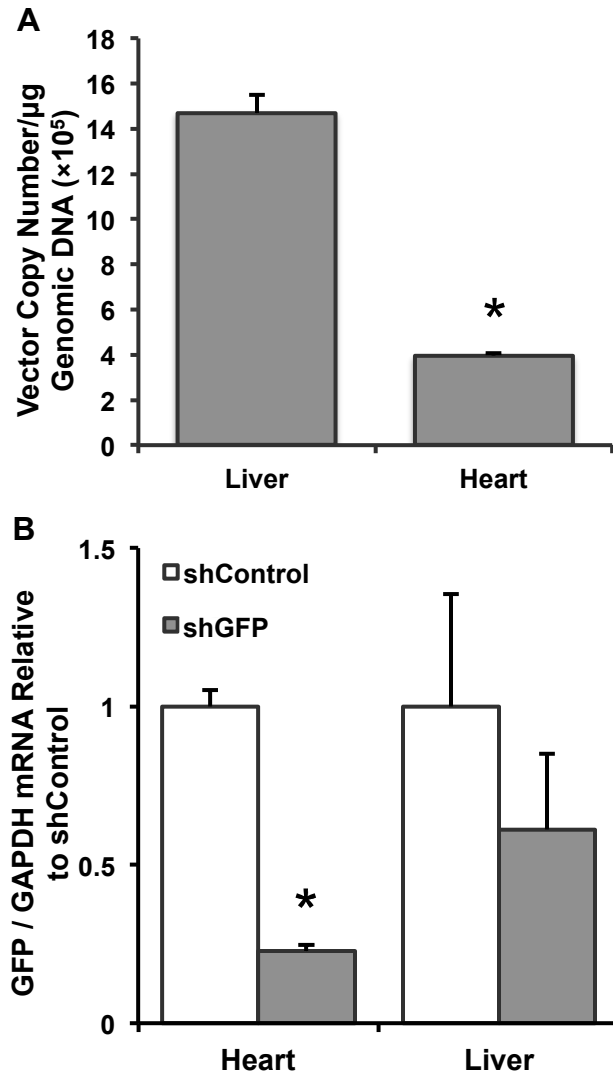


**Figure 2.7. Vector genomes and GFP mRNA in heart and liver.** (A) To determine viral distribution within the primary target tissues, genomic DNA (gDNA) was isolated from heart and liver and analyzed by qPCR to find average vector copy numbers per microgram of gDNA. Liver had approximately 3.7-fold more vector genomes than the heart ( $1.47 \times 10^6$  copies/ $\mu\text{g}$  gDNA versus  $3.97 \times 10^5$  copies/ $\mu\text{g}$  gDNA, respectively;  $n=6/\text{group}$ ,  $p<0.001$ ). (B) mRNA was also isolated from heart and liver, and GFP transcript levels were normalized by GAPDH. The shGFP group showed a 77% reduction in cardiac GFP mRNA compared to the shControl group ( $n=7/\text{group}$ ,  $p<0.0001$ ), and while the shGFP group showed a trend towards decreased mRNA in liver, it was not significant ( $n=7/\text{group}$ ,  $p=0.38$ ).

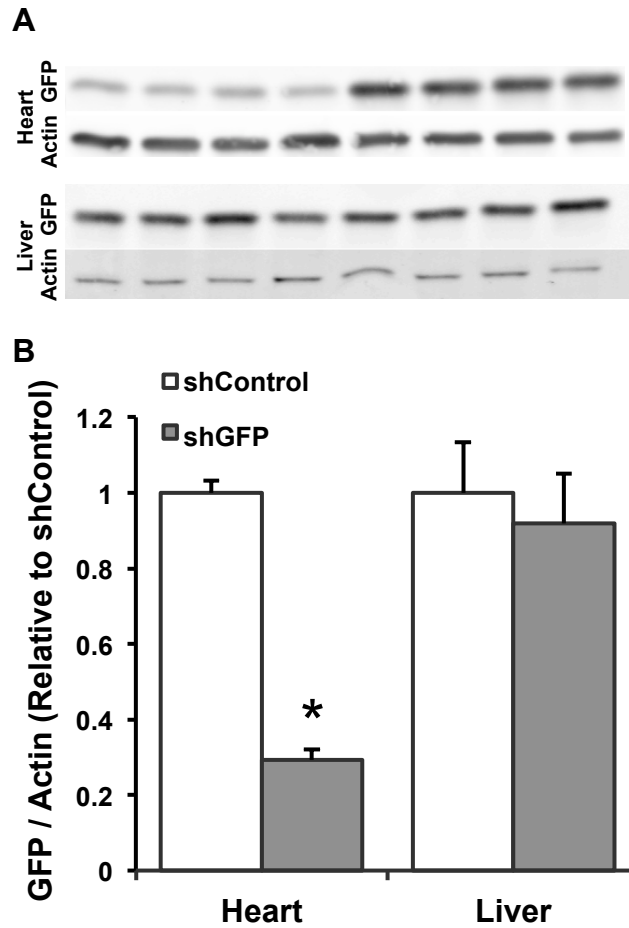


**Figure 2.8. GFP protein in heart and liver.** (A) Western blots of GFP in heart and liver tissues, with actin used as a loading control. The first four bands in each sample are from the shGFP group, while the second four bands are from the shControl group. (B) Quantitative analysis of the Western blots shows that actin-normalized GFP expression was reduced by 71% in the shGFP-treated group compared to the shControl group in heart ( $n=4/\text{group}$ ;  $p<0.0001$ ), but there was no difference in GFP expression between groups in the liver.



**Single- and Double-Stranded AAV Vectors Provide Similar Knockdown:** For the ss/ds experiment, mice were euthanized and their hearts, livers and gastrocnemius (GA) muscles were collected for analysis by fluorescence microscopy, as well as for analysis of AAV genomes, GFP mRNA and GFP protein. Six micron cryosections of heart, liver and GA tissue revealed a similar level of cardiomyocyte GFP knockdown between ss- and dsAAV treated groups versus controls (Fig. 2.9A-C) while there was no appreciable difference in fluorescence between groups in the liver (Fig. 2.9D-F) or GA (Fig. 2.9G-I) compared to controls. As previously, liver sections were stained with hematoxylin and eosin to detect potential liver tissue damage due to shRNA production. Representative H&E stained liver sections for a control AAV not expressing shRNA (Fig. 2.10A) and after treatment with either ssAAV (Fig. 2.10B) or dsAAV (Fig. 2.10C) showed no histological evidence of damage.

To assess the distribution of viral genomes, gDNA was isolated from heart, liver and GA and analyzed by qPCR to determine mean vector copy numbers per microgram of gDNA. Figure 2.11A shows that for ssAAV treated mice, liver had approximately 5-fold more vector genomes than the heart and 132-fold more than GA muscle ( $4.10 \times 10^5$  copies/ $\mu$ g gDNA,  $8.10 \times 10^4$  copies/ $\mu$ g gDNA, and  $3.11 \times 10^3$  copies/ $\mu$ g gDNA respectively;  $n=7-8$ /group,  $p<0.001$  for all groups compared by one-way ANOVA). dsAAV treated mice had a similar liver to heart ratio, with 1.9-fold more vector genomes in the liver than the heart but only 8-fold more in the liver than in GA muscle ( $8.93 \times 10^3$  copies/ $\mu$ g gDNA,  $4.76 \times 10^3$  copies/ $\mu$ g gDNA, and  $1.10 \times 10^3$  copies/ $\mu$ g gDNA respectively;  $n=6-7$ /group,  $p<0.05$  versus liver). In addition to gDNA, mRNA was also isolated from heart, liver and GA. After conversion

to cDNA, qPCR was performed to assess GFP transcript levels normalized by GAPDH transcripts in each tissue. Figure 2.11B shows the expression of GFP/GAPDH mRNA relative to the untreated controls. Compared to controls (n=5), the ssAAV group (n=8) demonstrated an 82% decrease in mRNA while the dsAAV group (n=7) showed knockdown of 79% ( $p < 0.001$  for both groups versus controls). In liver, the ssAAV group showed a 36% reduction in GFP mRNA versus controls and the dsAAV group showed a 27% knockdown ( $p < 0.01$  for both groups versus controls). Finally, the ssAAV group showed a nearly 20% reduction in GFP mRNA in GA muscle, but these results did not reach significance and the dsAAV group showed no reduction at all, but was significantly different from the ssAAV group (n=5-8/group,  $p < 0.05$  for the ssAAV versus dsAAV groups). These results show that when comparing AAV doses equalized by genomes, single-stranded vectors are equally or more capable of providing transcript knockdown compared to double-stranded vectors.

Finally, Western blot analysis was performed on protein isolated from heart, liver and GA (Fig. 2.12, n=4/group for all comparisons). GAPDH-normalized GFP expression was reduced by 51% in the ssAAV treated group and 45% in the dsAAV group compared to untreated controls in heart ( $p < 0.001$  for both groups versus control), but there was no difference in GFP expression between groups in the liver or GA muscle. These results corroborate the data from fluorescence microscopy of tissue sections and mRNA analysis, demonstrating that knockdown of GFP in the heart is very efficient with no significant reduction of GFP expression in liver or GA.

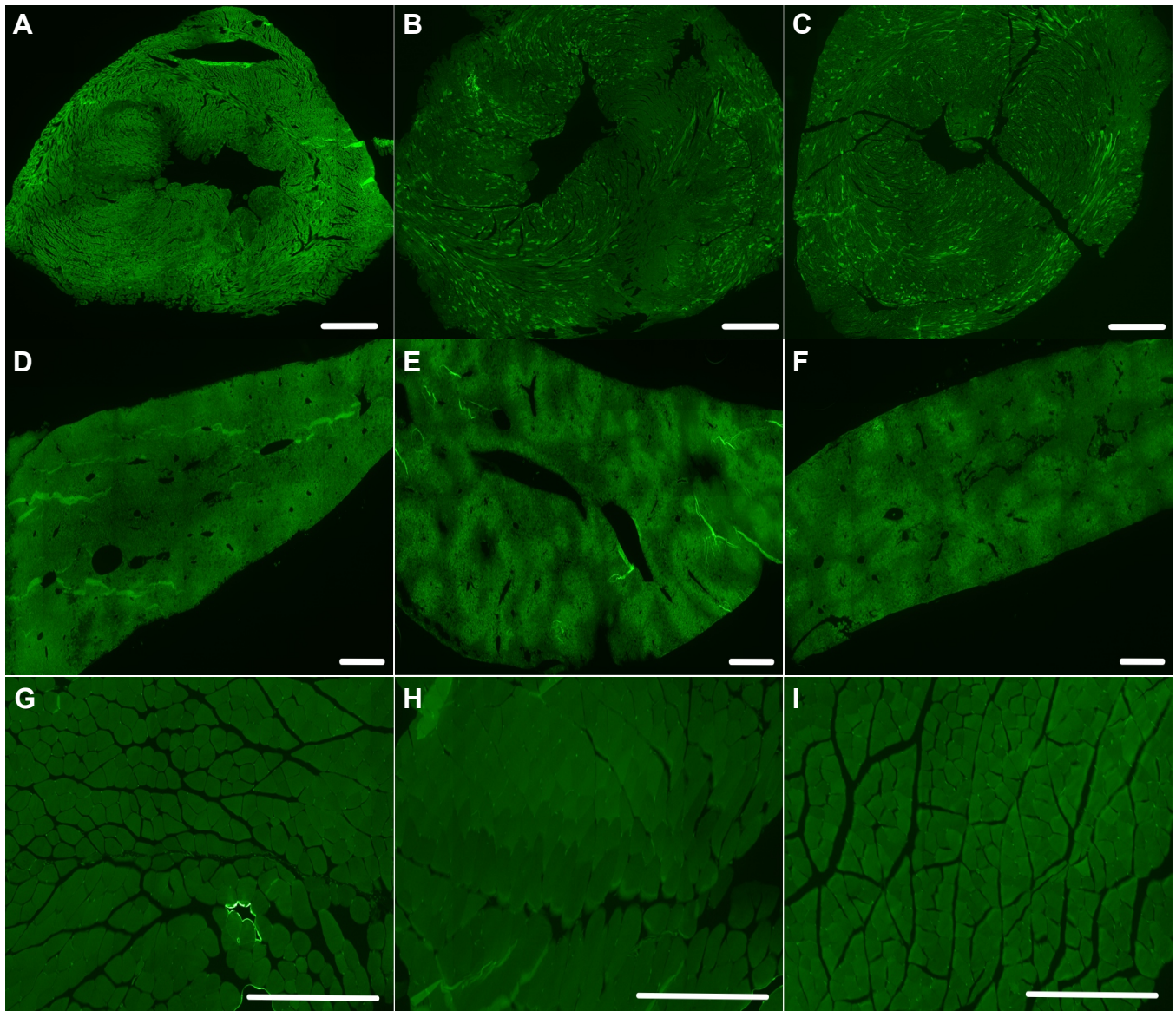


**Figure 2.9. Fluorescent sections show no difference in knockdown between ssAAV and dsAAV.** Mice were injected with AAV9 capsids containing the single-stranded pAUSiGrLuc vector or the double-stranded pAscUSiG vector, both expressing shGFP. Tissues were harvested 7 weeks after injection. (A) through (C) show heart after treatment with AAV9 expressing an off-target shRNA, ssAAV expressing shGFP or dsAAV expressing shGFP, respectively. (D) through (F) show liver after treatment with AAV9 expressing an off-target shRNA, ssAAV expressing shGFP or dsAAV expressing shGFP, respectively. (G) through (I) show GA muscle in an untreated mouse, or after treatment with ssAAV expressing shGFP or dsAAV expressing shGFP, respectively. All scale bars are 0.5 mm.

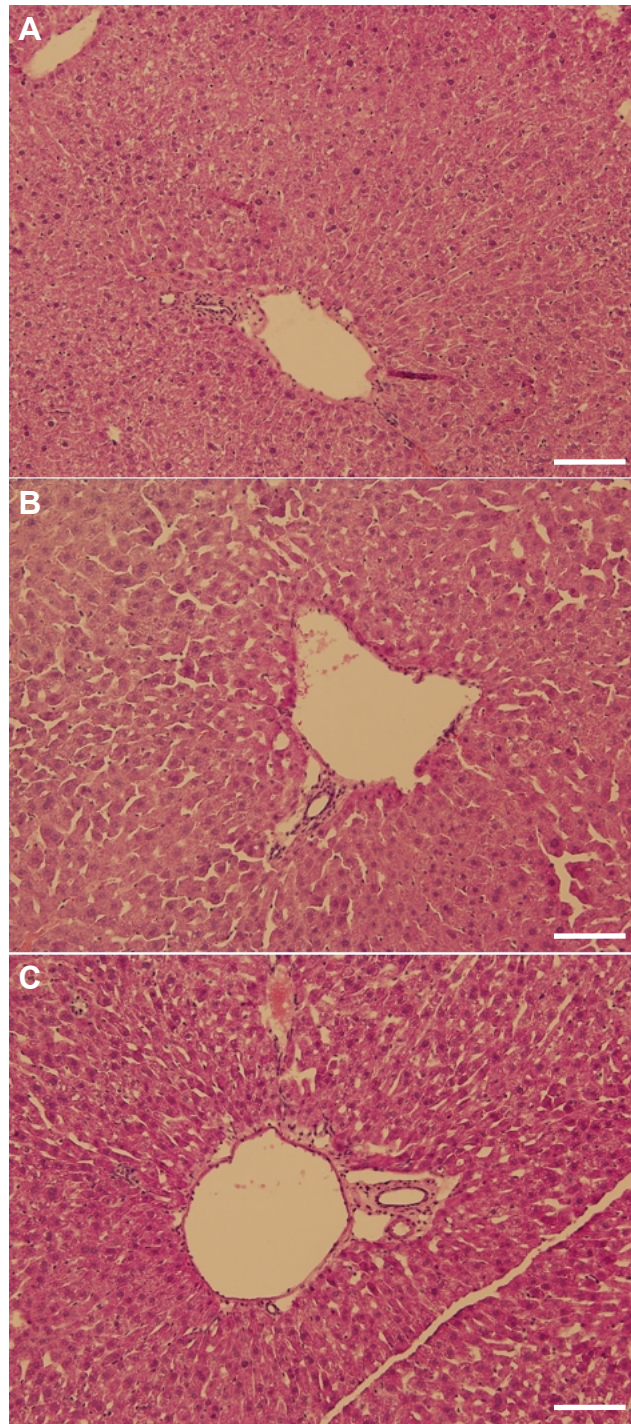


**Figure 2.10. H&E staining shows no histological evidence of liver damage after treatment with ssAAV or dsAAV.** Liver sections photographed after staining with hematoxylin and eosin show no signs of liver damage when comparing: (A) liver treated with a control AAV not expressing shRNA to (B) ssAAV packaged with pAUSiGrLuc and (C) dsAAV packaged with pAscUSiG. Scale bars are equal to 100 μm.



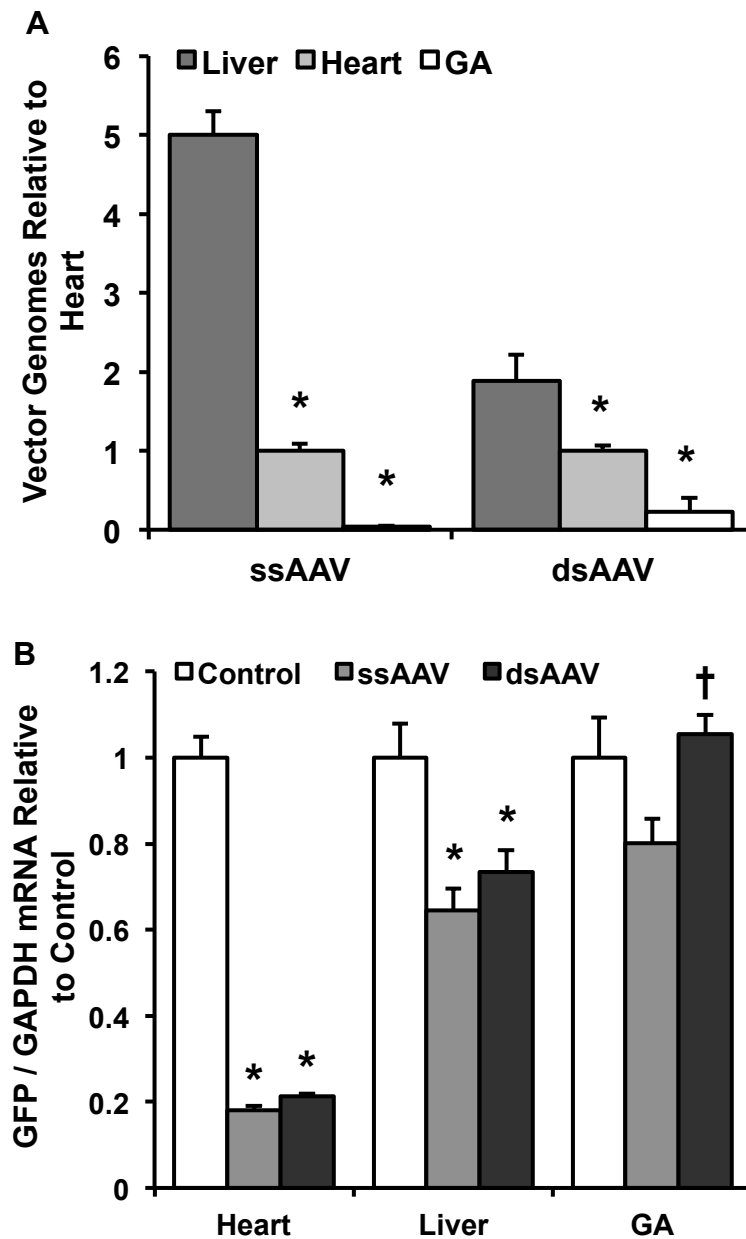


**Figure 2.11. Vector genomes and GFP mRNA after treatment with ssAAV and dsAAV.** (A) To determine viral distribution, genomic DNA (gDNA) was isolated from heart, liver and GA and analyzed by qPCR. Data are presented in terms of viral genomes relative to heart tissue. In mice treated with ssAAV, liver had approximately 5-fold more vector genomes than the heart and 132-fold more genomes than GA muscle ( $4.10 \times 10^5$ ,  $8.10 \times 10^4$ , and  $3.11 \times 10^3$  copies/ $\mu$ g gDNA respectively;  $n=7-8$ /group,  $p<0.001$  for all comparisons). In mice treated with dsAAV, liver had 1.9-fold more vector genomes than the heart and 8.1-fold more genomes than GA muscle ( $8.93 \times 10^3$ ,  $4.76 \times 10^3$ , and  $1.10 \times 10^3$  copies/ $\mu$ g gDNA respectively;  $n=6-7$ /group,  $p<0.001$  versus liver). (B) mRNA was also isolated from heart, liver and GA and GFP transcript levels were normalized by GAPDH. In the heart, the ss- and dsAAV groups showed reductions of 82% and 79%, respectively, compared to controls ( $n=5-8$ /group,  $p<0.001$  versus controls). In liver, the ss- and dsAAV groups showed reductions of 36% and 27%, respectively, compared to controls ( $n=5-8$ /group,  $p<0.01$  versus controls). In GA, only the ssAAV group showed a reduction in GFP mRNA versus controls though this difference was not significant. The dsAAV group was significantly different from the ssAAV group ( $n=5-8$ /group,  $p<0.05$ ). Asterisks (\*) indicate significance versus the control group and crosses (†) indicate significance between the ssAAV and dsAAV groups.

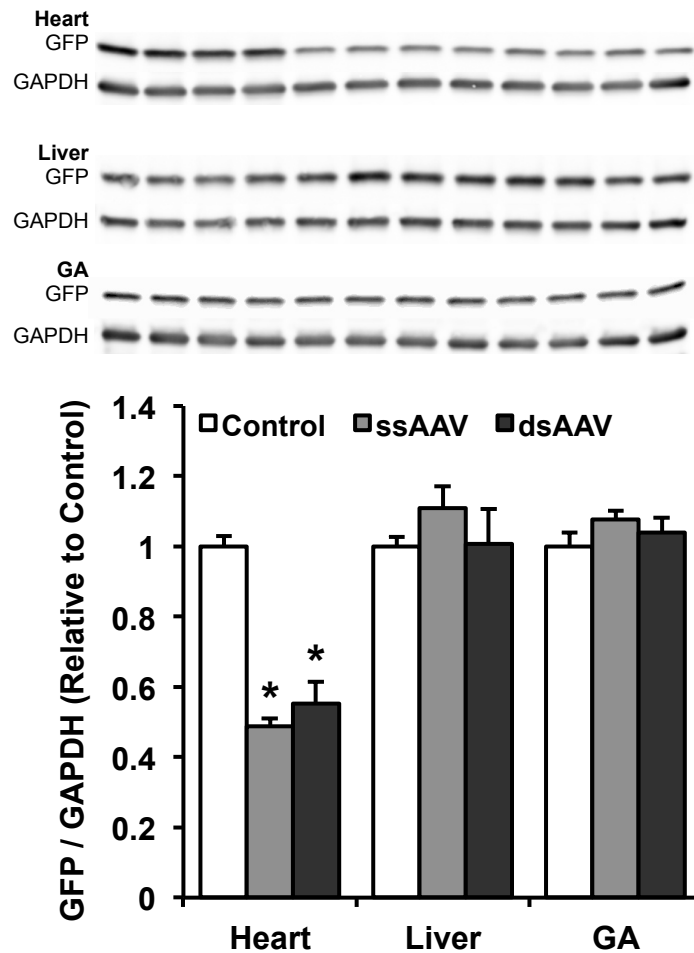


**Figure 2.12. GFP protein after treatment with ssAAV and dsAAV.** (A) Western blots of GFP in heart, liver and GA tissues, with GAPDH used as a loading control. The first four bands in each sample are from the control group (mice treated with AAV9 carrying an off-target shRNA in the case of heart and liver tissues, or untreated mice for the GA comparison), the second four bands are from the ssAAV group and the final four bands are from the dsAAV group. (B) Quantitative analysis of the Western blots shows that GAPDH-normalized GFP expression was reduced by 51% in the ssAAV-treated group and 45% in the dsAAV group compared to controls in heart (n=4/group;  $p < 0.001$  versus control), but there was no difference in GFP expression between groups in the liver or GA.

## Discussion

RNA interference-based gene therapy is an area of intense research with a great deal of potential for basic science investigation and clinical application. However, its implementation faces several challenges beyond those of traditional gene therapy. One is that gene knockdown is generally less predictable than gene overexpression. With a functioning promoter and cDNA, it is generally straightforward to overexpress any gene of interest. In contrast, it can often be challenging to identify the optimal region of a transcript for the most specific and efficiently targeted knockdown. Another challenge is attaining tissue-specific expression. mRNA transcripts are produced by RNA polymerase II promoters, which can be specific to a tissue of interest. Achieving adequate expression of interfering RNAs, however, is more efficiently achieved with RNA polymerase III promoters. This can make the task of targeting shRNA expression to a particular tissue of interest quite challenging.

Here, we report highly efficient knockdown of GFP in the heart but not in the liver after systemic injection of AAV9 carrying a single-stranded genome. To our knowledge, this is the first study to examine knockdown in heart and liver after systemic delivery of AAV9. This is an important comparison since AAV9 has been shown to traffic to these two tissues more than any other,<sup>37,38</sup> and previous reports have suggested the possibility of liver damage from shRNA expression.<sup>29</sup> We also describe the use of the luciferase reporter to confirm AAV9-mediated gene delivery prior to tissue level analysis of knockdown. Other labs have reported upon the use of AAV9 to knockdown genes in the heart,<sup>26-28</sup> but the reporter system we report

here with ubc-GFP mice provides new insights into the tissue-wide distribution of knockdown (e.g., Fig. 2.5B) that have not previously been described. The cell-to-cell variability in GFP signal intensity, notable particularly in the dosing study (Fig. 2.3), is complementary to results our laboratory has previously reported in mice injected with AAV9 carrying GFP under control of the cardiac troponin T promoter.<sup>13</sup> In addition, because AAV9 has not previously been shown to effectively target non-cardiomyocytes in the heart, the 71% reduction of GFP in heart tissue for the highest administered dose may be confined almost exclusively to cardiomyocytes. Since cardiomyocytes account for approximately 56% of cells in the heart,<sup>39</sup> it is possible that this approach is achieving cardiomyocyte knockdown of greater than 71%.

While AAV9 is extremely effective at programming RNA polymerase II-mediated overexpression in cardiac muscle and liver, there are relatively few reports of AAV9-mediated knockdown in liver. A study by Mayra et al.<sup>40</sup> described AAV9-mediated knockdown in cardiac and skeletal muscle after intraperitoneal delivery into neonatal mice, with no apparent shRNA production in the liver. As Mayra et al. speculate, it is probable that lack of liver expression in their study is due to the early post-natal time point of AAV injection, after which liver cells divide rapidly and viral genomes are likely degraded and/or diluted. Similarly, other studies have found low expression of transgene in liver after AAV injection into mice within 1-2 days after birth, further indicating that such early time points for AAV delivery are disadvantageous for achieving liver expression.<sup>41-43</sup> In contrast, mice injected in the current study were 8-10 days old, and we have previously observed



liver expression after AAV6 delivery to 7 day old mice and after AAV9 delivery to 8 day old mice (data not shown).<sup>13</sup> Indeed, in the current study we report 3.7-5 fold more AAV genomic DNA in the liver than in the heart 8 weeks after injection of single-stranded vectors (Fig. 2.7A), a ratio similar to what other studies have shown.<sup>37,44</sup>

We hypothesized that the lack of knockdown in the liver was the result of inefficient conversion of the single-stranded AAV9 genomes into the double-stranded DNA required by cells for transcription.<sup>34,45,46</sup> As a result of this limited hepatic conversion, several studies have directed liver expression using double-stranded AAV vectors, which obviate cellular conversion from single- to double-stranded DNA, although use of such vectors has been shown to cause toxicity in the liver at high doses.<sup>29,32,47-49</sup> However, in the current study comparing single- to double-stranded vectors we observed greater reduction of GFP transcript in the liver with ssAAV, and no reduction in liver protein with either ss- or dsAAV. Similarly, mRNA and protein analysis demonstrated that cardiac tissue knockdown was slightly improved with ssAAV over dsAAV. In GA muscle, ssAAV showed a slight but non-significant reduction in GFP transcript, while neither single- nor double-stranded vectors reduced GFP protein levels. The slight advantage of ss- over dsAAV here may be due to the relatively higher dose. For injection, an equal number of genomes were administered to both groups, i.e., twice as many single-stranded AAV particles were injected. Because our hypothesis was that single-stranded vectors were inefficiently converted in the liver, we decided that a dose of equivalent genomes would provide a more accurate test of our hypothesis than a dose of

equivalent viral particles. Compared to the initial single-stranded study, mRNA knockdown in cardiac tissue was similar (82% versus control), but protein knockdown was less robust (55% versus control). This is most likely due to the 20% reduction of viral dose in the ss/ds experiment and suggests that inhibition of translation, as well as transcript degradation, is integral to GFP knockdown in cardiac tissue.

These results indicate that although more AAV genomes are present in the liver than in other tissues, it is not conversion to double-stranded DNA but another mechanism that is responsible for decreased knockdown. Similar levels of knockdown with the pAUSiGTL and pAUSiGrLuc vectors (Fig. 1B and E) indicate that the cardiac selective knockdown is not due to the cardiac troponin T promoter affecting liver expression, which would not be expected given that it is located 3' from the knockdown cassette. A tissue level analysis of lacZ in cardiac, liver and skeletal muscle tissues by Inagaki et al. showed that to reach 83% transduction efficiency in liver and skeletal muscle required a 10-fold higher dose of AAV9 than that needed to achieve similar efficiency in the heart.<sup>38</sup> The contrast in tissue knockdown described here may therefore be due to the greater cardiac transduction efficiency of AAV9. A recent study by Lovric et al. implicates the activity of the Mre11/Rad50/Nbs1 heterotrimeric protein (MRN) DNA-damage response complex in lower AAV transduction.<sup>50</sup> In particular, it was shown that as cardiac MRN activity decreased in mice ranging from 1-21 days of age, cardiac transduction by AAV increased. They further showed that MRN activity is higher in liver than in heart and when MRN expression is decreased by siRNA, AAV transduction in liver increases.

However, a similar number of AAV genomes were present in liver regardless of MRN activity. While it was speculated that this transduction effect may be due to MRN recognition of single-stranded genomes, our experiments here suggest that double-stranded genomes fare no better. Since more genomes are present in the liver than in cardiac or skeletal muscle tissues, the most likely explanation for the lower knockdown we observed in liver may be transcriptional silencing by DNA-damage response proteins, as suggested by Lovric et al.

This study demonstrates that AAV9 vectors expressing shRNA can be used to achieve highly efficient cardiac-selective knockdown of GFP expression, with no change in liver expression despite a heavy accumulation of AAV genomes in the liver, or a change in GA muscle expression. Furthermore, this difference in expression is similar when either single- or double-stranded AAV9 genomes are employed. The mechanism for this remarkable contrast in expression may well relate to the activity of DNA-damage response proteins across the surveyed tissues and it suggests that the use of cardiac-specific promoters for gene knockdown may be unnecessary when using AAV9 due to its intrinsic affinity for cardiomyocytes.

Future studies will take advantage of the cardiac-selectivity of AAV9 to provide therapeutic cardiac gene knockdown. Indeed, several studies have looked at the effects of AAV9-mediated RNAi on cardiac function with transverse aortic constriction models of heart failure, including knockdown of phospholamban and the histidine-rich calcium binding protein.<sup>19,27</sup> Our lab is particularly well positioned to analyze the effect of gene knockdown on left ventricular remodeling after myocardial infarction, and a recent study showing that cardiomyocytes can be

efficiently targeted by AAV9 after reperfused myocardial infarction increases the clinical potential for therapeutic gene knockdown.<sup>16</sup> While the presence of feedback loops regulating gene expression may make knockdown of some genes more challenging than knockdown of GFP, a protein that is not expressed in wild-type mice, our data indicates that highly-efficient knockdown is possible. Furthermore, our inclusion of a cTnT promoter driving expression of luciferase shows that a knockdown cassette can be combined with an overexpression cassette, providing the ability to deliver cardiac-selective therapeutic knockdown along with cardiac-specific therapeutic overexpression, allowing for a multi-pronged approach to future cardiac gene therapies.

### **CHAPTER 3**

Myocardial Injury Independent of Ischemia/Reperfusion is Sufficient to Alter Viral Distribution and Transgene Expression and Simulates the Ischemic Induction of AAV9 Independent of the Compound Injected

## Introduction

Each year, over 790,000 Americans suffer a new or recurrent myocardial infarction (MI), making coronary disease the leading cause of death in the US.<sup>51</sup> Acute MI results in impairment of left ventricular (LV) function and progressive LV remodeling which can lead to heart failure. The goal of clinical therapy post-MI is to modulate the remodeling response to prevent deterioration of ventricular function. While gene therapy has been used in an experimental setting to reduce LV remodeling, it is currently not approved for any post-MI clinical treatments.

Because AAV9 provides such robust expression to the heart, it is a nearly ideal gene delivery vehicle for cardiomyocytes. However, to compensate for the transductional lag phase before AAV-mediated gene delivery reaches maximum expression, gene therapy for the treatment of LV remodeling is most often studied by delivering AAV several weeks prior to the ischemic insult.<sup>52-55</sup> In a clinical setting, patients surviving MI would ideally be treated in the hospital during their recovery period, and pretreatment would likely only be prescribed for those at risk of a recurring MI. Recently, our lab has shown that AAV9 provides robust and accelerated transduction to cardiomyocytes after ischemia and reperfusion.<sup>16</sup> While the mechanisms behind this ischemic induction effect remain to be proven, we hypothesized that they are related to increased tissue permeability and/or an unmasking of the AAV9 receptor on cardiomyocytes.

Inflammatory factors released during ischemia increase vascular permeability and the heart becomes edematous, an effect that may increase the extravasation of AAV into the heart, thus facilitating transduction.<sup>56,57</sup> Indeed, the

combination of papaverine (to increase vasodilation) and histamine (to increase vascular permeability) has long been known to provide increased AAV-mediated gene expression in skeletal muscle.<sup>58,59</sup> Furthermore, experiments using neuraminidase to remove sialic acids have demonstrated that AAV9 binds to *N*-linked glycans with terminal galactosyl residues.<sup>21</sup> Under normal conditions, these terminal galactosyl residues are usually sialylated, but ischemic conditions might unmask the AAV9 receptor by activating endogenous sialidases, increasing viral transduction.<sup>60</sup>

We hypothesized that by studying the effects of histamine/papaverine and neuraminidase, alone and in combination via intramyocardial (IM) injection, it would be possible to recapitulate the effects of ischemic induction on AAV9-mediated transduction of a vector expressing luciferase in a cardiac-specific manner and that the relative importance of each mechanism could be assessed. By comparing *in vivo* bioluminescence, cardiac luciferase activity and viral genomes, we determined that the tissue damage caused by intramyocardial injection was sufficient to alter viral distribution and transgene expression similarly to ischemic induction, regardless of the compound injected. We also carried out an additional study arm using the proteasome inhibitors MG132 and doxorubicin since previous studies have shown an increase in viral transduction after administration of these compounds and other proteasome inhibitors.<sup>11,61–63</sup> However, these compounds were also unable to boost transduction above that of the baseline tissue injury caused by IM injection.

## Materials and Methods

**Plasmid Design:** An initial pilot study described below used an AAV2 based plasmid construct with a cardiac-specific troponin T promoter driving firefly luciferase (pAcTnTLuc), as previously described by our lab.<sup>13</sup> The remaining experiments used a modified version of pAcTnTLuc with three miRNA-122 target sites inserted by BamHI restriction digestion into the 3'-untranslated region of the luciferase gene (pAcTnTLuc-miR122) to provide greater cardiac specificity.<sup>64,65</sup> Figure 3.1A-B shows plasmid constructs used for this experiment and Figure 3.1C shows the experimental study design.

**AAV Vector Production:** Vector genomes were cross-packaged into AAV9 capsids via triple transfection of AAV-293 cells (Agilent Technologies Inc., Clara, CA), then purified by ammonium sulfate fractionation and iodixanol gradient centrifugation. Titers of the AAV vectors [viral genomes (vg)/ml] were determined by qPCR. The following primers were used for amplifying luciferase: 5'-AAGATTCAAAGTGCCTGCTGGTG-3' (forward) and 5'-TTGCCTGATACCTGGCAGATGGAA-3' (reverse). Known copy numbers ( $10^5$ – $10^9$ ) of plasmids carrying the corresponding expression cassettes were used to construct standard curves for quantification.

**Animal Procedures:** The animal protocol used in this study was approved by the University of Virginia Institutional Animal Care and Use Committee (Protocol Number: 2802) and strictly conformed to the “Guide for the Care and Use of Laboratory Animals” (NIH Publication 85-23, revised 1985). Mice were maintained on a 12/12 hr light/dark cycle at 24°C and 60% humidity.



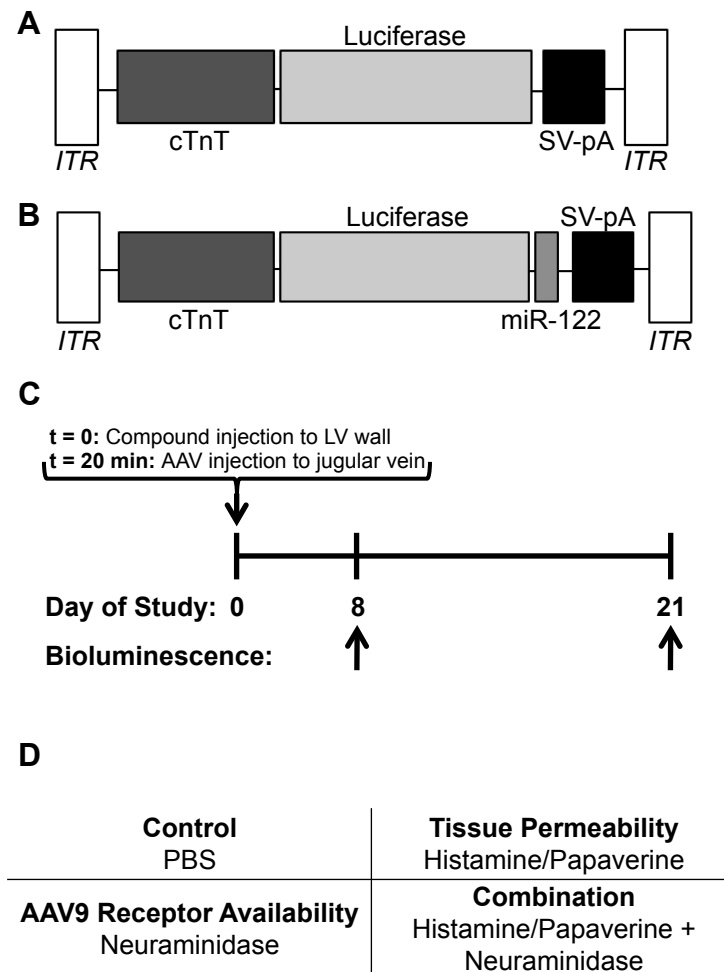


**Figure 3.1. AAV luciferase expression cassettes and experiment timeline.** (A) pAcTnTLuc, a previously described vector carrying a cardiac troponin T (cTnT) promoter driving firefly luciferase with an SV40 polyadenylation signal between the two AAV2 ITRs. (B) pAcTnTLuc-miR122, a modified version of pAcTnTLuc made by inserting three target sites for miRNA-122 into the 3'-untranslated region of luciferase. (C) Experimental timeline. Mice received 20  $\mu$ L intramyocardial injections of PBS, histamine/papaverine, neuraminidase, neuraminidase and histamine/papaverine, or MG132/ Doxorubicin, followed 20 minutes later by AAV9 administration to the jugular vein. Mice were subjected to in vivo bioluminescence imaging on days 8 and 21 after injection. (D) Summary of the four study groups to test the contributions of tissue permeability and AAV9 receptor availability. Two additional groups received either no cardiac injections or MG132 and doxorubicin.

Figure 3.1D shows a summary of the treatment groups in this study. To administer compounds to the myocardial wall, C56Bl/6 mice were anesthetized with sodium pentobarbital, placed in a supine position and orally intubated. Core body temperature was monitored throughout the operation with a rectal probe (Thermocouple Thermometer, Barnant Co, Barrington, IL) and maintained between 36.5-37.5°C with a heating lamp. The heart was then exposed by cutting the 3<sup>rd</sup> and 4<sup>th</sup> ribs with a cautery pen and the intercostal muscles with scissors. The compounds were injected as a 20 µL bolus into the anterior mid-wall of the left ventricle at concentrations of 10 mM histamine, 0.3 mg/mL papaverine, and 10 milliunits of neuraminidase, dissolved in water and PBS, as described previously.<sup>21,58,60</sup> For the proteasome inhibition arm, MG132 and doxorubicin were injected similarly at concentrations of 400 µM and 200 µM, respectively, as described previously.<sup>61</sup> Twenty minutes later, AAV was injected into the left ventricular chamber at a dose of  $1.5 \times 10^{11}$  viral genomes for the pilot study, or via the jugular vein at a dose of  $2 \times 10^{11}$  vg for the remaining studies.

**Lectin Staining and Fluorescence Microscopy:** To confirm neuraminidase activity for the time course planned for the AAV9 experiments, 20 µL of PBS or PBS containing 10 mU neuraminidase was injected into the LV wall of two groups of mice. After 20 minutes, the hearts were excised, fixed for 75 minutes in 4% paraformaldehyde, rinsed in PBS, and then frozen in OCT. Seven micron sections were blocked for 60 minutes at room temperature with 5% bovine serum albumin in PBS with streptavidin blocking (SP2002, Vector Laboratories, Burlingame, CA). Lectin staining was carried out with biotinylated Maackia amurensis lectin (MAL-I)

and Erythrina cristagalli lectin (ECL) (Vector Laboratories, Burlingame, CA). ECL sections were visualized with streptavidin-labeled Alexa Fluor 488 (Invitrogen, Carlsbad, CA) diluted 1:300 in PBS, and MAL sections were visualized with streptavidin Alexa 555 (Invitrogen) diluted 1:100. Sections were analyzed with an Olympus BX-41 Microscope (Olympus America, Inc., Center Valley, PA) with a Retiga-2000R camera (QImaging, Surrey, BC).

**Bioluminescence Imaging:** Luciferase expression was assessed in live mice using an in vivo bioluminescence imaging system (IVIS Spectrum, Caliper Life Sciences, Hopkinton, MA) as described previously.<sup>11,16,36</sup> Briefly, mice were anesthetized with isoflurane and injected with 150  $\mu$ L of 30 mg/mL D-luciferin (Gold Biotechnologies, Inc., St. Louis, MO) intraperitoneally. Images were collected 10-15 minutes after substrate injection and light output was quantified using Living Image software (Caliper Life Sciences).

**Tissue Analysis for Genomic DNA and Luciferase Activity:** Mice injected with AAV9 were euthanized on day 22 post-injection and their hearts were removed for analysis of viral genomes and luciferase activity. At the time of tissue collection, hearts were divided into injected and uninjected pieces so that the uninjected portions of the hearts could be used as internal controls. Luciferase activity was analyzed using the Promega (Madison, WI) luciferase assay kit, as described previously.<sup>11,66</sup> Briefly, hearts were homogenized in Promega reporter lysis buffer, incubated for 1 hour at 4°C and centrifuged at 10,000 $\times g$  for 10 minutes to collect protein extracts. A FLUOstar Optima microplate reader was used to assess relative light units per milligram of protein.

Total genomic DNA was isolated by passing the luciferase protein extracts through Qiagen DNA mini columns (Qiagen Inc., Valencia, CA). AAV vector genome copy numbers were determined by qPCR using the Bio-Rad iTaQ Universal SYBR Green Supermix PCR kit (Bio-Rad Laboratories, Hercules, CA) and a Bio-Rad CFX Connect real-time system. The following primers were used to amplify luciferase: 5'-AAGATTCAAAGTGGCTGCTGGTG-3' (forward) and 5'-TTGCCTGATACCTGGCAGATGGAA-3' (reverse). Known copy numbers ( $10^2$ – $10^7$ ) of the pAcTnTLuc-miR122 plasmid were used to construct the standard curve. Results are expressed as the number of vector copy numbers per  $\mu\text{g}$  of genomic DNA.

**Evans Blue Extraction:** To test the effects of histamine/papaverine (H&P) on vascular permeability, two groups of mice were injected with PBS or H&P to the LV wall as described above. Twenty minutes later, 50  $\mu\text{L}$  of 20 mg/mL Evans Blue was injected into the LV chamber. Forty-five minutes later, hearts were harvested and prepared for Evans Blue extraction by snap-freezing in liquid nitrogen. We adapted a protocol from Böhmer et al. to extract Evans Blue from heart.<sup>67</sup> Tissue samples were freeze-dried overnight on a VirTis system and then weighed. 300  $\mu\text{L}$  of formamide was added to each sample, which were then placed in a 60°C water bath for 2 hours, followed by incubation at room temperature for 10 hours. Absorption was measured using a FLUOstar Optima microplate reader (BMG Labtech, Durham, NC) at 595 nm with 100  $\mu\text{L}$  of each sample. A standard curve was prepared with 0–50  $\mu\text{g/mL}$  Evans Blue in formamide and data was expressed as the percent of the injected dose of Evans Blue per gram heart tissue.

**Statistical Analysis:** Data are expressed in figures as mean  $\pm$  SEM. Results were analyzed by Student's t-test or one-way ANOVA with the Tukey method to assess significance, where appropriate.

## **Results**

### **A Pilot Study with Neuraminidase, Histamine, and Papaverine Shows**

**Increased Expression After Injection with AAV9:** A pilot study was conducted to provide evidence for the hypothesis that the combination of neuraminidase and histamine/papaverine (NHP) could simulate the effects of ischemia-reperfusion on transduction and expression of AAV9. One mouse was injected with a 20  $\mu$ L bolus containing 10 mU neuraminidase, 10 mM histamine, and 0.3 mg/mL papaverine at the mid-wall on both sides of the left ventricle. At time = 0, the left side of the LV wall was injected. 18 minutes later, the right side was injected. 2 minutes after the second injection, AAV9 packaged with pAcTnTLuc was administered into the LV chamber at a dose of  $1.5 \times 10^{11}$  vg. Two control mice were treated similarly, but with PBS in place of NHP. In vivo bioluminescence imaging was performed at days 3, 7, 14 and 21 post-injection, and hearts were collected for in vitro luciferase activity on day 22. To assess any differences in the timing of NHP injection relative to AAV delivery, the left and right portions of the LV were isolated separately, homogenized in Promega Reporter Lysis Buffer, and equal amounts of protein, as determined by Bio-Rad Dc Protein Assay (Bio-Rad, Hercules, CA), were analyzed using a microplate reader.

Bioluminescence imaging revealed an approximately 2-fold difference between the NHP mouse and control mice starting at day 14 and persisting until day 21 (Fig. 3.2A-B). In vitro analysis showed similar results, with a 2-fold increase in luciferase activity in the NHP mouse compared to the average of the control mice (Fig. 3.2C). Additionally, the side of the heart treated 20 minutes before AAV injection showed 47% higher luciferase activity than the side of the heart treated 2 minutes before AAV injection. These results were taken as supporting the hypothesis that NHP can at least partially simulate ischemic induction of AAV9 and indicated that the doses and time points used were suitable for use in further studies.

#### **miRNA-122 Target Sites in the 3' Untranslated Region of Luciferase Provide**

**Increased Cardiac Specificity:** Our lab has previously published studies using the cardiac troponin T promoter to provide cardiac specific expression of luciferase and GFP.<sup>13</sup> These experiments were largely performed by injecting one-week old mice with a dose of  $1 \times 10^{11}$  vg/mouse. In recent experiments, we have used a similar dose of AAV9 in adult mice with an 8-10 fold greater body mass. In such mice luciferase expression is prevalent in liver as well as heart (i.e., Fig. 3.2A). It is unknown whether this effect is due to a relative decrease in viral dose versus body mass, a change in AAV9 receptors in older mice, or a dilution of viral genomes in the liver as it develops in younger mice, but we decided that a restoration of cardiac specificity to what was seen in younger mice would be highly advantageous for in vivo bioluminescence quantification of cardiac signal.

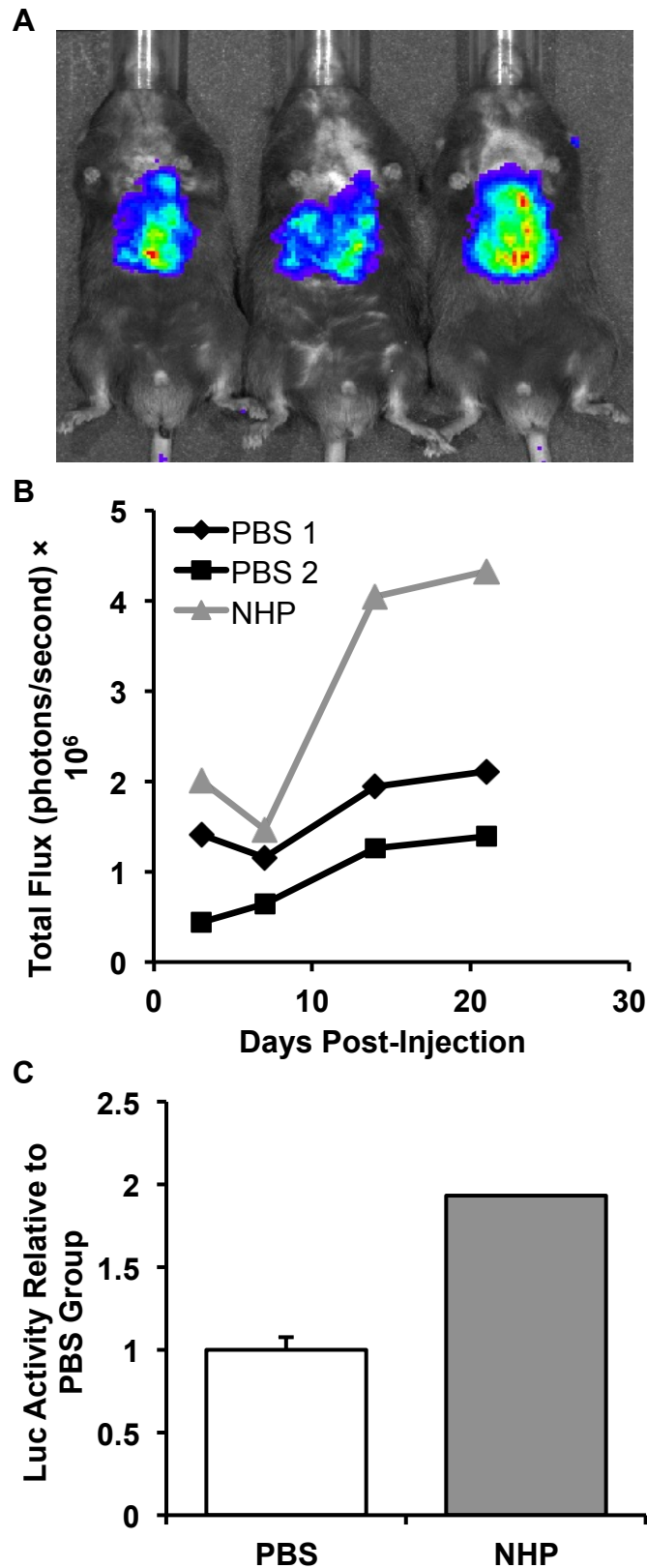


**Figure 3.2. A pilot study with NHP shows increased expression compared to PBS-injected mice.** (A) Bioluminescence image showing increased expression in a mouse injected with neuraminidase, histamine and papaverine (NHP, right) compared to control mice injected with PBS (left, middle). (B) Quantification of in vivo bioluminescence signal shows approximately 2-fold higher expression in the NHP-injected mouse compared to the PBS-injected mice by days 14 and 21. (C) Luciferase activity on protein extracted from hearts 22 days after injection also demonstrates 2-fold higher expression in the NHP-injected mouse compared to PBS-injected mice.

Geisler et al. and Qiao et al. both described embedding target sites for miRNA-122 (miR122), which is highly expressed in and specific to the liver, into the 3'-untranslated region of their expression cassettes, leading to highly effective prevention of AAV-mediated transgene expression in liver tissue.<sup>64,65</sup> We adopted this approach by incorporating miR122 sites into the pAcTnTLuc plasmid, and tested the new pAcTnTLuc-miR122 vector alongside the original to analyze tissue distribution. FVB mice were subject to bioluminescence imaging 14 days post-injection (Fig. 3.3), and luciferase expression was confined to the upper chest region with the vector containing miR122 target sites. This vector was used for subsequent experiments with AAV9.

#### **Neuraminidase Effectively Desialylates AAV9 Receptors Within 20 Minutes of**

**Administration:** To confirm that neuraminidase (NAD) is active over the planned time course of the study, two groups of mice were injected with either PBS (n=2) or NAD (n=2). Twenty minutes later, the hearts were harvested, fixed and frozen for sectioning and staining with Maackia amurensis lectin (MAL-I) and Erythrina cristagalli lectin (ECL). ECL binds to desialylated galactose residues, while MAL binds to sialic acid residues. Therefore, regions with increased ECL binding should show a corresponding decrease in MAL binding. Such regions are visible in Figure 3.4 in which areas of greater green staining on ECL sections correspond to areas of lower red staining on MAL sections from the two NAD-treated mice. In contrast, the PBS mouse shows uniform staining for both ECL and MAL. The results from this experiment indicate that NAD is capable of unmasking the AAV9 receptor within 20 minutes of intramyocardial injection.



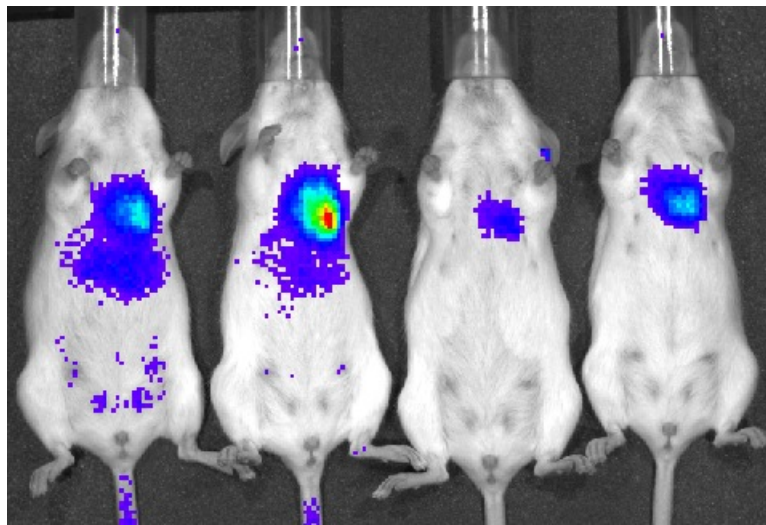


**Figure 3.3. miR122 target sites increase cardiac specificity from the cTnT promoter.**

Bioluminescence image acquired 14 days after mice were injected with AAV9 packaged with pAcTnTLuc (two left mice) or pAcTnTLuc-miR122 (two right mice), demonstrating luciferase expression confined to the thoracic cavity and absent from liver.

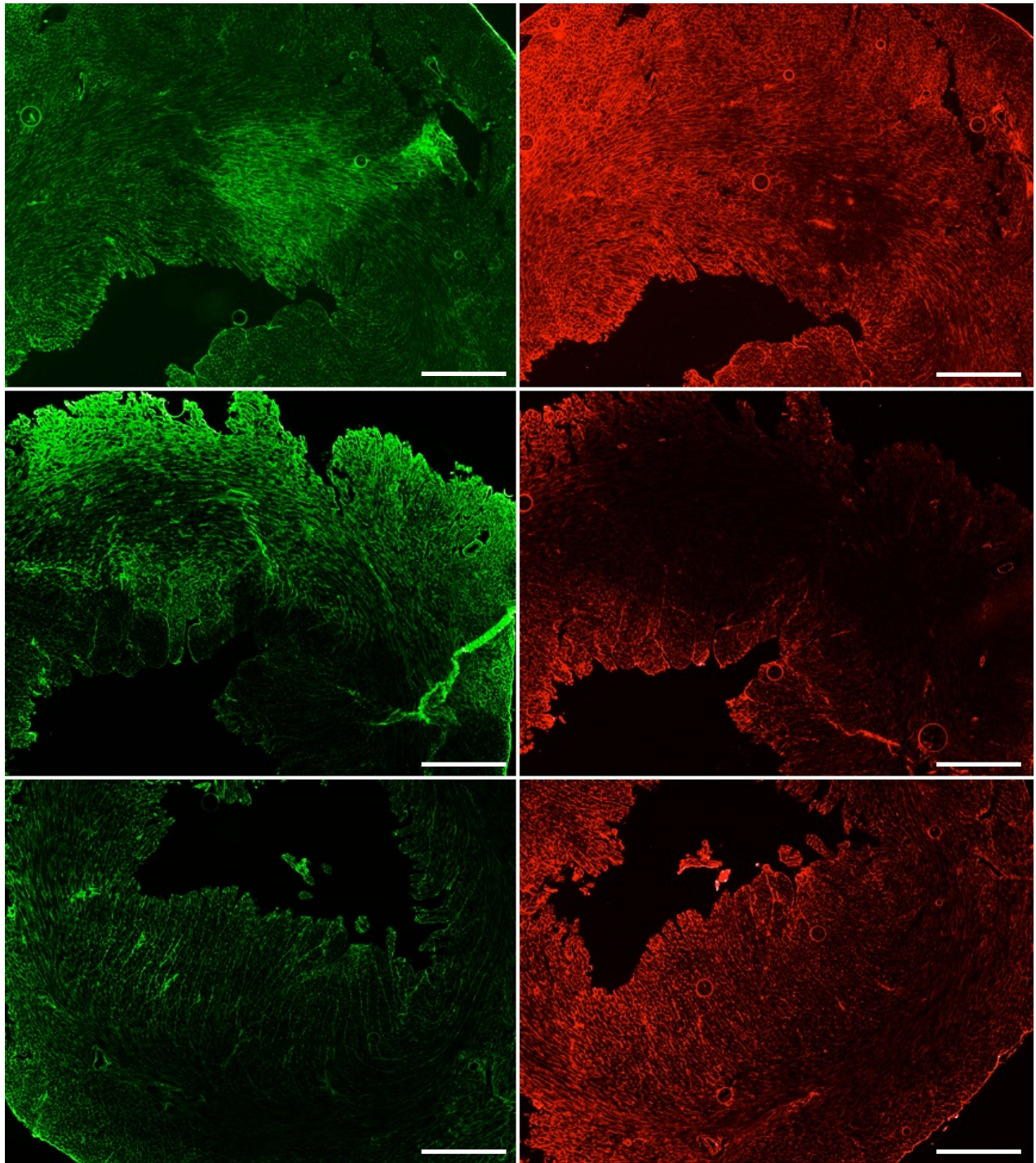


**Figure 3.4. Neuraminidase increases binding of ECL and decreases binding of MAL 20 minutes after intramyocardial injection.** Mice were injected IM with PBS or neuraminidase (NAD) and 20 minutes later, hearts were removed, fixed and frozen for lectin staining with ECL and MAL. The NAD injected regions (top and middle) show a higher ECL intensity and a reduced MAL intensity compared to the PBS control (bottom), indicating effective desialylation of cell surface glycans by NAD 20 min after injection. Scale bars = 100  $\mu$ m.

**Intramyocardial Injection Increases Luciferase Expression Independent of the Injected Compound:**

To test the effect of histamine/papaverine and neuraminidase alone and in combination, 4 groups of mice (n=4-6 per group) received the following injections: 1) PBS, 2) histamine/papaverine, 3) neuraminidase, and 4) neuraminidase and histamine/papaverine (NHP). Two additional groups of mice, one that received AAV but no injection to the myocardium, and the group that received MG132 and doxorubicin (MG132/Dox), were also included for comparison by bioluminescence imaging. Twenty minutes after IM injection, AAV9 packaged with pAcTnTLuc-miR122 was administered into the jugular vein at a dose of  $2 \times 10^{11}$  vg. In vivo bioluminescence imaging was performed using an IVIS Spectrum at 8 and 21 days post-injection (Fig. 3.5A). Light output was quantified at each time point and is displayed in Figure 3.5B. At both time points, the groups of mice that received IM injections displayed higher bioluminescence signal than mice that received no injection (at day 8:  $1.58 \times 10^6$  for uninjected controls,  $4.38 \times 10^6$  PBS group,  $2.91 \times 10^6$  H&P group,  $4.19 \times 10^6$  NAD group,  $3.99 \times 10^6$  NHP group, and  $2.66 \times 10^6$  MG132/Dox group; at day 21:  $2.56 \times 10^6$  for uninjected controls,  $5.94 \times 10^6$  PBS group,  $5.84 \times 10^6$  H&P group,  $7.83 \times 10^6$  NAD group,  $5.88 \times 10^6$  NHP group, and  $8.32 \times 10^6$  MG132/Dox group; all measurements in photons/second). While bioluminescence from the NAD and MG132/Dox groups trended higher than other injected groups by day 21, they did not demonstrate a significant difference as determined by one-way ANOVA. Furthermore, the NAD group also displayed higher bioluminescence signal than the group injected with both H&P and neuraminidase, suggesting that the increased signal was not due to the action of neuraminidase. These results indicate that

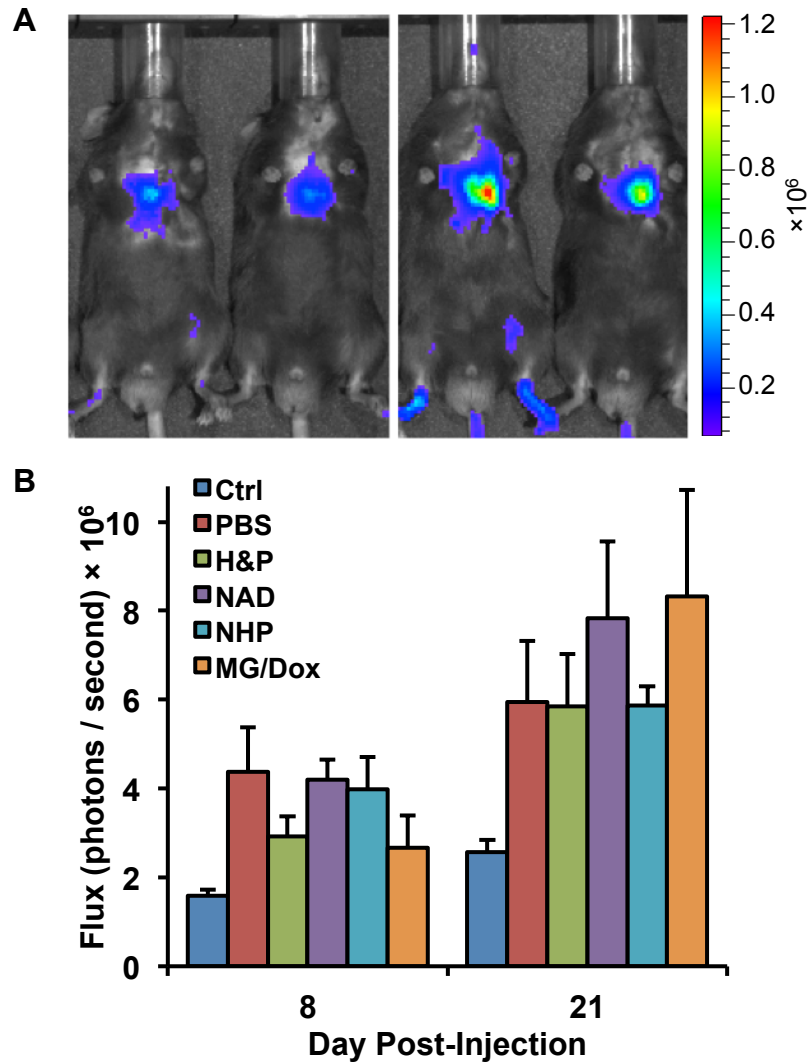


**Figure 3.5. Intramyocardial injection increases luciferase expression independent of the injected compound.** (A) Representative images of in vivo bioluminescence in mice from day 8 (left) and day 21 (right) post-injection, showing an increase in luciferase expression over the time course of the experiment. (B) Bioluminescence signals from days 8 and 21 were quantified and plotted for mice injected with AAV9 packaged with pAcTnTLuc-miR122 in the absence of a thoracotomy and IM injection (Ctrl), or 20 minutes after injection with: PBS, histamine/papaverine (H&P), neuraminidase (NAD), histamine/papaverine in combination with neuraminidase (NHP), or a combination of MG132 and doxorubicin (MG/Dox).

intramyocardial injection (and more generally, myocardial injury) is sufficient to increase bioluminescence signal intensity regardless of the compound injected.

**Injected Myocardium Contains More Viral Genomes and Increased Luciferase**

**Activity Compared to Uninjected Myocardium:** At day 22 post-injection, after bioluminescence imaging was completed, mice were euthanized and their hearts were removed for tissue level analysis of viral genomes and luciferase activity.

Hearts were divided into injected and uninjected portions, and the same portions of each were used to obtain gDNA and luciferase protein. Figure 3.6A shows vector copy numbers per microgram of genomic DNA for groups injected with PBS, H&P, NAD and NHP and the corresponding uninjected portions from each group. Copy numbers for injected heart fragments averaged 9436 copies/ $\mu$ g, 6724 copies/ $\mu$ g, 9363 copies/ $\mu$ g and 9297 copies/ $\mu$ g for the PBS, H&P, NAD and NHP groups, respectively, while the uninjected pieces averaged 5860 copies/ $\mu$ g, 3882 copies/ $\mu$ g, 4604 copies/ $\mu$ g and 3917 copies/ $\mu$ g for the PBS, H&P, NAD and NHP groups, respectively. The NHP group was the only group found to have a significant difference between injected and uninjected portions as measured by one-way ANOVA. Fold changes between injected and uninjected heart fragments were measured by taking the average number of copies in the injected pieces for each group and dividing by the average number of copies in uninjected pieces for each group (1.61, 1.73, 2.03 and 2.37 for the PBS, H&P, NAD and NHP groups, respectively), or by taking the same ratio for the individual mice and averaging over the entire group (1.72, 1.95, 2.22, and 2.78 for the PBS, H&P, NAD and NHP groups, respectively) (Fig. 3.6C-D).

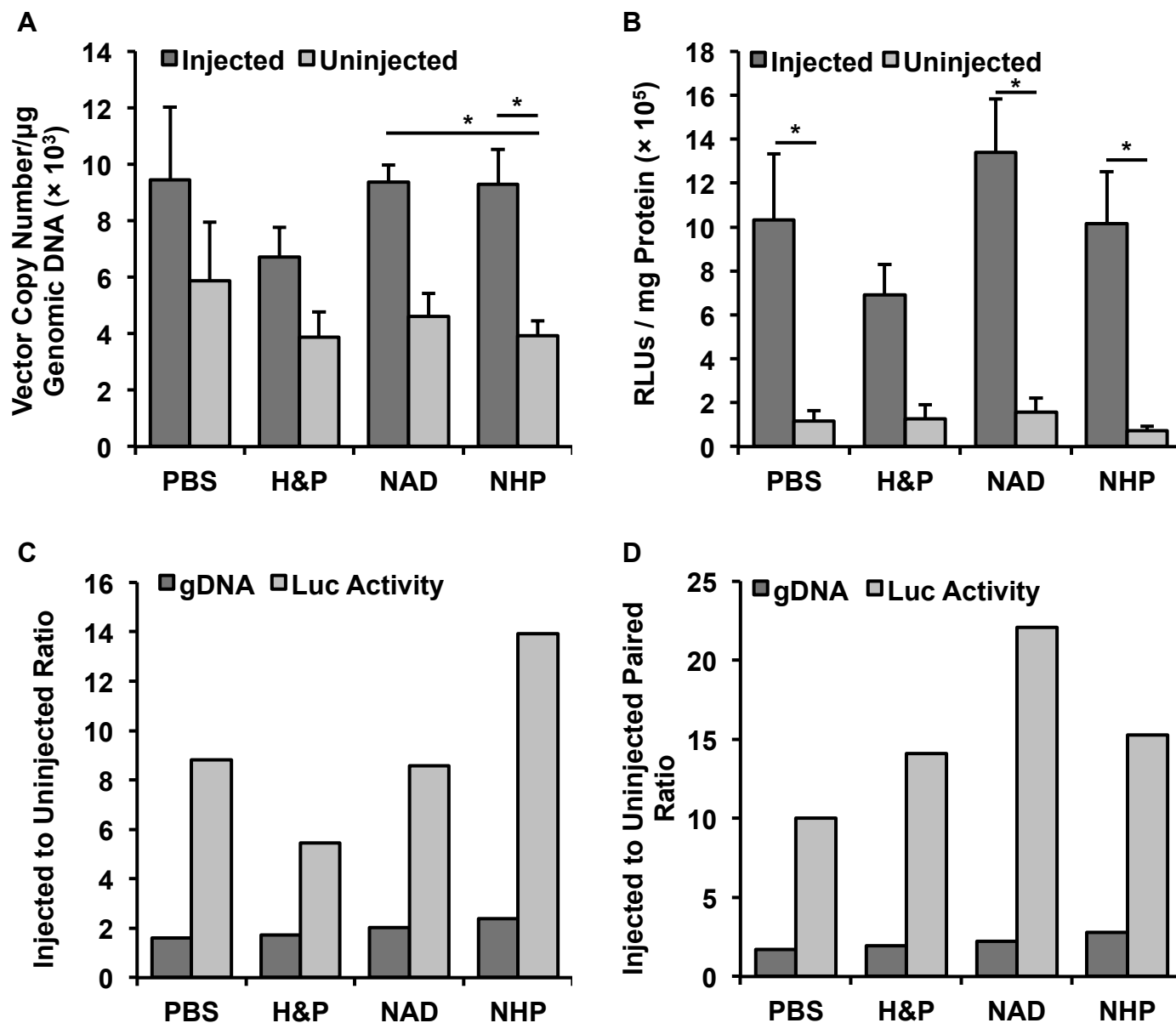


**Figure 3.6. Injected myocardium contains more viral genomes and greater luciferase activity than uninjected myocardium.** Hearts were removed from mice and divided into injected and uninjected pieces, which were processed for genomic DNA and luciferase protein. (A) AAV vector copy numbers per microgram of genomic DNA for groups injected with PBS, histamine/papaverine (H&P), neuraminidase (NAD), and histamine/papaverine in combination with neuraminidase (NHP). Groups that were significantly different as measured by one-way ANOVA are denoted with asterisks (\*). (B) Luciferase activity in injected and uninjected hearts, expressed as relative light units (RLUs) per milligram of protein. Except for the histamine/papaverine group, all injected heart samples were significantly different from all uninjected heart samples, as measured by one-way ANOVA. (C) Injected to uninjected ratios of gDNA and luciferase activity for each group. Averages were calculated for each group, and the ratios of the averages were plotted. (D) Injected to uninjected paired ratios of gDNA and luciferase activity for each group. For each animal, the injected to uninjected ratios were calculated, and the averages within each group were then plotted.



Figure 3.6B shows luciferase activity expressed as relative light units (RLUs) per milligram protein for injected and uninjected heart samples for groups injected with PBS, H&P, NAD and NHP. For injected samples, RLUs/mg protein averaged  $1.03 \times 10^6$ ,  $6.91 \times 10^5$ ,  $1.34 \times 10^6$ , and  $1.02 \times 10^6$  for the PBS, H&P, NAD and NHP groups, respectively, and for uninjected samples RLUs/mg protein averaged  $1.17 \times 10^5$ ,  $1.27 \times 10^5$ ,  $1.56 \times 10^5$ , and  $7.30 \times 10^4$  for the PBS, H&P, NAD and NHP groups, respectively. Except for the H&P group, all injected samples were found to have significantly greater luciferase expression than their corresponding uninjected samples, as measured by one-way ANOVA. Fold changes between injected and uninjected hearts were measured by taking the average luciferase activity in the injected pieces for each group and dividing by the average luciferase activity in uninjected pieces for each group (8.80, 5.45, 8.59 and 13.92 for the PBS, H&P, NAD and NHP groups, respectively), or by taking the same ratio for the individual mice and averaging over the entire group (10.03, 14.12, 22.07 and 15.27 for the PBS, H&P, NAD and NHP groups, respectively) (Fig. 3.6C-D).

### **Intramyocardial Injection of Histamine/Papaverine Does Not Increase Evans**

**Blue Extravasation into Cardiac Tissue:** In an attempt to detect a change in tissue permeability after administration of histamine/papaverine, mice were treated with either H&P (n=4) or PBS (n=5) to the LV wall 20 minutes prior to intraventricular chamber injection with Evans Blue. Hearts were removed 45 minutes later and freeze dried overnight (Fig. 3.7A), after which Evans Blue was extracted from heart samples and expressed as percentage of injected dose per gram tissue (Fig. 3.7B).

**A**



**B**

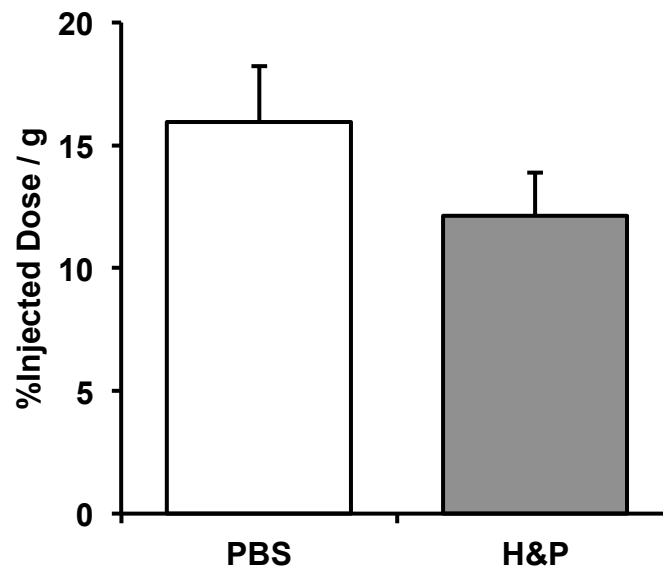


**Figure 3.7. Intramyocardial injection of histamine/papaverine does not increase Evans Blue extravasation into the injected region.** (A) Mice were injected IM with PBS (top) or histamine/papaverine (H&P) (bottom) at t=0 min, followed by systemic injection of Evans Blue at t=20 min. Hearts were removed after 45 minutes and assayed for Evans Blue content. Photographs were taken after freeze-drying hearts overnight. (B) Evans Blue was extracted from freeze-dried heart samples and expressed as the percentage of the injected dose of Evans Blue per gram tissue. There was a trend towards increased Evans Blue in PBS-treated mice, but the difference was not significant.



While there was a trend towards increased Evans Blue content in the hearts of PBS-treated mice, the difference was not significant ( $p = 0.23$ ).

## **Discussion**

AAV9-based gene therapy has demonstrated a great deal of promise for the treatment of post-MI left ventricular remodeling. Until recently, however, it has been thought that the transductional lag phase of AAV9 prior to maximum transgene expression would limit its clinical utility. Recent evidence published by our lab shows that AAV9 provides robust and accelerated transduction to cardiomyocytes after ischemia and reperfusion.<sup>16</sup> Understanding the mechanisms by which this ischemic induction of AAV9 occurs could allow for the development of new strategies to target gene therapy to both ischemic and non-ischemic tissues.

We hypothesized that by increasing vascular permeability and AAV9 receptor availability through a combination of histamine/papaverine and neuraminidase, we could partially recapitulate the ischemic induction of AAV9. Furthermore, the study was designed to elucidate the importance of each mechanism by administering the compounds alone and in combination, with injection of PBS serving as a control. However, analysis of bioluminescence signal, luciferase activity and viral genomes showed that intramyocardial injection confounds the ability to determine the relative contributions of the proposed mechanisms and provided evidence that those mechanisms are secondary to one of greater importance.

While there was no significant difference among injected groups as measured by in vivo bioluminescence imaging, all groups had higher signals than the

uninjected control group, especially the neuraminidase and MG132/Dox groups. These results suggested that intramyocardial injection alone was enough to increase AAV9-mediated transgene expression, but analysis of vector genomes and luciferase activity from harvested hearts provided more insight into the mechanisms involved. At the time of tissue collection, hearts were divided into injected and uninjected fragments since only the anterior LV wall was injected and the rest of the heart could act as an internal control. Among all groups, there were roughly 2-fold more viral genomes in the injected myocardium compared to uninjected myocardium, similar to the increase in viral genomes in post-ischemic versus sham-operated hearts.<sup>16</sup> While there were relatively minor differences in average viral genome injected-to-uninjected ratios between groups, the PBS group demonstrated the smallest change, followed by the H&P, NAD, and NHP groups. This is the pattern we initially predicted, but with smaller changes than anticipated, and no statistical significance. An experiment we performed that used Evans Blue to measure permeability after IM injection with PBS and H&P confirmed that injection of PBS alone was enough to increase tissue permeability to AAV. We initially speculated that Evans Blue would provide a poor proxy for AAV given that the protein complex that comprises the AAV capsid is 60× greater in size than the albumin to which Evans Blue binds. However, the data from the Evans Blue experiment explain why the histamine/papaverine-treated groups did not show an increase in AAV transduction over PBS-treated groups, despite a dose of H&P comparable to or higher than other studies.<sup>58,68,69</sup> This data indicates that the tissue damage and the resulting inflammatory response from needle insertion and/or IM injection was

sufficient to increase vascular permeability and diminish the effect of the H&P injection. While histamine/papaverine has previously been used to increase AAV transduction to skeletal muscle, that procedure involved vein isolation and arterial perfusion of H&P over several minutes.<sup>58</sup> Similar efforts have been used to increase adenovirus delivery to dog heart,<sup>70</sup> but such a procedure would be extraordinarily technically challenging in a mouse. The trend towards increased viral genomes in groups injected with neuraminidase suggests that it may have been very slightly effective in increasing AAV9 uptake, but it was not possible to isolate the effect of NAD injection from the effect of injecting a 20  $\mu$ L bolus into the LV wall.

While the injected-to-uninjected ratio of viral genomes in heart samples increased steadily among the treatment groups, the same effect did not hold for luciferase activity, which ranged from 5.5- to 14-fold greater among the injected samples compared to uninjected samples, also similar to the increase in luciferase activity in post-ischemic versus sham-operated hearts.<sup>16</sup> The non-linear relationship between increased viral genomes and increased luciferase activity suggests what is likely the most important mechanism behind the ischemic induction of AAV9. A paper recently published in collaboration with our lab studied a similar ischemic induction effect in skeletal muscle with a mouse model of peripheral artery disease.<sup>71</sup> In this study, AAV1 was used as a control for AAV9 since it binds to sialic acid rather than the *N*-linked glycans with terminal galactosyl residues that are unmasked when sialic acids are removed, as with AAV9.<sup>21</sup> In contrast to AAV9-delivered genomes, which were found in greater abundance in ischemic hindlimb, more AAV1 vector genomes were found in the corresponding non-ischemic

hindlimb. Despite more vector genomes in the non-ischemic hindlimb, however, the ischemic limb of AAV1 injected mice displayed greater transgene expression, albeit much less than what was provided by AAV9. These results provide support for our hypothesis involving post-ischemic availability of the AAV9 receptor, but indicate that post-entry cellular processing of AAV, altered by ischemia, provides the most important component to the ischemic induction effect. IM injection of PBS or the other compounds in the current study likely stresses heart tissue in a manner similar to ischemia, increasing transgene expression disproportionately to the additional genomes that enter the tissue. This change in cellular processing of AAV may well relate to activity of DNA damage response proteins.

The previous chapter described a study by Lovric et al. that implicates the activity of the DNA-damage response MRN complex in lower AAV transduction of several tissues, including the liver.<sup>50</sup> AAV transduction was higher in tissues in which the MRN proteins showed lower expression, including the heart. In addition, it has previously been shown that the MRN complex localizes to sites of DNA damage and that this is advantageous for AAV transduction, likely because it reduces direct binding of MRN proteins to AAV genomes.<sup>72-75</sup> Therefore, decreased expression or altered activity of the MRN complex seems to allow greater viral transduction and transgene expression by AAV. Similarly, use of proteasome inhibitors in several studies has led to increased AAV transduction.<sup>11,61-63</sup> We tried to amplify this effect by injecting mice with the proteasome inhibitors MG132 and doxorubicin. These mice had a slightly higher average bioluminescence signal than the other groups, but the proteasome inhibitors were unable to significantly boost

expression above what was caused by the IM injection injury. The demonstrated increase in viral genomes and luciferase activity in injected versus uninjected heart samples that we witnessed is comparable to the increases between ischemic and sham-operated cardiac tissue we previously described, and probably due to a similar mechanism.<sup>16</sup>

The evidence presented here suggests that the proposed ischemic induction of AAV9 caused by an altered DNA damage response greatly outweighs the previously hypothesized mechanisms of increased tissue permeability and AAV9 receptor availability. Therefore, it may be fair to ask whether the latter mechanisms have any relative importance, and how they might be studied. Systemic injection of histamine/papaverine and neuraminidase would likely alter AAV9 uptake throughout the body. For example, a study published by Shen et al. demonstrated a biodistribution of AAV9-delivered genomes and gene expression that was decreased in the heart and increased in the liver after IV injection of neuraminidase.<sup>76</sup> An alternative approach may be to clamp the aorta and pulmonary arteries and deliver the compounds directly into the left ventricle. While this approach has previously been used to deliver AAV to rats and mice, it is extremely technically challenging.<sup>69,77</sup> Furthermore, while the duration of the clamp would be confined to a minute or less, that period may be enough to stimulate DNA damage response proteins throughout the heart. Since ischemic induction has also been demonstrated in skeletal muscle, the relative contributions of vascular permeability and AAV9 receptor availability may be best tested there. It is easier to isolate the circulation of the hindlimbs, after which the compounds could be perfused alone and in

combination, as was previously described for histamine/papaverine.<sup>58</sup> Though this method would not definitively elucidate the relative contributions of these mechanisms in the heart, it could provide for a reasonable approximation.

The goal of this study was to elucidate the relative importance of the proposed mechanisms behind the ischemic induction of AAV9, namely increased vascular permeability and AAV9 receptor availability. The results show that intramyocardial injection confounds the ability to determine the relative contributions of these mechanisms and, indeed, that these mechanisms are likely less important than an alteration of the DNA damage response mechanism induced by ischemia or general tissue injury. However, these results are illuminating in and of themselves, particularly the confirmation of a non-linear relationship between genome entry and transgene expression in injected versus uninjected tissue, similar to the relationship previously described between ischemic and sham-operated cardiac tissue.<sup>16</sup> Even though this data does not directly explain the mechanism behind ischemic induction, it provides greater evidence for it, which may be used to inform future research and clinical therapies. Increased AAV9 efficiency post-ischemia and reperfusion has clear clinical implications for the delivery of therapeutic genes, and an understanding of the mechanisms may enhance the targeting of ischemic tissues while eliminating off-target effects in other tissues and result in the application of novel strategies to target non-ischemic tissues more effectively.

## **CHAPTER 4**

AAV-Mediated Delivery of a Modified Periostin Promoter Driving Cre Recombinase  
Activates Gene Expression in Cells that Express Markers for Hematopoietic Stem  
Cells in the Infarct Borderzone After Reperfused Myocardial Infarction

## Introduction

Adeno-associated virus has been used to direct gene transfer to a variety of tissues, including heart, liver, skeletal muscle, brain, kidney and lung.<sup>10,37</sup> AAV9, in particular, provides highly efficient transduction to cardiac muscle.<sup>38,54</sup> However, it has not previously been shown to effectively target fibroblasts, including cardiac fibroblasts.

Studies by Zak<sup>78</sup> and Nag<sup>79</sup> demonstrated that fibroblasts account for over half of the cardiac cell population in adult rats, though more recent studies have shown that this fraction is lower in mice.<sup>17</sup> After injury, cardiac fibroblasts differentiate into myofibroblasts, which are integral to the post-MI wound healing process.<sup>39,80</sup> The ability to modulate myofibroblast behavior would be extremely valuable, in particular by opening new avenues of potential therapy to treat LV remodeling in patients recovering from MI. In vitro studies of AAV6, 8 and 9 in human corneal fibroblasts have demonstrated 25-50 fold greater transgene expression in AAV6 compared to the other two serotypes.<sup>22</sup> However, another study in cultured mouse embryonic fibroblasts indicated an approximately 10-fold increase in expression from AAV1 compared to AAV6.<sup>23</sup> We therefore considered AAV serotypes 1 and 6 to be leading candidates over AAV9 for providing maximal gene expression in cardiac fibroblasts in vivo after IV injection.

While AAV1 and 6 may transduce cardiac fibroblasts efficiently, both serotypes will also transduce cardiomyocytes after systemic administration.<sup>13,37</sup> As a result, any therapy aimed at cardiac fibroblasts would benefit from a promoter excluding transcription of the AAV genome from cardiomyocytes to avoid off-target



effects. Lindsley et al. described a 3.9 kilobase promoter responsible for controlling the transcription of periostin, an epithelial ligand and matricellular protein commonly expressed by fibroblasts.<sup>81</sup> We PCR amplified regions corresponding to an enhancer and minimal promoter and combined them to create a modified periostin promoter of reduced size for use in our AAV vectors. We hypothesized that a combination of the periostin promoter and AAV1 or -6 capsids could provide efficient expression to cardiac fibroblasts but not cardiomyocytes.

We tested the ability of the periostin promoter to drive Cre recombinase expression in two different strains of reporter mice that express GFP or luciferase after Cre-mediated recombination. This reporter system was useful for validating the periostin vector construct in vivo because a short duration of Cre expression can activate long-term reporter gene expression and allows for lineage tracking after differentiation or proliferation. While little to no expression was evident after AAV6 delivery to normal, healthy mice, robust cardiac GFP expression was seen when vector was injected two-days after reperfused MI, with only rare borderzone cardiomyocytes expressing GFP. We then analyzed expression with AAV1, -6 and -9 and found that AAV9 activated greater reporter gene expression than either AAV1 or AAV6. Cre-mediated reporter gene expression was also shown to be approximately two-fold higher after AAV9 delivery two days post-MI compared to delivery at reperfusion. Finally, immunofluorescence analysis of Cre-activated GFP-positive cells revealed that they lacked characteristic fibroblast markers such as  $\alpha$ -smooth muscle actin and DDR2. Instead, the majority of GFP expressing cells were positive for VEGFR-2, with a smaller subset of cells demonstrating expression of the

pan-leukocyte marker CD45, indicating AAV transduction of hematopoietic stem cells rather than cardiac fibroblasts.

## **Materials and Methods**

**Plasmid Design:** We initially set out to construct an expression cassette that would provide transgene expression in cardiac fibroblasts but not cardiomyocytes.

Lindsley et al. described a 3.9 kilobase periostin promoter,<sup>81</sup> from which we PCR amplified sequences containing an 804 bp enhancer and 423 bp minimal promoter to create a shorter 1395 bp promoter. PCR was completed with Phusion high-fidelity master mix (Thermo Scientific, Waltham, MA) to avoid errors in amplification. This smaller periostin promoter, which was found by Lindsley et al. to provide stronger expression than its full-length wild-type counterpart, was inserted by quadruple ligation with a linker oligonucleotide in place of the cardiac troponin T promoter in plasmids carrying either a Cre recombinase gene codon-optimized for eukaryotic expression,<sup>82</sup> or a GFP expression cassette. The new plasmids, pAPiCre and pAPGFP, were sequenced to confirm accurate amplification of the periostin promoter.

Further experiments were carried out by modifying the pAPiCre vector with three target sites for miRNA-122, as described in the previous chapter, to reduce liver expression.<sup>64,65</sup> The target sites were inserted into a BamHI site in the 3' untranslated region of Cre and confirmed to be in the correct orientation by restriction digestion and sequencing. All expression cassettes used in this chapter are shown in Figure 4.1A-C.

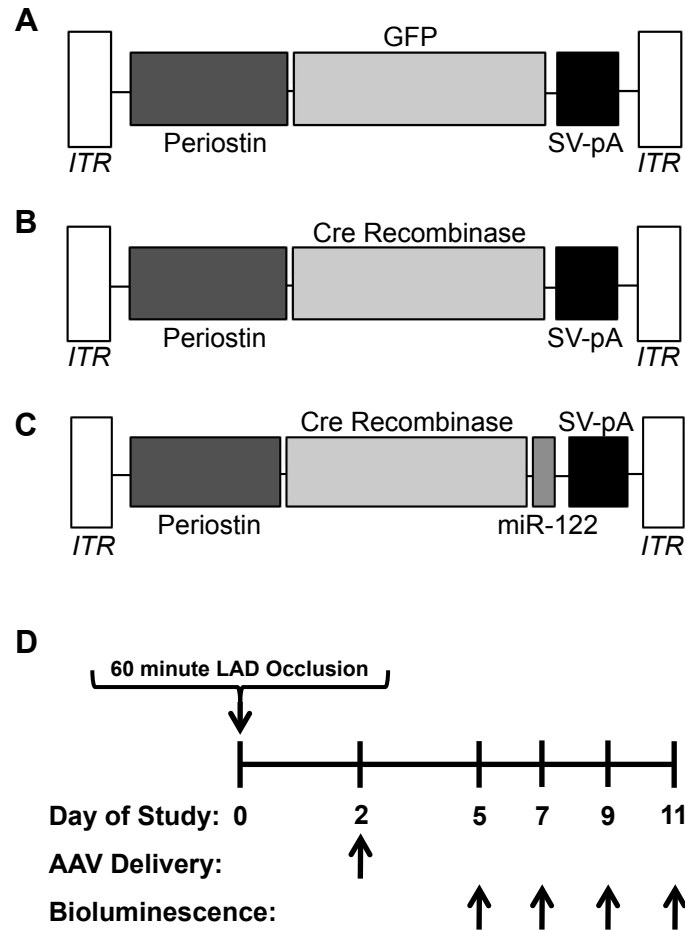


**Figure 4.1. AAV expression cassettes containing a modified periostin promoter and experimental design.** A modified periostin promoter was constructed by PCR amplifying regions surrounding the 804 bp enhancer and 423 bp minimal periostin promoter as described by Lindsley et al. These were cloned into plasmids containing either (A) a GFP reporter, pAPGFP, or (B) a Cre recombinase gene codon optimized for eukaryotic expression, pAPiCre. (C) The expression cassette with Cre was modified by inserting target sequences for miRNA-122 into the 3' untranslated region of Cre to prevent transgene expression in the liver (pAPiCre-miR122). (D) General timeline for experiments carried out in this chapter. Most mice were injected with AAV two days after reperfusion MI and bioluminescence imaging was employed in several experiments by imaging mice between days 5 and 11 post-MI.

**In Vitro Testing of pAPGFP:** To test the ability of the modified periostin promoter to provide transcription, AAV-293 cells were transfected via the calcium phosphate method with pAPGFP and compared to a plasmid expressing GFP from the cytomegalovirus (CMV) promoter. Briefly, plasmid DNA was added to a mixture containing water and 500 mM CaCl<sub>2</sub> before mixing drop-wise with 2× hepes-buffered saline. The transfection mixture was added to the cell media at 1/10<sup>th</sup> the volume and cells were monitored until day 3 by fluorescence microscopy to confirm GFP expression. Three wells were transfected with 0.5 µg and three wells with 1 µg of each plasmid. On day 3, fluorescence from the periostin and CMV promoters was quantified with a FLUOstar Optima plate reader (BMG Labtech, Durham, NC).

**AAV Vector Production:** Vector genomes were cross-packaged into AAV1, -6 and -9 capsids via double or triple transfection of AAV-293 cells (Agilent Technologies Inc., Clara, CA), then purified by ammonium sulfate fractionation and iodixanol gradient centrifugation. Titers of the AAV vectors [viral genomes (vg)/ml] were determined by qPCR. The following primers were used for amplifying periostin: 5'-TCCGTGTTCTGCTGTGGAGTGATT-3' (forward) and 5'-TAGGGATCTCTCTGCCTTCTGTCT-3' (reverse). Known copy numbers (10<sup>5</sup>–10<sup>9</sup>) of plasmids carrying the corresponding expression cassettes were used to construct standard curves for quantification.

**Animal Procedures:** The animal protocol used in this study was approved by the University of Virginia Institutional Animal Care and Use Committee (Protocol Number: 2802) and strictly conformed to the “Guide for the Care and Use of

Laboratory Animals” (NIH Publication 85-23, revised 1985). All mice were maintained on a 12/12 hr light/dark cycle at 24°C and 60% humidity.

Two transgenic mouse lines were used in this chapter for in vivo testing of AAV packaged with the periostin promoter driving Cre recombinase. Figure 4.2 shows a summary of the transgenic expression cassettes in these mice. When Cre is expressed in these strains it recognizes LoxP sites flanking a transcriptional stop sequence between a promoter and a reporter gene and removes the stop sequence, allowing expression of a reporter gene. B6.Cg-Gt(ROSA)26Sor<sup>tm6(CAG-ZsGreen1)Hze</sup>/J (Flox-GFP) mice are on a C57Bl/6 background and express ZsGreen1, an enhanced green fluorescent protein, from the CMV-enhanced chicken beta-actin promoter (CAG).<sup>83</sup> FVB.129S6(B6)-Gt(ROSA)26Sor<sup>tm1(Luc)Kael</sup>/J (Flox-Luc) mice are on an FVB background and express luciferase under control of the ROSA26 promoter.<sup>84</sup>

Most mice in this study were treated with AAV after reperfused myocardial infarction. Male mice from 9 to 19 weeks of age were anesthetized with sodium pentobarbital, placed in a supine position and orally intubated. Core body temperature was monitored throughout the operation with a rectal probe (Thermocouple Thermometer, Barnant Co, Barrington, IL) and maintained between 36.5-37.5°C with a heating lamp. The heart was exposed by cutting the 3<sup>rd</sup> and 4<sup>th</sup> ribs with a cautery pen and the intercostal muscles with scissors. MI was induced by passing a 7-0 silk suture beneath the left anterior descending coronary artery (LAD) at the level of the lower left atrium and tying it over a piece of PE-50 tubing to achieve occlusion. Reperfusion was performed by untying the ligature and removing the tubing. Mice were injected with AAV at the time of reperfusion by intravenous

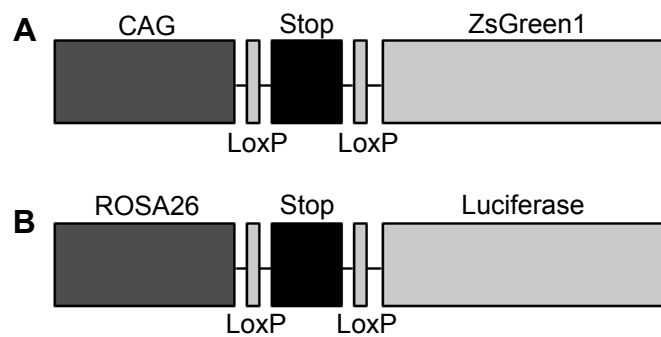


**Figure 4.2. Transgenic mouse strains expressing a green fluorescent protein or luciferase upon Cre-mediated recombination.** Two transgenic mouse lines were used in this chapter to test AAV packaged with periostin plasmid constructs *in vivo*. When Cre is expressed in these strains it recognizes the LoxP sites flanking a stop sequence and removes the stop sequence, allowing expression of the reporter gene. (A) B6.Cg-Gt(ROSA)26Sor<sup>tm6(CAG-ZsGreen1)Hze</sup>/J mice, abbreviated Flox-GFP and on a C57Bl/6 background, express ZsGreen1, an enhanced green fluorescent protein, from the CMV enhanced chicken beta-actin promoter (CAG). (B) FVB.129S6(B6)-Gt(ROSA)26Sor<sup>tm1(Luc)Kael</sup>/J mice, abbreviated Flox-Luc and on an FVB background, express luciferase under control of the ROSA26 promoter.

injection via the jugular vein, or 1, 2 or 3 days after MI via the tail vein. An additional group of mice was also treated with virus in the absence of MI by tail vein injection. Mice received between  $1 \times 10^{11}$  to  $3 \times 10^{11}$  viral genomes for all studies. A generalized experimental design used for most animal studies is shown in Figure 4.1D.

**Bioluminescence Imaging:** Luciferase expression was assessed in live Flox-Luc mice using an in vivo bioluminescence imaging system (IVIS Spectrum, Caliper Life Sciences, Hopkinton, MA) as described previously.<sup>11,16,36</sup> Briefly, mice were anesthetized with isoflurane and injected with 150-300  $\mu$ L of 30 mg/mL D-luciferin (Gold Biotechnologies, Inc., St. Louis, MO) intraperitoneally. Images were collected 10-30 minutes after substrate injection and light output was quantified using Living Image software (Caliper Life Sciences).

**Tissue Analysis for Luciferase Activity:** Mice injected with AAV1, -6 or -9 were euthanized on days 9-15 post-MI and their hearts were removed for analysis of luciferase activity. Luciferase activity was analyzed using the Promega (Madison, WI) luciferase assay kit, as described previously.<sup>11,66</sup> Briefly, hearts were homogenized in Promega reporter lysis buffer, incubated for 1 hour at 4°C and centrifuged at  $10,000 \times g$  for 10 minutes to collect protein extracts. A FLUOstar Optima microplate reader was used to assess relative light units per milligram of tissue.

**Immunofluorescence and Image Acquisition:** For fluorescence microscopy of Flox-GFP mice, hearts were excised 9 days post-MI and fixed for one hour at room temperature in 4% PFA, rinsed in PBS, and incubated overnight at 4°C in 30% sucrose in PBS before embedding in OCT. Six micron cryosections were cut from

each tissue and coverslipped using Prolong Gold anti-fade reagent (Life Technologies Corp., Carlsbad, CA), with or without DAPI, to preserve GFP signal. Sections were also incubated with a variety of primary antibodies to identify additional markers of GFP-positive cells (Table 4.1 contains a full list of the primary antibodies used). Briefly, the staining protocol involved rinsing OCT from slides with PBS, and blocking with 5% bovine serum albumin (BSA) in PBS with 0.3 M glycine and 0.05% Tween-20 for one hour at room temperature. Primary antibodies were incubated at dilutions ranging from 1:50 to 1:1000 for one hour at room temperature with 1% BSA and 0.05% Tween-20 in PBS. Secondary antibodies to goat, rat or rabbit containing Alexa Fluors 546, 555, 594 or 647 (Life Technologies Corp.) were incubated at dilutions of 1:200 for one hour at room temperature with 1% BSA and 0.05% Tween-20 in PBS.

Images were acquired with an Olympus BX-41 Microscope (Olympus America, Inc., Center Valley, PA) with a Retiga-2000R camera (QImaging, Surrey, BC) using a FITC (41004, Chroma Technology Corp., Bellows Falls, VT), Texas Red (41004, Chroma) or Cy5.5 (41023, Chroma) filter set. Further imaging was performed using an Olympus IX81 inverted microscope with a 10× UPlanFLN 0.30 NA objective, Orca-AG CCD camera (Hamamatsu, Bridgewater, NJ), automated stage (Prior Scientific, Rockland, MA), and IPLab software (Scanalytics, Fairfax, VA).

For confocal microscopy, 1 mm short axis segments from the infarct zone were whole mounted using 50% glycerol in PBS after fixing in PFA and sucrose as described above. Imaging was performed on a Nikon TE 2000-E2 microscope equipped with a Melles Griot Argon Ion Laser System and Nikon D-Eclipse C1



Antibody	Target Cells	Company	Catalog #	Dilution	Signal
alpha-SMA	Fibroblasts, smooth muscle	Sigma	C6198	100	- HS
SM-MHC	Smooth muscle	Kamiya	MC-352	100	- HS
Vimentin	Fibroblasts, mesenchymal cells	Cell Signaling	5741	100	- NSI
		Abcam	ab92547	200	- NSI
DDR2	Fibroblasts	Santa Cruz	sc-7555	50	- HS
Periostin	Fibroblasts, epithelial cells	Abcam	ab14041	400	- NSI
FSP-1	Fibroblasts	Millipore	ABF32	200	- TBO
Collagen I	Collagen	Santa Cruz	sc-28654	100	- NSI
Collagen III	Collagen	Santa Cruz	sc-28888	100	- NSI
Isolectin IB4	Endothelial cells	Invitrogen	I32450	200	- HS
CD31	Endothelial cells	BD	550274	50	- HS
CD34	Endothelial cells, BMDCs	Abcam	ab8158	400	- NS - ECM
		eBiosciences	14-0341	200	- NS - ECM
CD45	Leukocytes	BD	553076	200	+ HS
CD54	Endothelial cells, T & B cells, macrophages	Biologend	116114	50	- S
CD68	Macrophages	Biologend	137002	400	+ HS
CD86	Antigen presenting cells, T & B cells	Biologend	105002	50	- TBO
CD105	Endothelial cells, monocytes	Biologend	120414	200	- S
CD206	Macrophages, dendritic cells	NA	NA	100	- HS
VEGFR-2	Hemangioblasts, HSCs	Novus	NB100-686	50	+ HS
Ki-67	Proliferation	Acris	AM11168PU-T	100	+ HS
Sca-1	HSCs, peripheral B lymphocytes	Biologend	108114	200	- S
c-kit	HSCs, cardiac stem/progenitor cells	Santa Cruz	sc-5535	50	- NP
		R&D Systems	AF1536	200	- TBO
Nkx2.5	Cardiomyocytes, cardiac progenitor cells	Santa Cruz	sc-8697	50	+CM HS
Myoglobin	Cardiomyocytes	Santa Cruz	sc-25607	500	+CM HS
Cardiac TnT	Cardiomyocytes	Abcam	ab45932	400	+CM HS

**Table 4.1. Primary antibodies used to identify GFP-positive cells 9 days post-MI after treatment with AAV6 packaged with pAPiCre or AAV9 packaged with pAPiCre-miR122.** Cell abbreviations: BMDCs, bone marrow-derived cells; HSCs, hematopoietic stem cells. Signal abbreviations: +, colocalizes to GFP<sup>+</sup> cells; -, does not colocalize to GFP<sup>+</sup> cells; +CM, colocalizes to GFP<sup>+</sup> cardiomyocytes; HS, highly specific; S, specific; NSI, non-specific infarct zone staining; NS - ECM, non-specific staining of extracellular matrix, including the infarct zone; TBO, to be optimized; NP, no signal present.

accessories (Nikon Instruments Inc., Melville, NY). Digital confocal images of GFP-positive cells in the infarct and border zones were acquired using a  $\times 20/0.75$  NA oil-immersion objective (Nikon Instruments Inc.) or a  $\times 60/1.45$  NA oil-immersion objective (Nikon Instruments Inc.), and Nikon EZ-C1 software (Nikon Instruments, Inc.).

**Statistical Analysis:** Data are expressed as mean  $\pm$  SEM where appropriate.

Nonparametric Kruskal-Wallis analysis was used to assess significance.  $P < 0.05$  was considered significant in all comparisons.

## Results

**Periostin Provides GFP Expression After Transfection into 293 Cells:** The ability of the modified periostin promoter to provide gene expression was analyzed in vitro by transfecting AAV-293 cells via the calcium phosphate method with either pAPGFP or a plasmid expressing GFP from the CMV promoter. Figure 4.3 shows cells transfected with 1  $\mu\text{g}$  of plasmid. Cells were monitored until day 3 by fluorescence microscopy to confirm GFP expression. Plate reader-measured fluorescence showed 14.8-fold greater fluorescence with the CMV promoter when cells were transfected with 0.5  $\mu\text{g}$  of plasmid but only 5.5-fold greater fluorescence when cells were transfected with 1  $\mu\text{g}$  of plasmid (Fig. 4.3C).

**AAV Packaged with pAPiCre Provides Robust Cardiac Expression in Mice After MI but not in Absence of MI:** After confirming in vitro periostin-driven GFP expression, pAPiCre was cross-packaged into AAV6 for in vivo testing. Two 4 week old Flox-GFP mice were injected via the tail vein with either  $2.6 \times 10^{10}$  or  $1 \times 10^{11}$  viral

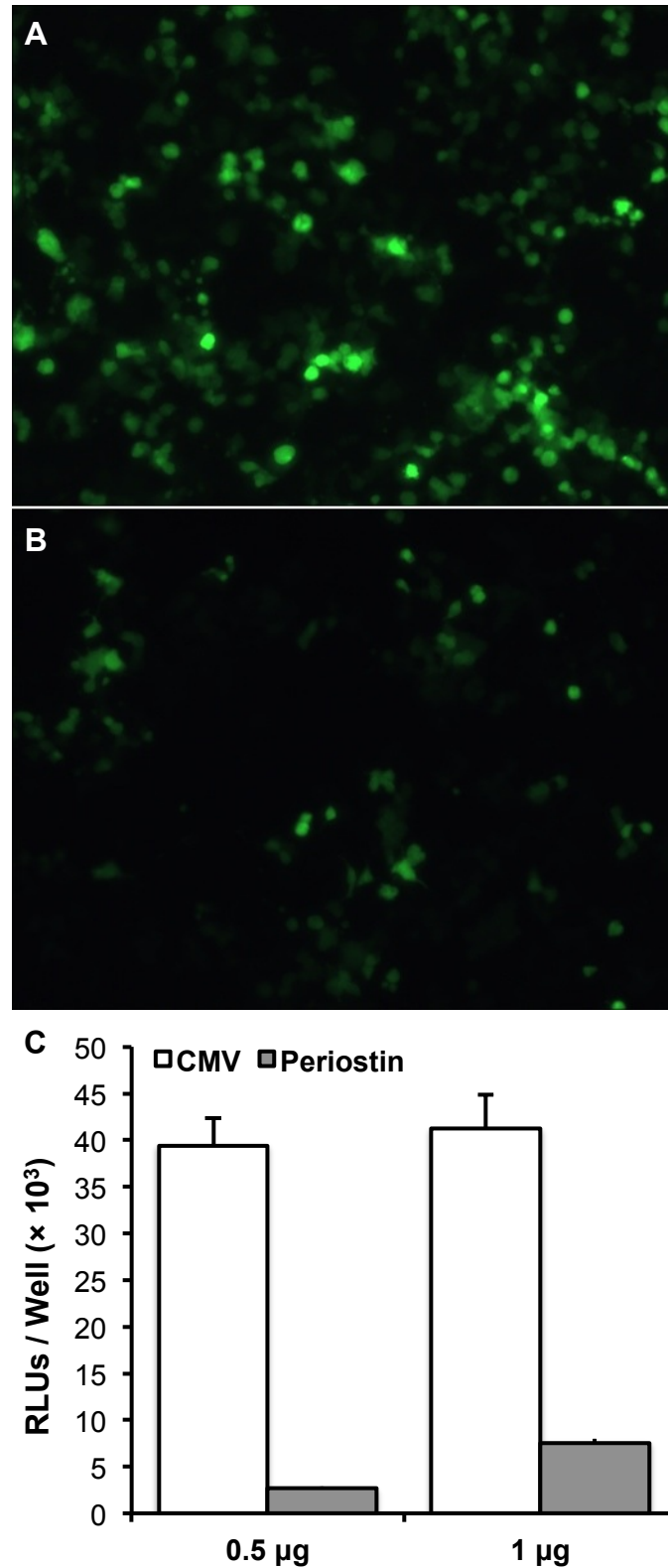


**Figure 4.3. In vitro expression of GFP from the periostin promoter.** The ability of the modified periostin promoter to provide expression was analyzed in vitro by transfecting AAV-293 cells via the calcium phosphate method with a plasmid expressing (A) GFP from the CMV promoter or (B) pAPGFP. Cells were monitored until day 3 by fluorescence microscopy to confirm GFP expression. (C) Plate reader-measured fluorescence showed 14.8-fold greater fluorescence with the CMV promoter when cells were transfected with 0.5  $\mu$ g of plasmid but only 5.5-fold greater fluorescence when cells were transfected with 1  $\mu$ g of plasmid, as in (A) and (B).

genomes. A control mouse received no injection. Successful expression of Cre recombinase was expected to result in GFP-positive cells. Mice were euthanized 4 weeks after injection and no GFP expression was seen in the untreated control mouse or the mouse that received the low dose of AAV. For the mouse that received the higher dose, very few GFP-positive cells were visible by fluorescence microscopy. Figure 4.4A shows only one GFP-positive cell in the field of view – typical 6 micron sections contained no more than one or two GFP-positive cells.

To test whether periostin would provide higher expression in cardiac cells activated through injury, as described previously,<sup>24,80,85</sup> we employed AAV6 packaged with pAPiCre in the setting of reperfused MI. Three 8 week old male Flox-GFP mice were subjected to 60 minutes of coronary occlusion followed by reperfusion. Two days after MI, allowing for full activation of the cardiac wound healing response,<sup>86,87</sup>  $1 \times 10^{11}$  vg of AAV6 were injected into the tail vein of each mouse. One week later, mice were euthanized and hearts were collected for analysis by fluorescence microscopy. In contrast to the previous results in non-infarcted mice, we observed many GFP-positive cells, both in the infarct and border zones of the heart (Fig. 4.4B). Interestingly, we witnessed rare GFP-positive cardiomyocytes confined strictly to the infarct borderzone. These cells contained striations characteristic of cardiomyocytes and express cardiomyocyte markers myoglobin and cTnT (Figure 4.15E and F, respectively). Though periostin expression would have been required to activate GFP expression in these cardiomyocytes, it is unknown if they belong to a small population of cardiomyocytes that experience an

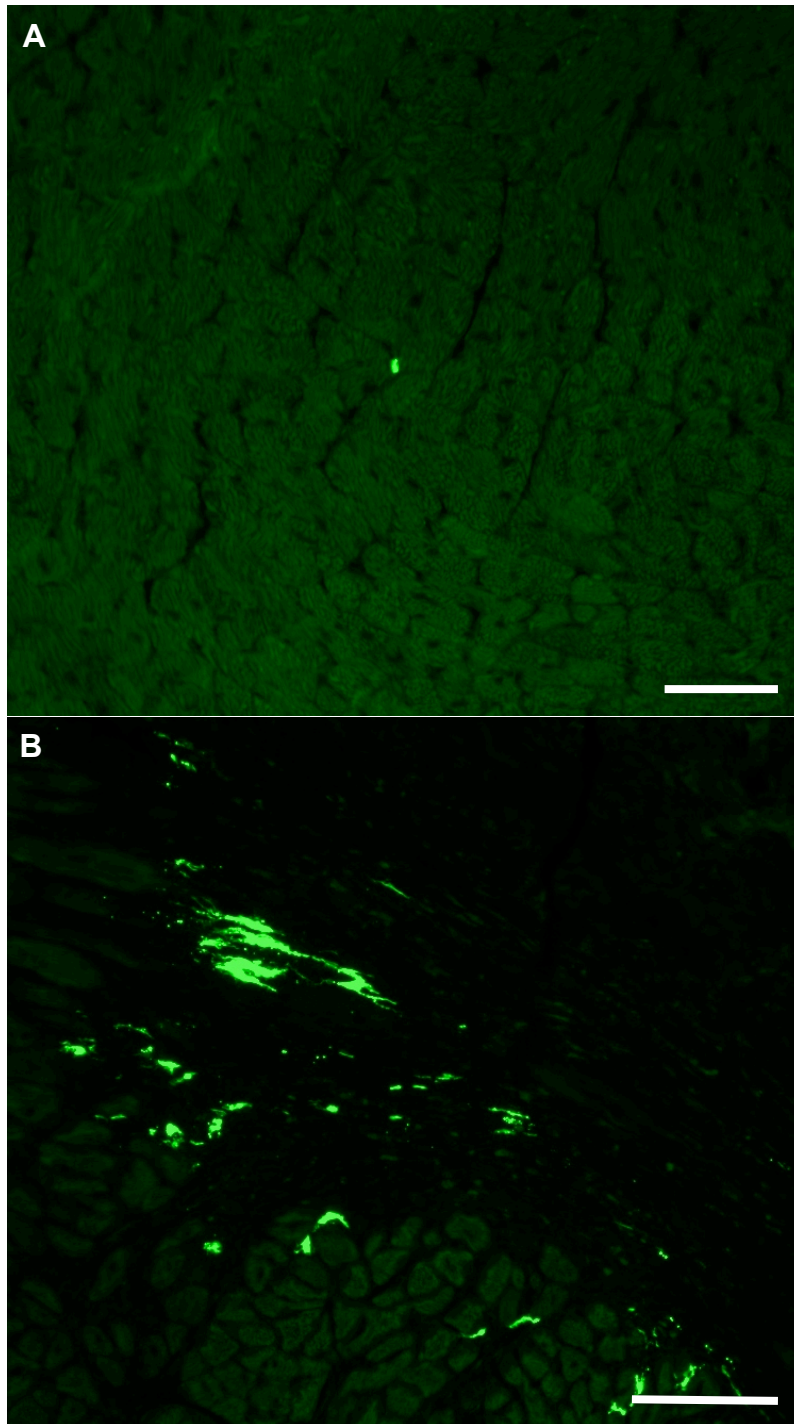


**Figure 4.4. Expression in Flox-GFP mice treated with AAV in the absence of myocardial infarction and after MI.** (A) Poor GFP expression in an otherwise untouched Flox-GFP mouse injected with AAV6-pAPiCre compared to (B) a mouse injected with the same AAV vector 2 days after reperfusion MI, which shows prevalent GFP expression in cells activated in the infarct and border zones as a result of ischemic injury. Scale bars = 50 microns.

upregulation in periostin expression at some point after MI or whether they differentiated from cells that previously expressed periostin.

### **AAV1 and -6 Injected 3 Days Post-MI Do Not Activate Detectable Cardiac**

**Luciferase Expression:** Previous reports of in vitro studies have indicated that AAV1 and AAV6 are both more effective at targeting fibroblasts (the cells we initially set out to target) than AAV9.<sup>22,23</sup> Therefore, we decided to compare AAV1 and -6 Cre-mediated activation of luciferase expression in Flox-Luc mice. 13-19 week old mice were treated with  $1 \times 10^{11}$  vg AAV1 (n=2) or -6 (n=3) packaged with pAPiCre via tail vein injection 3 days after reperfused MI. Mice were subject to bioluminescence imaging at days 5, 9, 10 and 14 post-MI but no bioluminescence was detected in the thoracic cavity, though liver expression increased throughout the duration of the study (Fig. 4.5A). Hearts were removed 15 days post-MI for luciferase activity measurement, but no luciferase activity was detectable.

### **AAV9 Packaged with pAPiCre-miR122 Activates Robust Cardiac Luciferase Expression Post-MI and Eliminates Liver Luciferase Expression in Flox-Luc**

**Mice:** Since we had difficulty producing large titers of AAV1, we decided to test AAV9 with the periostin promoter driving Cre, despite evidence that it would provide lower expression in fibroblasts than AAV1 or -6.<sup>22</sup> Additionally, to reduce liver signal and increase accuracy of bioluminescence quantification, we introduced target sites for miRNA122 into the 3' untranslated region of pAPiCre, as described above. Four 11 week old male Flox-Luc mice were injected with  $1 \times 10^{11}$  or  $3 \times 10^{11}$  viral genomes of AAV9 packaged with pAPiCre-miR122 (n=2/group) 2 days after reperfused MI. Mice were imaged at day 9 post-MI and showed clear

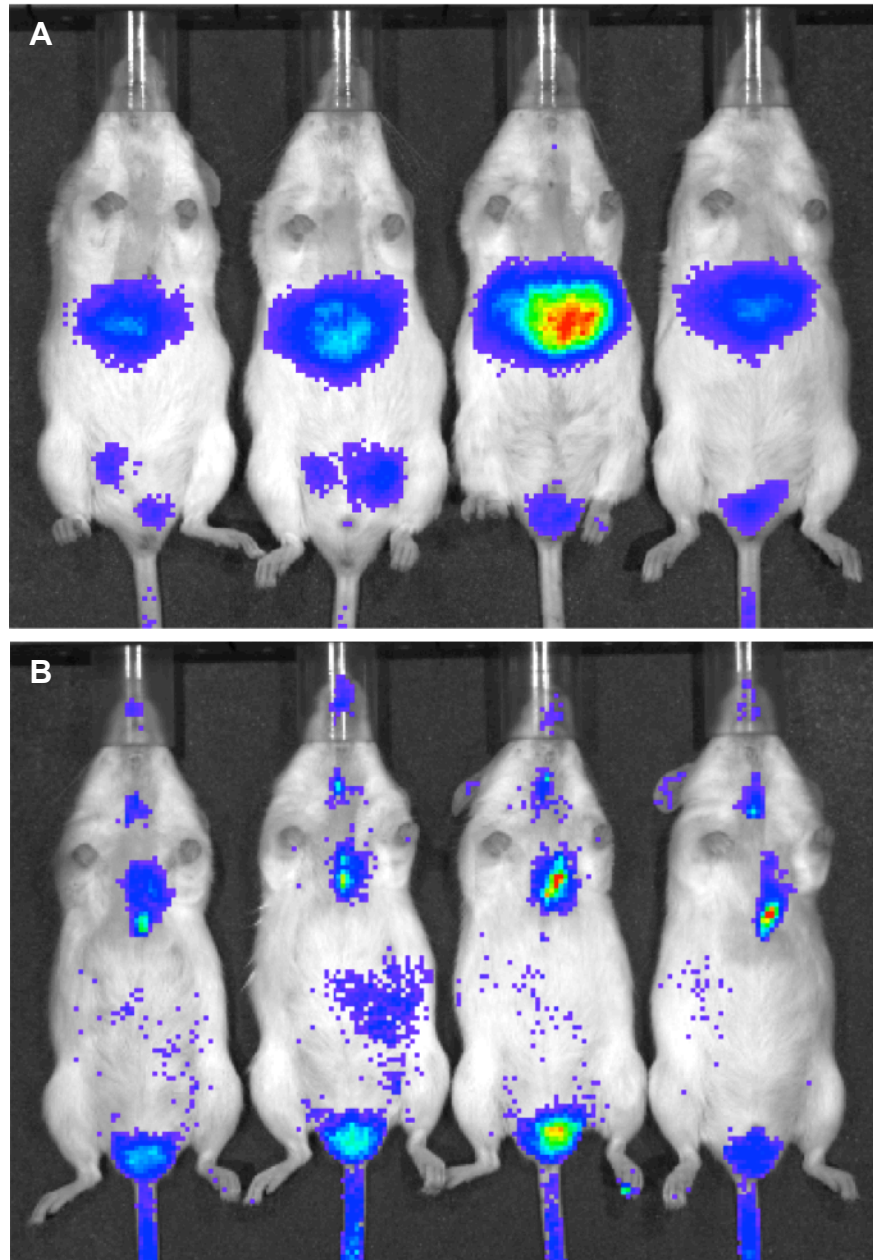


**Figure 4.5. Flox-Luc mice treated with AAV1 and AAV6 packaged with pAPiCre and AAV9 packaged with pAPiCre-miR122.** (A) Mice were treated with  $1 \times 10^{11}$  vg AAV1 or -6 packaged with pAPiCre via tail vein injection 3 days after reperfusion MI and subject to bioluminescence imaging at days 5, 9, 10 and 14 post-MI. No bioluminescence was detected in the thoracic cavity, though liver expression increased throughout the study. Hearts were removed 15 days post-MI for luciferase activity measurement, but no luciferase activity was detectable. The figure shows a bioluminescence image of mice from day 14 post-MI. The left-most mouse was injected with AAV1, the other three received AAV6. (B) Mice treated with  $1 \times 10^{11}$  vg (2 left) or  $3 \times 10^{11}$  vg (2 right) AAV9 packaged with pAPiCre-miR122 two days post-MI demonstrate cardiac but not liver bioluminescence. Mice were imaged 9 days post-MI (7 days post-injection).

bioluminescence signal from the thoracic cavity. In addition, while other bioluminescence signal was present, notably from a small incision site on the neck, liver expression was eliminated by the miR122 target sites. Mice were euthanized 10 days post-MI and their hearts were saved for luciferase activity processing in tandem with mice described below. The pAPiCre-miR122 vector was utilized for all future experiments.

#### **AAV9 Provides Greater Expression than AAV6 When Injected 2 Days Post-MI:**

Two days after reperfusion MI, Flox-Luc mice were injected with  $1 \times 10^{11}$  vg AAV6 (n=3) or AAV9 (n=2) packaged with pAPiCre-miR122. Mice were imaged on days 5, 7, 9 and 11 post-MI, and hearts were collected after the last imaging time point on day 11. Figure 4.6A shows bioluminescence imaging with luciferase expression only slightly above background for AAV6-treated mice while mice treated with AAV9 consistently showed a higher signal. Quantification of bioluminescence demonstrated that AAV9 had a significantly higher signal as determined by Kruskal-Wallis analysis on day 9 post-MI, at which point the two AAV9 mice that received  $1 \times 10^{11}$  vg from the previous experiment were included, compared to all other time points at which only two AAV9 mice were imaged. On day 9, AAV9 mice demonstrated a 4.3-fold increase in bioluminescence signal compared to AAV6 mice, and this difference was similar throughout the duration of the experiment (Fig. 4.6B). After tissue harvest, hearts were processed for luciferase protein. Mice from the previous experiment with AAV9 were included for the luciferase activity assay so that final numbers of animals were n=3 for  $1 \times 10^{11}$  vg of AAV6, n=4 for  $1 \times 10^{11}$  vg of AAV9 and n=2 for  $3 \times 10^{11}$  vg of AAV9. In vitro luciferase activity was higher for



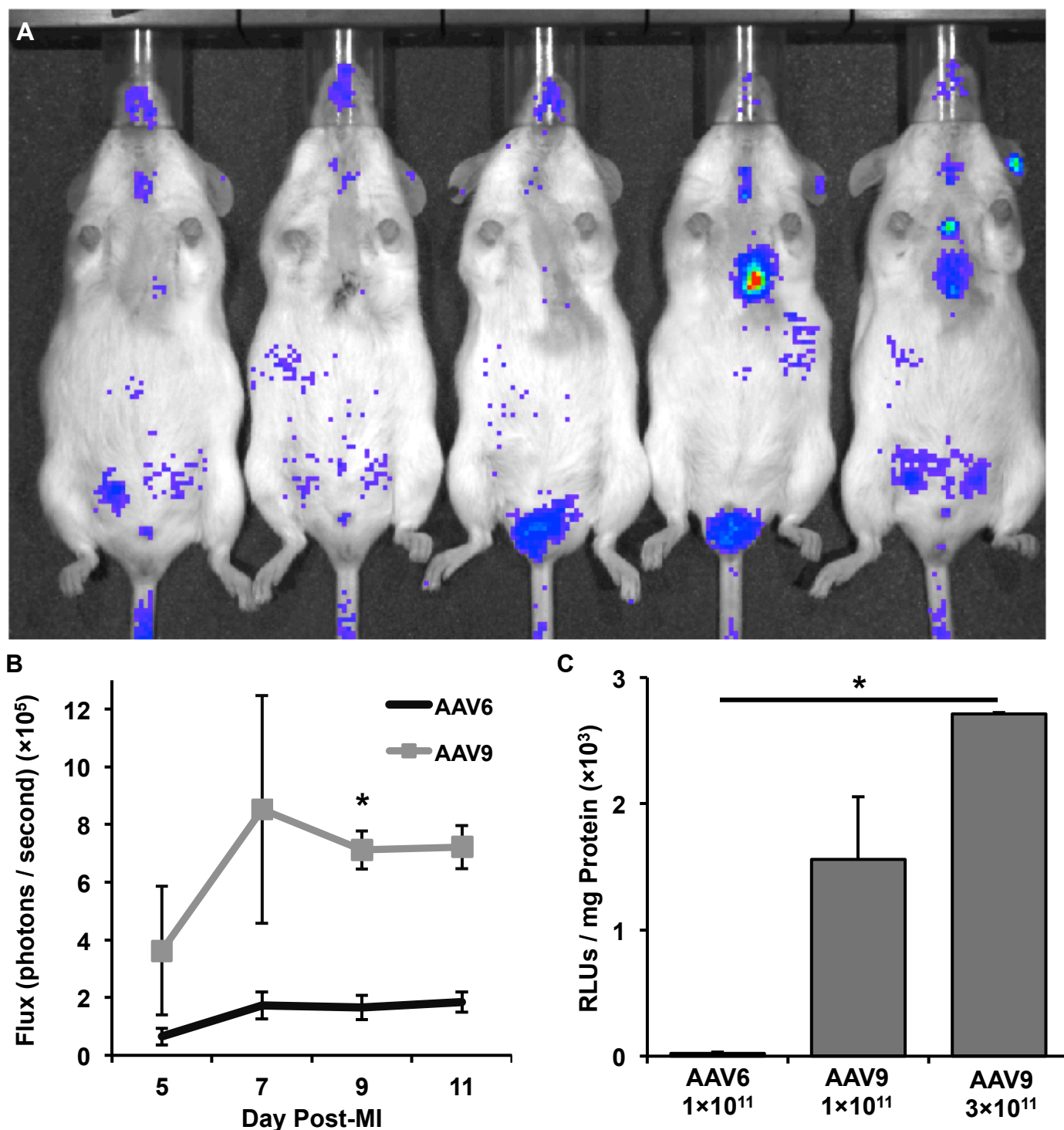


**Figure 4.6. AAV9 packaged with pAPiCre-miR122 provides greater expression than AAV6 when injected two days post-MI.** Two days after reperfusion MI, Flox-Luc mice were injected with  $1 \times 10^{11}$  vg AAV6 or -9 packaged with pAPiCre-miR122. Mice were imaged on days 5, 7, 9 and 11 post-MI, and hearts were collected after the last imaging time point on day 11. (A) Bioluminescence imaging revealed expression only slightly above background for AAV6-treated mice (3 mice on left), while mice treated with AAV9 constantly showed a higher signal (two mice on right). (B) Quantification of bioluminescence demonstrated that AAV9 had a significantly higher signal as determined by Kruskal-Wallis analysis on day 9, at which point  $n=3$  AAV6 and  $n=4$  AAV9 mice were imaged, compared to all other time points at which  $n=3$  AAV6 and  $n=2$  AAV9 mice were imaged. (C) Hearts were processed for luciferase protein and in vitro luciferase activity demonstrated higher signal for AAV9-treated mice, in accordance with bioluminescence imaging results. AAV6 signal was barely detectable above background, while luciferase activity was easily detectable in AAV9-treated mice. Two additional mice were injected with  $3 \times 10^{11}$  vg AAV9, which showed significantly higher signal than AAV6 mice, as determined by Kruskal-Wallis analysis.

AAV9-treated mice, in accordance with bioluminescence imaging results. Luciferase signal from AAV6-treated hearts was barely detectable above background, while luciferase activity was easily detectable in AAV9-treated mice (Fig. 4.6C). Mice treated with the high dose of AAV9 showed significantly higher signal than AAV6 mice, as determined by Kruskal-Wallis analysis.

AAV6 and -9 were also compared after injection of Flox-GFP mice 2 days post-MI. Figure 4.7 shows fluorescence micrograph mosaics of cardiac sections from mice injected with AAV6 packaged with pAPiCre or AAV9 packaged with pAPiCre-miR122. GFP-positive cells can be seen clearly in the infarct and border zones of each section. While the relative number of cells has not been quantified, the AAV9 treated mouse visibly has several times the number of GFP-positive cells compared to the AAV6 mouse, consistent with bioluminescence and luciferase activity results from Flox-Luc mice. Figure 4.8 shows 20× confocal z-stacks from a GFP-Flox mouse treated with AAV9, giving a clearer demonstration of the morphology of the GFP-positive cells.

**Delivery of AAV9 Two Days After Reperfused MI Provides Higher Luciferase Expression than AAV Delivery at Reperfusion:** Flox-Luc mice were injected at reperfusion (n=2), or at day 1 (n=1) or day 2 (n=3) after reperfused MI with  $1.5 \times 10^{11}$  vg AAV9 packaged with pAPiCre-miR122 and imaged at days 7 and 9 post-MI. Bioluminescence imaging from day 9 post-MI (Fig. 4.9A) demonstrated that mice injected at day 2 and day 1 post-MI had comparable expression, while mice injected at reperfusion had approximately 2-fold lower bioluminescence signal (Fig. 4.9B,  $p=0.083$  by Kruskal-Wallis analysis).

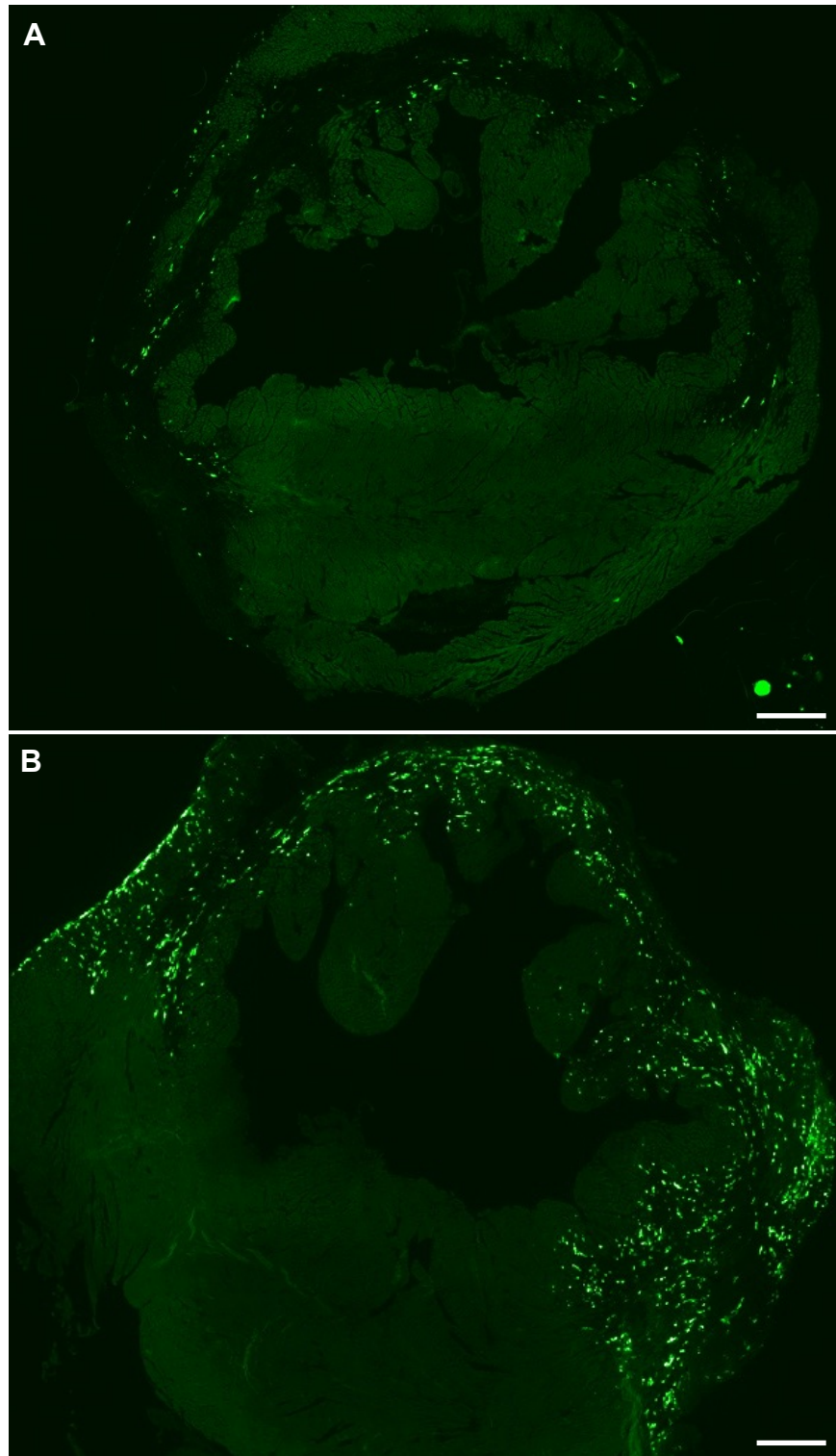


**Figure 4.7. Flox-GFP mice contain more GFP-positive cells after treatment with AAV9 than with AAV6.** Mice were injected 2 days post-MI with  $1 \times 10^{11}$  vg (A) AAV6 or (B) AAV9 packaged with pAPiCre or pAPiCre-miR122. Hearts were removed 9 days after MI, fixed, frozen, sectioned, and imaged by fluorescence microscopy. Both hearts contain GFP-positive cells restricted almost exclusively to the infarct and border zones of the heart, but AAV9 provides much more GFP expression than AAV6. Scale bars = 0.5 mm.

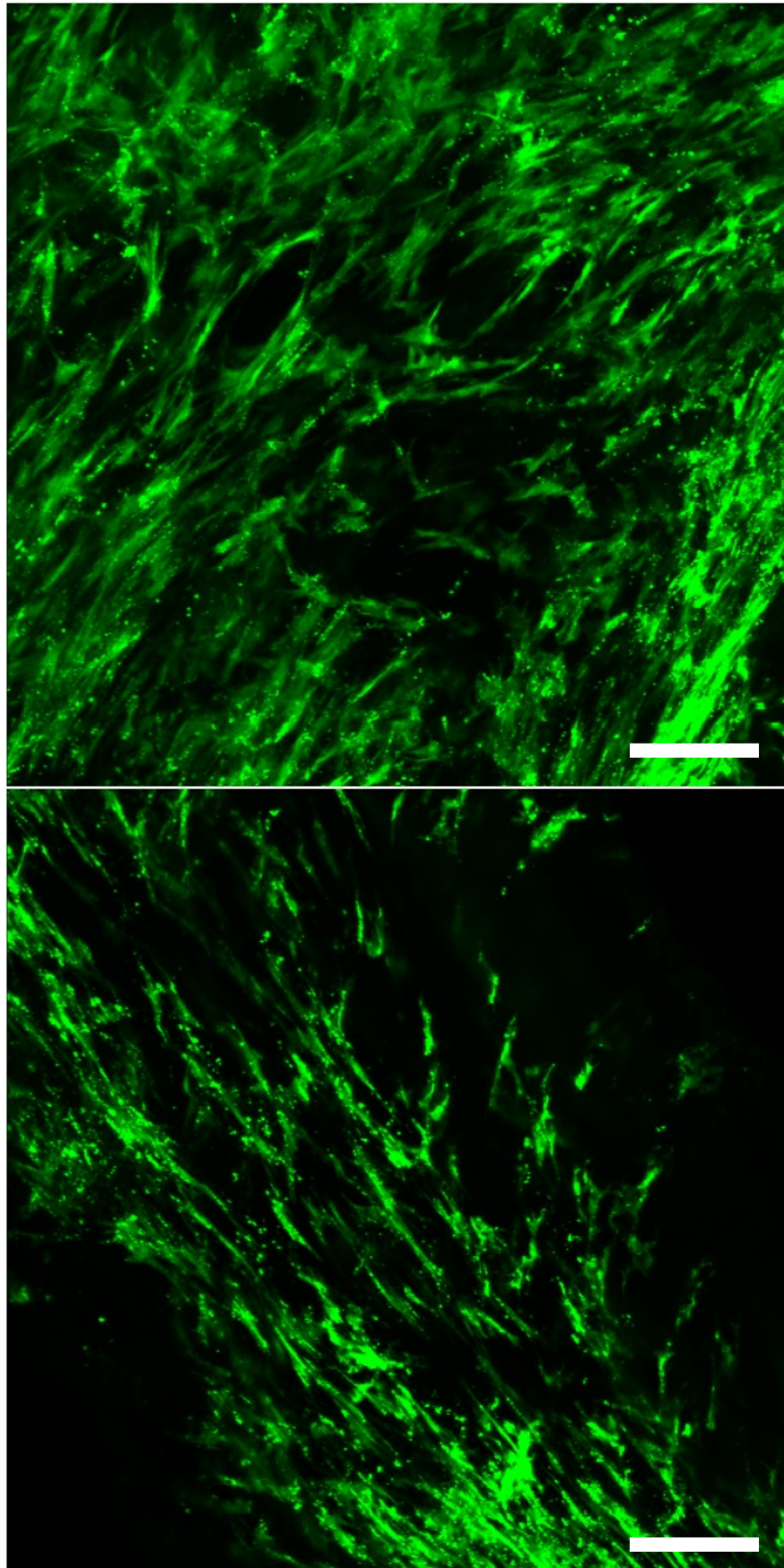


**Figure 4.8. Confocal z-stacks of GFP-positive cells from mice treated with AAV9.** At the time of tissue harvest, Flox-GFP hearts from mice treated with AAV9 packaged with pAPiCre-miR122 were sliced into three pieces, including a 1 mm short axis segment from the infarct zone which was whole mounted for confocal microscopy. These 20× z-stacks show GFP-positive cells in the infarct/border zone. Scale bars = 100 microns.



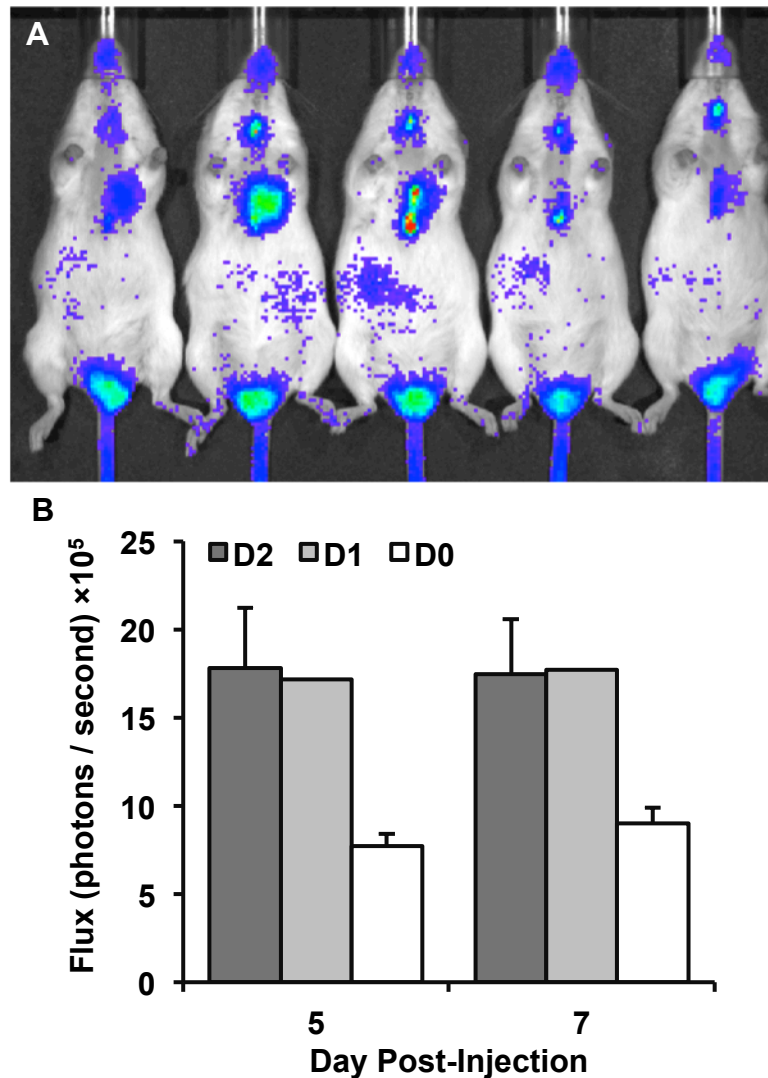
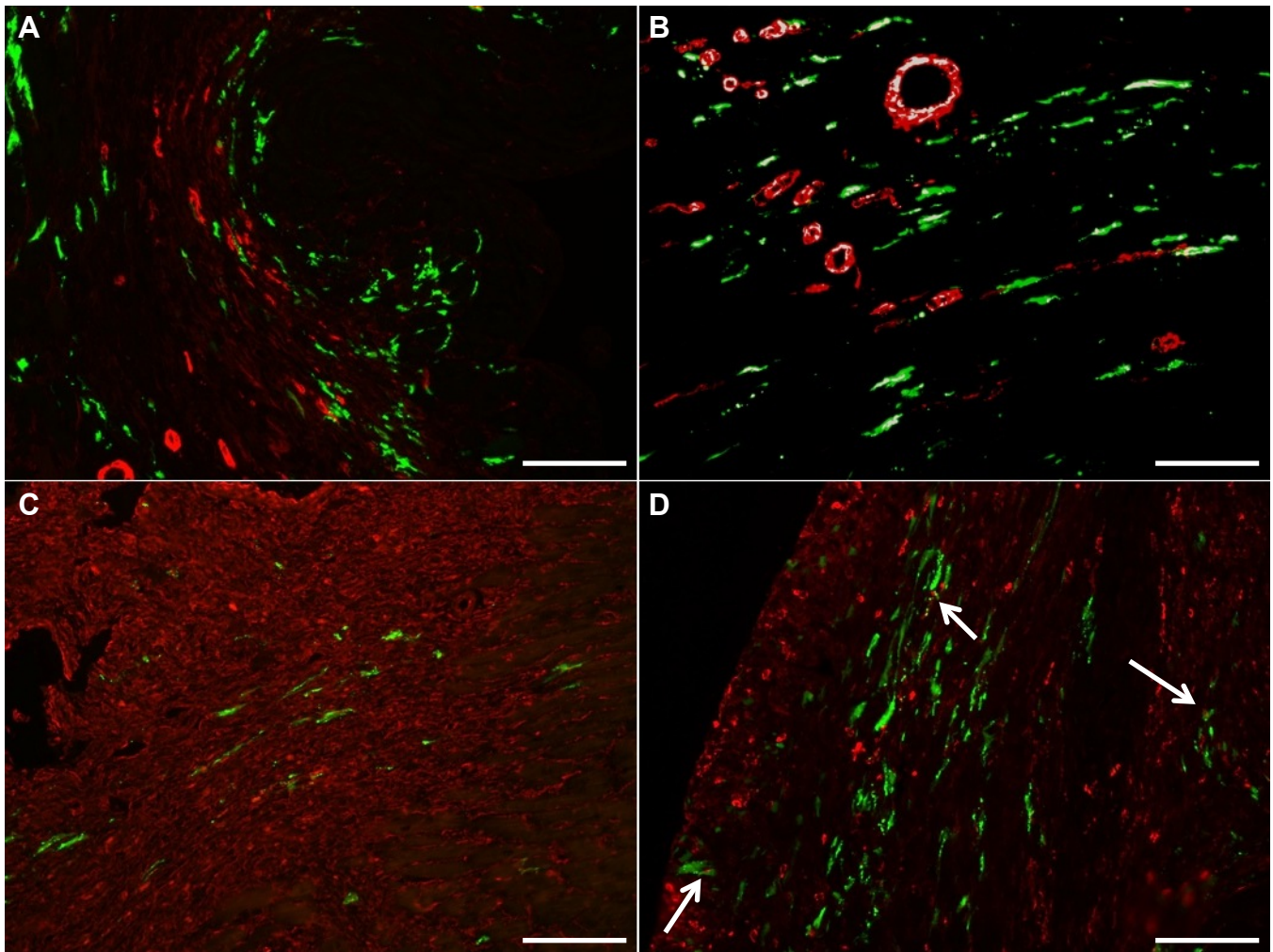


**Figure 4.9. Mice treated with AAV9 two days after reperfusion MI show higher luciferase expression than mice that receive AAV at reperfusion.** Flox-Luc mice were injected at reperfusion (n=2) or at day 1 (n=1) or day 2 (n=3) after reperfusion MI with  $1.5 \times 10^{11}$  vg AAV9 packaged with pAPiCre-miR122 and imaged at day 7 and 9 post-MI. (A) Bioluminescence image from day 9 post-MI showing mice injected at day 2 post-MI (three on left) and at reperfusion (2 on right). An additional mouse injected with AAV9 at day 1 post-MI is not shown. (B) Quantification of bioluminescence intensity shows that mice injected at 2 days post-MI (D2) have approximately 2-fold greater expression than mice injected at reperfusion (D0;  $p=0.083$  by Kruskal-Wallis analysis).

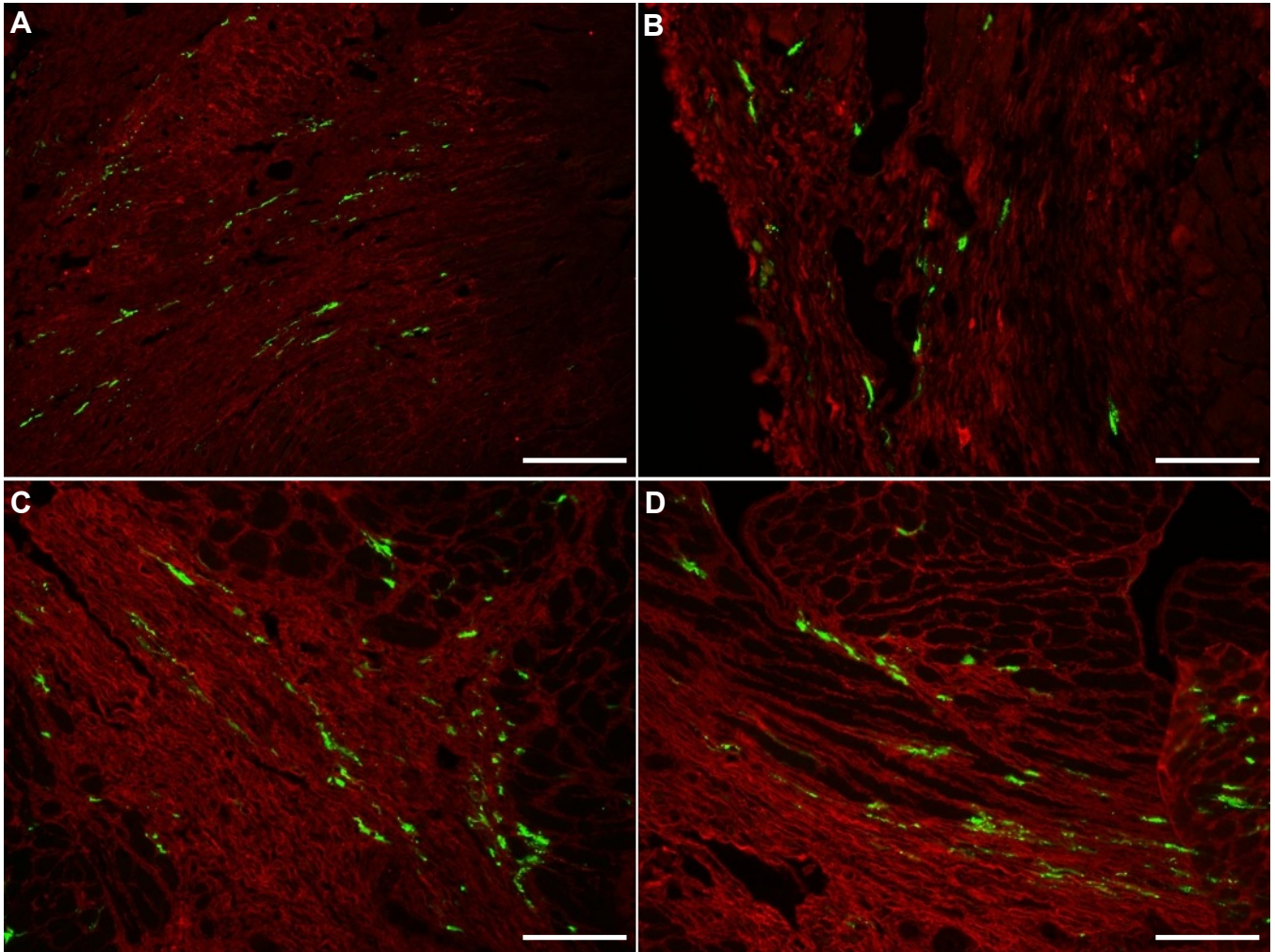
## **GFP-Positive Cells Lack Characteristic Fibroblast Markers but Express**

**Markers for Hematopoietic Stem Cells:** Cardiac sections from Flox-GFP mice treated with AAV6 and AAV9 were analyzed with 27 primary antibodies (Table 4.1). Markers that are typically expressed on cardiac fibroblasts and myofibroblasts include  $\alpha$ -smooth muscle actin, vimentin and discoidin domain receptor 2 (DDR2). These antibodies, along with smooth muscle myosin heavy chain (SM-MHC), are shown in Figure 4.10. While DDR2 colocalizes with GFP to a small degree,  $\alpha$ -smooth muscle actin and SM-MHC do not appear to colocalize with GFP-positive cells. Results with vimentin have proven inconclusive since the majority of GFP-positive cells are located in the infarct and border zones and the vimentin antibodies employed stain these regions with a high degree of non-specificity. Other antibodies shown in Figure 4.11 include periostin, fibroblast-specific protein 1 and collagens I and III. Staining with periostin would be especially valuable to ascertain whether the GFP-positive cells still express periostin at day 9 post-MI, but these antibodies have all proven inconclusive due to a high degree of non-specific staining in the infarcted regions (though this was not unexpected with the collagen antibodies due to the high level of collagen deposition in the infarct zone).

A variety of other antibodies were tested to look for signs that GFP-positive cells expressed markers for endothelial, inflammatory, progenitor or stem cells. Figure 4.12 shows immunofluorescence for CD34, CD45 and CD68. Two clones of CD34, a marker for endothelial and bone marrow-derived cells, showed non-specific staining of the extracellular matrix in the infarct and border zones in between

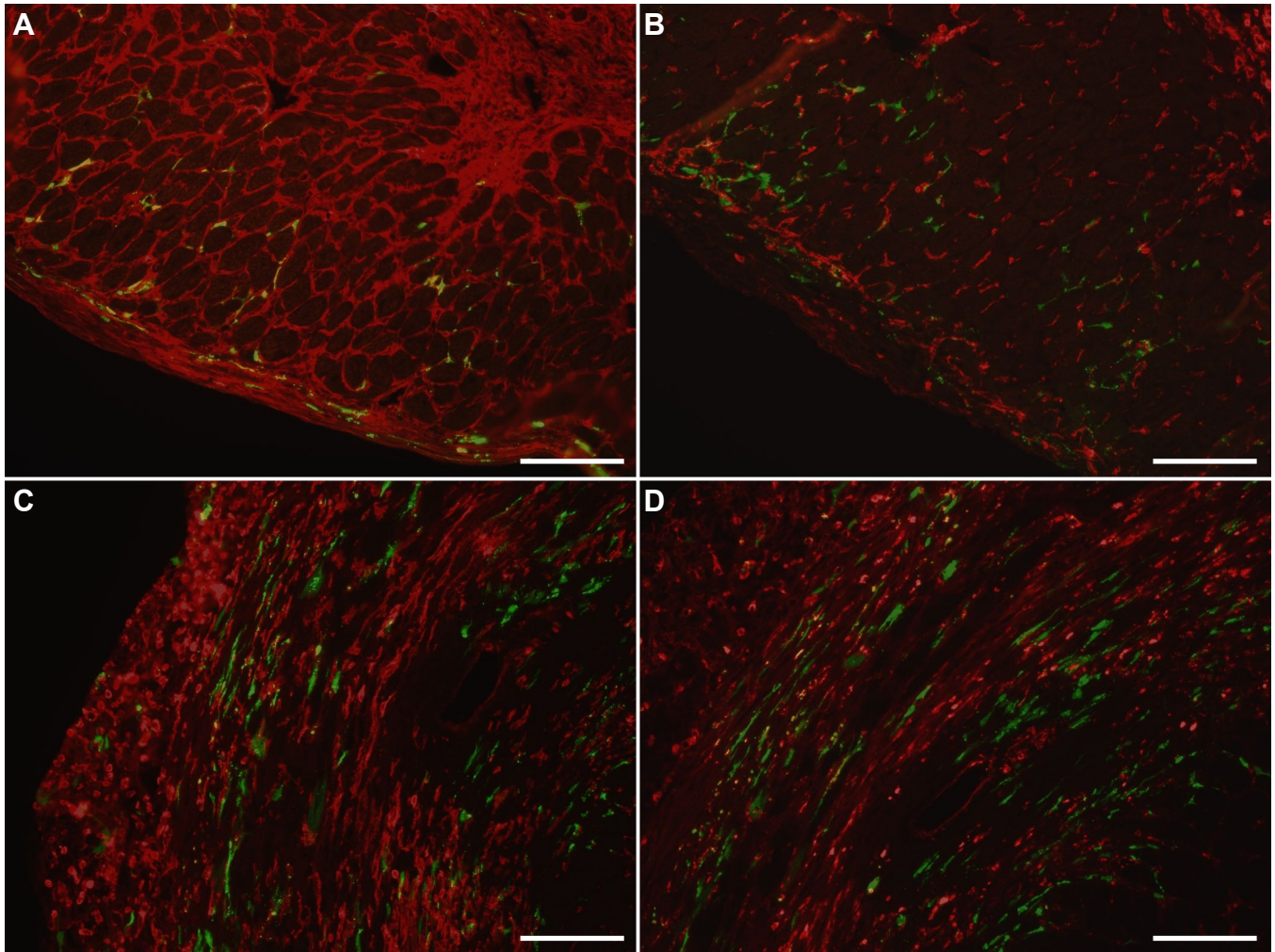


**Figure 4.10. Flox-GFP cardiac sections treated with antibodies targeting smooth muscle and fibroblasts.** 20× fluorescence micrographs showing GFP-positive cells in green and (A)  $\alpha$ -smooth muscle actin, (B) smooth muscle myosin heavy chain, (C) vimentin and (D) DDR2 in red. Some colocalization was seen with DDR2 (arrows) but no colocalization with GFP was witnessed with the other antibodies. Scale bars = 100  $\mu$ m.



**Figure 4.11. Flox-GFP cardiac sections treated with antibodies targeting fibroblasts and collagen.** 20× fluorescence micrographs showing GFP-positive cells in green and (A) periostin, (B) FSP1, (C) collagen 1, and (D) collagen III in red. Little to no colocalization with GFP was witnessed with these antibodies. Scale bars = 100  $\mu\text{m}$ .

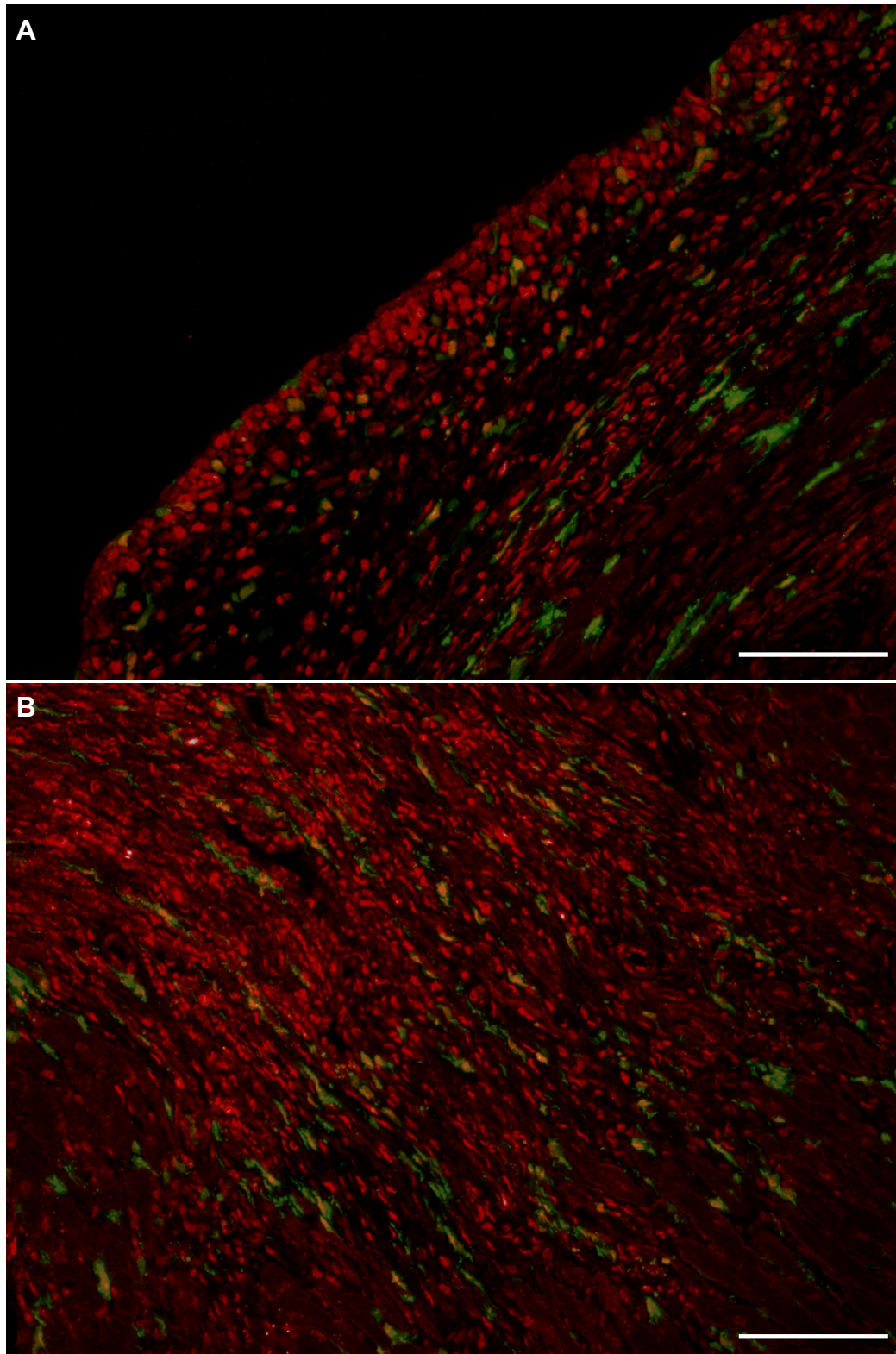




**Figure 4.12. Flox-GFP cardiac sections treated antibodies targeting with CD34, CD45 and CD68.** 20× fluorescence micrographs showing GFP-positive cells in green and, in red, (A) CD34 in the epicardial borderzone, (B) CD45 in the epicardial borderzone, (C) CD45 in the infarct and (D) CD68 in the infarct. CD34 appeared to bind largely to extracellular matrix. CD45 and CD68 both showed colocalization with GFP in the infarct and border zones. Scale bars = 100 μm.

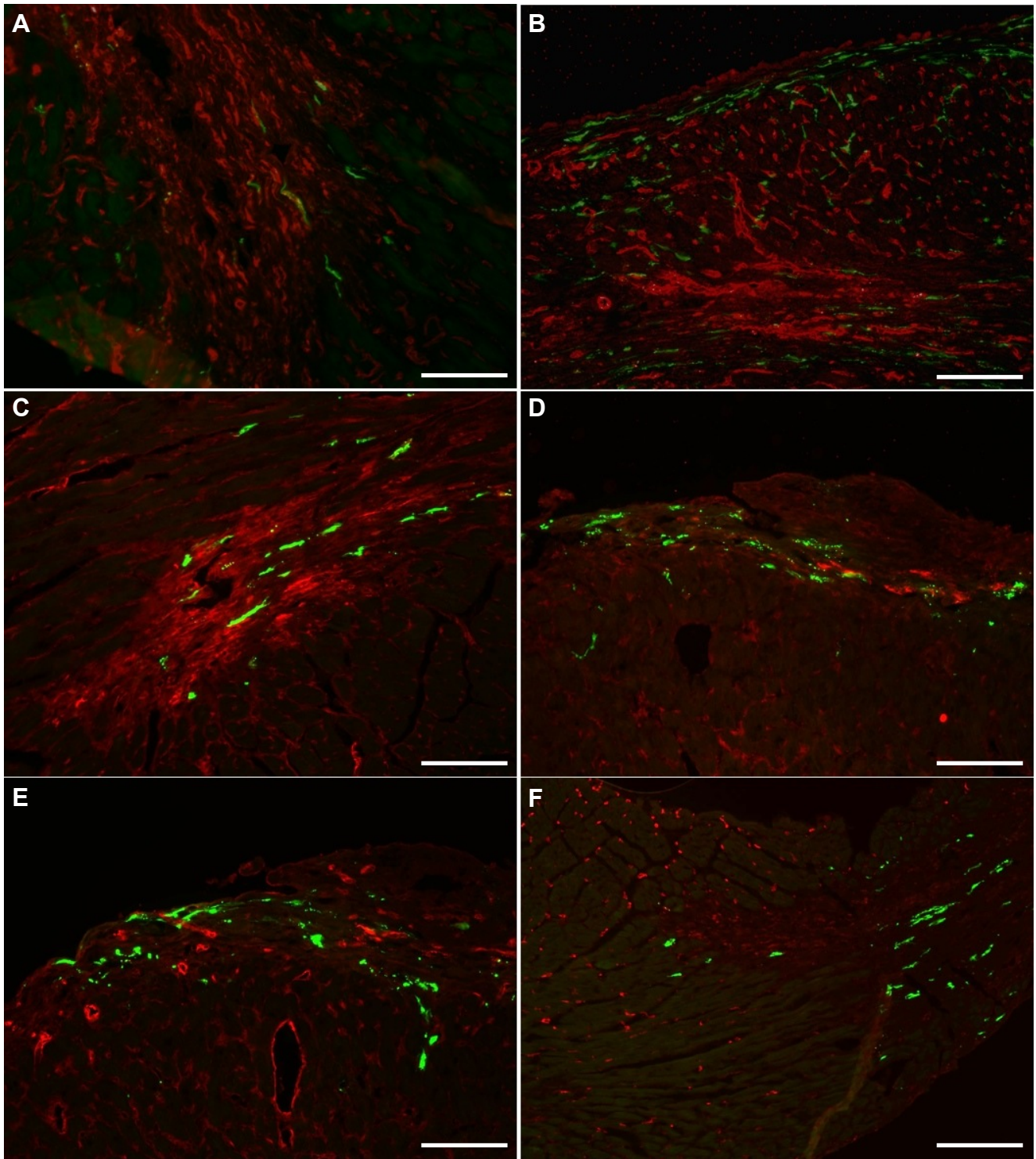
cardiomyocytes (Fig. 4.12A). However, the leukocyte common antigen CD45 colocalized to a population of GFP-positive cells in the infarct and border zones (Fig. 4.12B&C). A subset of GFP<sup>+</sup> cells were also positive for the macrophage marker CD68 (Fig. 4.12D), though we were not able to co-stain with these two antibodies since they were from the same host. Additional signs of hematopoietic lineage was indicated with the colocalization of vascular endothelial growth factor receptor 2 (VEGFR-2), which a majority of GFP<sup>+</sup> cells expressed (Fig. 4.13) in the infarct and border zones of the heart.

Figure 4.14 shows immunofluorescence for additional endothelial and inflammatory cell markers. Little to no colocalization with GFP was seen with Isolectin IB<sub>4</sub>, CD31, CD54, CD86, CD105 or CD206. To look for signs of cardiac stem or progenitor cells, we also performed immunofluorescence with Ki-67, Sca-1 and Nkx2.5. Myoglobin and cTnT were used to confirm that GFP-positive cardiomyocyte-like cells expressed cardiomyocyte markers. Ki-67 expression confirmed the presence of a small population of proliferating GFP<sup>+</sup> cells in the infarct and border zones (Fig 4.15A&B), though Sca-1 and Nkx2.5 showed no overlap with GFP<sup>+</sup> cells (Fig. 4.14C&D, respectively). Myoglobin and cTnT expression confirmed the presence of some GFP<sup>+</sup> cardiomyocytes in the borderzone (Fig. 4.15E&F).



**Figure 4.13. Flox-GFP cardiac sections treated with an antibody targeting VEGF receptor 2.** 20× fluorescence micrographs showing GFP-positive cells in green and VEGFR-2 in red. Significant overlap was seen between GFP and VEGFR-2 in all areas of the heart including (A) the epicardial borderzone and (B) the infarct. Scale bars = 100  $\mu$ m.





**Figure 4.14. Flox-GFP cardiac sections treated with antibodies targeting endothelial, inflammatory and progenitor cells.** 20× fluorescence micrographs showing GFP-positive cells in green and (A) Isolectin IB<sub>4</sub>, (B) CD31, (C) CD54, (D) CD86, (E) CD105 and (F) CD206 in red. Little to no colocalization with GFP was witnessed with these antibodies. Scale bars = 100 μm.

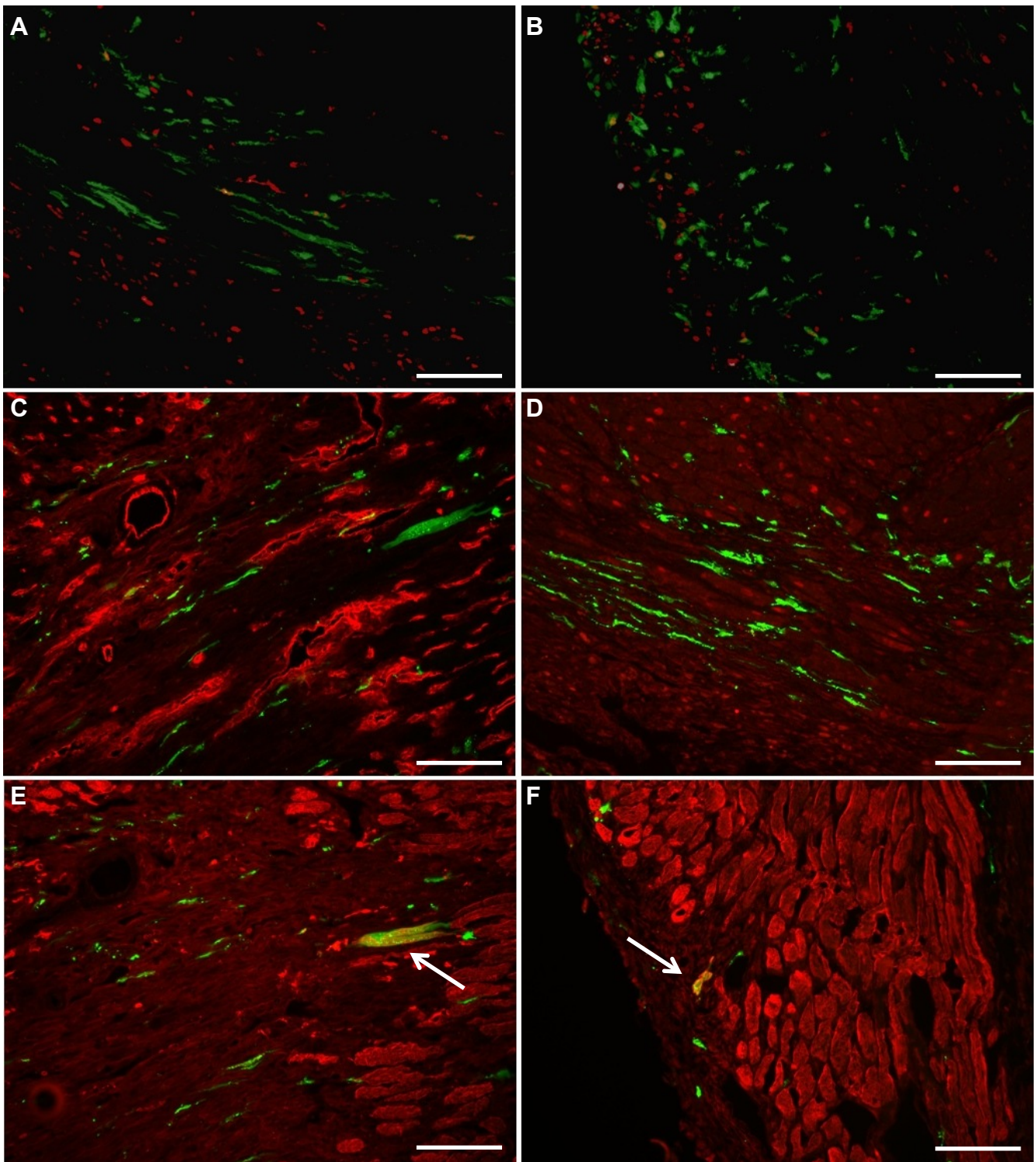


**Figure 4.15. Flox-GFP cardiac sections treated with markers of proliferation, cardiac stem cells and cardiomyocytes.** Fluorescence micrographs showing GFP-positive cells in green and, in red, (A) Ki-67 in the infarct zone, (B) Ki-67 in the epicardial borderzone, (C) Sca-1, (D) Nkx2.5, (E) myoglobin and (F) cTnT. Ki-67 staining shows occasional overlap with GFP-positive cells. No co-localization is visible between the majority of GFP-positive cells and the other antibodies, but GFP-positive cardiomyocytes are confirmed here with myoglobin and cTnT colocalization (arrows). Scale bars = 100 μm.

## Discussion

The ability to target fibroblasts in the remodeling heart with adeno-associated virus could open many new avenues into cardiac gene therapy, including the possibility of reprogramming fibroblasts into functional cardiomyocytes.<sup>88-92</sup> The modified periostin promoter used for these experiments was designed to restrict expression in the heart to fibroblasts using AAV1 or -6, which had been shown in other studies to be capable of transducing fibroblasts in vitro.<sup>22,23</sup> Figure 4.3 shows that our newly constructed periostin promoter functions in vitro, providing GFP expression in AAV-293 cells. It has further been proven to provide Cre-mediated recombination in vivo, activating reporter gene expression in cells present in the infarct and border zones after reperfused MI in Flox-GFP and Flox-Luc mice. However, while we anticipated that our vector would target cardiac fibroblasts, it appears instead to target hematopoietic stem cells, as indicated by co-expression of CD45, CD68 or VEGFR-2 on GFP-positive cells.

We have shown here that in the absence of MI, Flox-GFP mice express very low amounts of GFP in the heart when injected with AAV6 packaged with pAPiCre. In contrast, when the same mice receive viral delivery after reperfused MI, GFP-positive cells are found in abundance in the infarct and border zones. We initially assumed this indicated that we had targeted fibroblasts activated through cardiac injury, since other studies have shown that activated fibroblasts express periostin.<sup>24,80,85</sup> In addition, the number of GFP<sup>+</sup> cells increased when the same vector was packaged into AAV9 instead of AAV6. Similarly, AAV9 provided several times the expression of AAV6 when injected into Flox-Luc mice at an equivalent



dose, and higher expression is obtained in mice injected with AAV two days post-MI compared to mice injected at the time of reperfusion. These transgenic mouse strains were ideal for validating the periostin vector construct in vivo because even a short duration of Cre expression would lead to long-term reporter gene expression in a cell and the progeny of that cell. Additionally, at least in the case of Flox-GFP mice under control of the strong CAG promoter, the fluorescent protein is likely expressed at much higher levels than it would be with our construct directly expressing GFP from the periostin promoter. A difference in promoter strength between the Flox-GFP and Flox-Luc strains may explain why luciferase activity was difficult to detect in AAV1 and -6 injected mice, since the ROSA26 promoter used to drive luciferase in Flox-Luc mice is considerably less robust than the CAG promoter.<sup>93</sup> Future experiments with pAPGFP or a vector driving luciferase from the periostin promoter would be useful for determining the duration of periostin promoter activity after MI which could help to better assess the therapeutic viability of targeting expression with the periostin promoter.

Periostin is a predominantly extracellular protein found in a variety of cells, including epithelial cells, several types of cancer cells, and fibroblasts.<sup>80,94</sup> It has been shown to be involved in embryonic development of the heart and is critical to repair of cardiac injury, including ischemia and transverse aortic constriction.<sup>24,80,85,95</sup> Additionally, delivery of extracellular periostin has been found to promote cardiac wound healing by coaxing cardiomyocytes back into the cell cycle.<sup>96</sup> Expression of periostin has also been demonstrated in bone marrow-derived cells (BMDCs). In particular, co-expression of periostin with CD45 was

shown in a lineage tracing study of BMDC contribution to cardiac valve interstitium.<sup>97</sup> However, in the setting of myocardial infarction, such BMDC lineage tracing studies often link periostin expression to bone marrow-derived fibrocytes or fibroblasts.<sup>17,97-99</sup> Since fibrocytes express CD34 and CD45,<sup>100</sup> a subset of the GFP<sup>+</sup> cells we see here may indeed be fibrocytes; however, lack of substantial overlap between GFP<sup>+</sup> cells and mature myofibroblast markers such as  $\alpha$ -smooth muscle actin and DDR2 suggests otherwise. Instead, co-expression of CD45, also called the leukocyte common antigen, and CD68 with GFP indicates a leukocyte population derived from hematopoietic stem cells (HSCs). Furthermore, strong co-expression of GFP with VEGFR-2 indicates another subset of HSCs, possibly endothelial progenitors.

VEGFR-2 has previously been described as a marker to distinguish hematopoietic stem cells from hematopoietic progenitors.<sup>101</sup> Additionally, periostin and VEGFR-2 expression from recruited bone marrow-derived cells have been linked to tumor angiogenesis.<sup>102-104</sup> Shao et al. showed that overexpression of periostin leads to tumor growth through upregulation of VEGFR-2, and when the activity of VEGFR-2 was blocked tumor growth was reduced.<sup>102</sup> In the case of the remodeling heart, periostin and VEGFR-2 may be similarly linked, but as a normal part of the wound healing response to provide neovasculature. Indeed, bone marrow-derived endothelial progenitor cells have been demonstrated to mobilize in the blood after myocardial infarction and circulating CD34<sup>+</sup>/VEGFR-2<sup>+</sup> cells are associated with cardiovascular risk factors.<sup>105,106</sup> Furthermore, injection of CD34<sup>+</sup>



BMDCs showing high expression of c-kit, GATA-2 and VEGFR-2 have led to increased ventricular function after infarction through increased angiogenesis.<sup>107</sup>

The nature of endothelial progenitor cells is controversial, with their origins, plasticity and therapeutic potential a subject of ongoing research.<sup>108-110</sup> Since our data currently provides a snapshot of the heart 9 days after MI (7 days after injection of AAV), we do not know the long-term fate of the GFP<sup>+</sup> cells, including their potential for engraftment in the heart. However, any cells that are present in the infarct zone in such high numbers are ideal targets for gene therapy. Until now, the practicality of targeting any cells with AAV so quickly after myocardial infarction has been completely unrealized, with the exception of cardiomyocytes as described in the previous chapter. Furthermore, the GFP<sup>+</sup> cells described here are likely a population not previously targeted in vivo with AAV. Prior efforts to target hematopoietic stem cells have been accomplished in vitro, and stably transduced cells have then been transplanted back into animals.<sup>111-113</sup> However, this is the first study we are aware of in which HSCs of any kind have been successfully transduced by AAV in vivo. More extensive characterization of the GFP<sup>+</sup> cells is required, but based on the current data it is possible to say that the GFP<sup>+</sup> cells in the infarct and border zones are largely VEGFR-2<sup>+</sup>, while smaller subsets are positive for CD45 and CD68, all of which indicates a bone marrow origin. Furthermore, Ki-67 staining indicates that a fraction of the cells in the heart are still proliferating at nine days post-MI. Additionally, evidence from other studies (summarized below) suggests that the GFP-positive cardiomyocytes witnessed in the borderzone may also arise from bone marrow-derived cells.

Over the last decade a variety of studies have attempted to improve cardiac function after myocardial infarction through transplantation of bone marrow-derived cells. Results have been highly conflicting, with several groups reporting that BMDCs contribute to new cardiomyocytes after delivery to infarcted hearts, and other studies reporting that they do not.<sup>114-116</sup> A lineage tracing study by Visconti and Markwald used GFP-labeling of hematopoietic stem cells to track their infiltration to normal hearts and after permanent ligation.<sup>98</sup> While most GFP-positive bone marrow-derived cells contributed primarily to the myofibroblast population, they also saw rare GFP-positive cardiomyocytes in the infarct borderzone. However, they also witnessed GFP<sup>+</sup> cardiomyocytes with equal frequency in non-infarcted hearts. In our experiments, the modified periostin promoter was utilized in part to exclude expression from cardiomyocytes. Nevertheless, GFP-positive cardiomyocytes are visible particularly in Flox-GFP mice treated with AAV9, though they are confined strictly to the borderzone, indicating that the periostin promoter is not active in the overwhelming majority of cardiomyocytes. We also have seen very rare GFP-positive cardiomyocytes in non-infarcted AAV6-treated mice 4 weeks after injection. This pattern is remarkably consistent with the results of Visconti and Markwald. We do appear to see a higher frequency of GFP-positive cardiomyocytes, but that may be a difference between the permanent ligation model of MI that they employed versus our reperfused model, which allows greater influx of cells to the infarct zone and dramatically alters the remodeling response.<sup>117</sup> While it is possible that some cardiomyocytes in the borderzone express periostin, the greater number of GFP<sup>+</sup> cardiomyocytes in AAV9-

treated mice compared to AAV6-treated mice correspond directly to the greater number of total GFP<sup>+</sup> cells. Additionally, AAV6 and -9 are both effective at transducing cardiomyocytes, and the reporter system employed should require a relatively low amount of Cre activity to activate reporter gene expression. Taken together, this indicates that the GFP<sup>+</sup> cells may have regenerative potential.

The initial goal of this aim was to target cardiac fibroblasts with AAV. Instead, the majority of cells targeted by AAV show markers for hematopoietic stem cells and/or endothelial progenitor cells which may or may not derive from the bone marrow. While there are a wide variety of targets for gene therapy in cardiac fibroblasts, the original impetus for our aim was the possibility of reprogramming fibroblasts into cardiomyocytes for cardiac regeneration post-MI. Though the origins of the GFP-positive cardiomyocytes we have witnessed in the borderzone have yet to be proven, it is possible that the AAV vectors expressing periostin are targeting a population of cells with endogenous regenerative potential. Indeed, other groups have reported on bone marrow-derived cellular contribution to new cardiomyocytes post-infarction, though few if any have done so in the setting of reperfused MI. Immunofluorescence analysis failed to provide evidence of colocalization of typical cardiac progenitor markers such as Sca-1 or c-kit to GFP<sup>+</sup> cells, but this may be due to the time point of our analysis 9 days post-MI. In addition to the possibility of using gene therapy to amplify cardiomyocyte regeneration, the prevalence of GFP<sup>+</sup>/VEGFR-2<sup>+</sup> cells indicates a significant potential for using AAV-mediated gene therapy to modulate the angiogenic response after reperfused MI.

Future studies will focus on further developing several aspects of this aim. One goal will be to analyze reporter gene expression at different time points and further elucidate the exact type or types of cells in which AAV-mediated, periostin-driven expression is active. Analysis of earlier time points may show GFP<sup>+</sup> cells in a less differentiated state, while analysis at later time points will determine the long-term fate of these cells in the remodeling heart. Furthermore, the use of vectors expressing GFP or luciferase from the periostin promoter will determine the length of time during which periostin promoter-driven gene therapy might be effective. Better characterization of the GFP<sup>+</sup> cells may point to a promoter that is more suitable than periostin for driving longer-term or higher maximum expression of transgene. Finally, the effect of therapeutic genes on post-MI left ventricular remodeling will need to be assessed. The exact genes to analyze will be best determined after further elucidation of the cell type(s) being targeted, but there should be no shortage of potential therapeutic avenues to explore.<sup>118,119</sup>

## **CHAPTER 5**

### **Dissertation Conclusions and Future Directions**

The goal of this dissertation was to bioengineer adeno-associated viral vectors to investigate several challenges in cardiac-targeted gene therapy. The specific challenges we focused on were to provide greater cardiac-selective knockdown with AAV-mediated shRNA expression; to elucidate the mechanisms behind the ischemic induction of AAV9; and to target AAV-directed gene therapy to cardiac fibroblasts to open new therapeutic possibilities in the post-ischemic heart. The previous chapters provide extensive detail into the experiments undertaken to investigate these challenges, which resulted in several interesting findings and unexpected outcomes.

In the first aim, to provide cardiac-selective knockdown, we were successful in restricting knockdown primarily to cardiac tissue, with slight mRNA knockdown but no protein reduction in liver. However, since AAV-mediated liver knockdown has previously been demonstrated,<sup>29,30</sup> we wanted to determine the mechanisms behind the pattern we witnessed. Ultimately, our hypothesis for low liver knockdown – inefficient conversion of single-stranded AAV genomes into double-stranded DNA in the liver – was not supported by the data, with cardiac, liver and skeletal muscle knockdown being comparable between ss- and dsAAV. Instead, recent studies by other groups suggest that the activity of DNA damage response proteins, namely the MRN complex, is most responsible for the contrasting transduction efficiencies in cardiac and liver tissues.<sup>50</sup>

The same fundamental mechanism may also explain the ischemic induction of AAV9. While we hypothesized that a combination of vascular permeability and AAV9 receptor availability was partly responsible for increased AAV9 transduction after MI, our experiments indicated that these potential mechanisms are secondary

to a more important one. Tissue level analysis of luciferase activity, which distinguished between injected and uninjected regions of the heart, revealed no significant differences between the various treatments we administered, but large differences between injected and uninjected regions. This indicated that damage caused by needle insertion or injection to the myocardium was sufficient to increase viral transduction similarly to the increase previously demonstrated after myocardial infarction.<sup>16</sup> This effect, too, may be related to the activity of the MRN complex, which localizes to sites of DNA damage and may therefore allow for greater transduction of AAV after tissue injury through reduced binding of MRN proteins to AAV.<sup>72-75</sup>

Whether the results from the third aim are also tied to this mechanism is for now a matter of complete conjecture. In this aim, we set out to deliver gene therapy to cardiac fibroblasts but appear to have instead targeted a population of hematopoietic stem cells. Leukocyte infiltration to the post-ischemic heart is well documented and a required part of the wound healing response,<sup>86,87</sup> and studies have also demonstrated BMDC contributions to various cell types in the healthy and remodeling heart.<sup>97-99</sup> Though these results are not what we anticipated, they are equally exciting from the standpoint of AAV-mediated cardiac gene therapy. To date, HSCs have only been successfully transduced by AAV in vitro for transplantation back into animals. However, the reasons for our success in delivering genes to these cells in vivo is, for now, a largely unanswered question. The previous chapter describes two healthy mice that were injected with AAV6 packaged with pAPiCre in the absence of MI. Four weeks after injection, these mice contained only rare GFP-

positive cells in their hearts. Mice injected after reperfused MI, however, contain a large number of GFP<sup>+</sup> cells. Some of this difference in expression is likely a result of the cell type(s) being transduced by AAV which may only be present in the healthy LV in small quantities. However, it remains a question whether these cells express transgene due to activation of the periostin promoter after injury or due to more successful AAV transduction after ischemia, or both. In the previous two aims, the MRN complex is implicated due to its higher baseline activity in liver than in heart and, in the case of ischemic induction, because it translocates to sites of DNA damage after injury, allowing for greater transduction of AAV.<sup>50,72-74</sup> A similar mechanism may be involved here with HSCs, though the potential transcriptional changes driving differentiation in these cells may also create a favorable environment for AAV transduction.

There remain a great many directions to explore in future work developing AAV-mediated cardiac gene therapy. Based on our data, gene knockdown with AAV9 is cardiac-selective using either ssAAV or dsAAV in 8-10 day old mice. However, in cases where genes are expressed at a lower level than GFP in ubc-GFP mice, cardiac-selectivity may not be sufficient to completely prevent liver or other off-target tissue knockdown of a given gene. Recent studies have embedded interfering RNAs inside microRNA backbones instead of shRNAs.<sup>120-122</sup> Transcripts based on these constructs tend to be much longer than shRNA sequences and could potentially be modified with miR122 target sites to eliminate liver expression, as described for vectors in Chapters 3 and 4. The longer expression cassettes can be transcribed by



transcribed by tissue-specific RNA polymerase II promoters, but in some cases these may not be strong enough to provide robust expression for knockdown.

Future experiments exploring ischemic induction of AAV9 will likely focus on the DNA damage response elements presumed to be responsible for increased transduction. The proteins of the MRN complex (Mre11, Rad50 and Nbs1) have previously been shown to associate directly with AAV genomes, which likely inhibits transcription.<sup>50,74,75</sup> Cervelli et al.<sup>75</sup> demonstrated that in cells treated with hydroxyurea, which induces double-stranded DNA breaks, transduction of AAV was more efficient and fewer genomes were bound to Mre11, as determined by chromatin immunoprecipitation (ChIP). ChIP could likewise be used to analyze the number of AAV genomes bound to Mre11, Rad50 or Nbs1 after ischemia and reperfusion compared to sham-operated mice, or after intramyocardial injection compared uninjected tissue. A similar experiment could be undertaken after systemic injection of MG132 and/or doxorubicin, which also induce double-stranded DNA breaks.<sup>61</sup> We employed intramyocardial injection of these compounds for the experiments in Chapter 3 to remain consistent with the other branches of the study, but systemic administration at the time of AAV9 injection would avoid the cardiac injury confounding our current results while providing a potentially large increase in viral transduction. Analysis of AAV genome association with MRN proteins by ChIP could also be performed in the context of this study to ascertain the exact mechanism of proteasome inhibition on AAV transduction. Regardless of the exact approach employed, the mechanism behind ischemic induction will need to be determined because it greatly increases the effectiveness of AAV9 and allows

for practical application of AAV gene therapy post-MI.<sup>16</sup> A comprehensive understanding of this mechanism could potentially allow it to be applied to other diseases and in other tissues, increasing the flexibility and power of AAV-based gene therapies.

Finally, the ability to target what are most likely a population of hematopoietic stem cells, including various cells that express markers for CD45, CD68, VEGFR-2 and the proliferation marker Ki-67, is an incredibly exciting new opportunity with great potential. Future experiments should provide better characterization of the targeted cells including analysis at various time points, as discussed in the previous chapter. Treatment with therapeutic genes to improve cardiac function and possibly regeneration post-MI should be investigated with a well-reasoned selection of candidate genes. More mechanistic studies are also necessary to determine under what conditions these cells become susceptible to AAV transduction and transgene expression. A fuller understanding of these parameters and mechanisms could allow for therapies to be applied in settings beyond myocardial infarction, creating entirely new possibilities for wound healing and tissue regeneration.

## References

1. Crystal, R. G. *et al.* Analysis of Risk Factors for Local Delivery of Low- and Intermediate-Dose Adenovirus Gene Transfer Vectors to Individuals with a Spectrum of Comorbid Conditions. *Hum. Gene Ther.* **13**, 65–100 (2002).
2. Fisher, K. J. *et al.* Recombinant adeno-associated virus for muscle directed gene therapy. *Nat Med* **3**, 306–312 (1997).
3. Flotte, T. R. *et al.* Stable in vivo expression of the cystic fibrosis transmembrane conductance regulator with an adeno-associated virus vector. *Proc. Natl. Acad. Sci. U. S. A.* **90**, 10613–10617 (1993).
4. Snyder, L. L., Esser, J. M., Pachuk, C. J. & Steel, L. F. Vector design for liver-specific expression of multiple interfering RNAs that target hepatitis B virus transcripts. *Antiviral Res.* **80**, 36–44 (2008).
5. Berns, K. & Linden, R. The cryptic life style of adeno-associated virus. *Bioessays* **17**, 237–245 (1995).
6. Berns, K. I. Parvovirus replication. *Microbiol Mol Biol Rev* **54**, 316–329 (1990).
7. Samulski, R. J., Chang, L. S. & Shenk, T. A recombinant plasmid from which an infectious adeno-associated virus genome can be excised in vitro and its use to study viral replication. *J Virol* **61**, 3096–3101 (1987).
8. Goncalves, M. A. Adeno-associated virus: from defective virus to effective vector. *Virol J* **2**, 517–534 (2005).
9. Grimm, D., Kern, A., Rittner, K. & Kleinschmidt, J. A. Novel Tools for Production and Purification of Recombinant Adenoassociated Virus Vectors. *Hum. Gene Ther.* **9**, 2745–2760 (1998).
10. Wu, Z., Asokan, A. & Samulski, R. Adeno-associated Virus Serotypes: Vector Toolkit for Human Gene Therapy. *Mol. Ther.* **14**, 316–327 (2006).
11. Prasad, K.-M. R. *et al.* Topoisomerase Inhibition Accelerates Gene Expression after Adeno-associated Virus-mediated Gene Transfer to the Mammalian Heart. *Mol. Ther.* **15**, 764–771 (2007).
12. Aikawa, R., Huggins, G. S. & Snyder, R. O. Cardiomyocyte-specific Gene Expression Following Recombinant Adeno-associated Viral Vector Transduction. *J Biol Chem* **277**, 18979–18985 (2002).
13. Prasad, K. M. R., Xu, Y., Yang, Z., Acton, S. T. & French, B. A. Robust cardiomyocyte-specific gene expression following systemic injection of AAV: in vivo gene delivery follows a Poisson distribution. *Gene Ther.* **18**, 43–52 (2011).
14. Flotte, T. *et al.* A Phase I Study of an Adeno-Associated Virus-CFTR Gene Vector in Adult CF Patients with Mild Lung Disease. Johns Hopkins Children's Center, Baltimore, Maryland. *Hum. Gene Ther.* **7**, 1145–1159 (1996).
15. Aldag, J., Herklots, H. & Sinclair, M. uniQure's Glybera® First Gene Therapy Approved by European Commission. (2012). at <http://www.uniquire.com/news/167/182/uniQure-s-Glybera-First-Gene-Therapy-Approved-by-European-Commission.html>
16. Konkalmatt, P. R. *et al.* Adeno-associated virus serotype 9 administered systemically after reperfusion preferentially targets cardiomyocytes in the infarct border zone with pharmacodynamics suitable for the attenuation of left ventricular remodeling. *J. Gene Med.* **14**, 609–620 (2012).

17. Souders, C. A., Bowers, S. L. K. & Baudino, T. A. Cardiac Fibroblast The Renaissance Cell. *Circ. Res.* **105**, 1164–1176 (2009).
18. Shan, Z. *et al.* Involvement of the Brain (Pro)renin Receptor in Cardiovascular Homeostasis. *Circ. Res.* **107**, 934–938 (2010).
19. Suckau, L. *et al.* Long-Term Cardiac-Targeted RNA Interference for the Treatment of Heart Failure Restores Cardiac Function and Reduces Pathological Hypertrophy. *Circulation* **119**, 1241–1252 (2009).
20. Hirai, T. *et al.* Intrathecal shRNA-AAV9 Inhibits Target Protein Expression in the Spinal Cord and Dorsal Root Ganglia of Adult Mice. *Hum. Gene Ther. Methods* **23**, 119–127 (2012).
21. Shen, S., Bryant, K. D., Brown, S. M., Randell, S. H. & Asokan, A. Terminal N-Linked Galactose Is the Primary Receptor for Adeno-associated Virus 9. *J. Biol. Chem.* **286**, 13532–13540 (2011).
22. Sharma, A., Ghosh, A., Hansen, E. T., Newman, J. M. & Mohan, R. R. Transduction efficiency of AAV 2/6, 2/8 and 2/9 vectors for delivering genes in human corneal fibroblasts. *Brain Res. Bull.* **81**, 273–278 (2010).
23. Kaminsky, P. M., Keiser, N. W., Yan, Z., Lei-Butters, D. C. & Engelhardt, J. F. Directing Integrin-linked Endocytosis of Recombinant AAV Enhances Productive FAK-dependent Transduction. *Mol. Ther.* **20**, 972–983 (2012).
24. Takeda, N. *et al.* Cardiac fibroblasts are essential for the adaptive response of the murine heart to pressure overload. *J. Clin. Invest.* **120**, 254–265 (2010).
25. Ku, G. & McManus, M. T. Behind the Scenes of a Small RNA Gene-Silencing Pathway. *Hum. Gene Ther.* **19**, 17–26 (2008).
26. Fechner, H. *et al.* Cardiac-targeted RNA interference mediated by an AAV9 vector improves cardiac function in coxsackievirus B3 cardiomyopathy. *J. Mol. Med.* **86**, 987–997 (2008).
27. Park, C. S. *et al.* AAV-Mediated Knock-Down of HRC Exacerbates Transverse Aorta Constriction-Induced Heart Failure. *Plos One* **7**, e43282 (2012).
28. Miyazaki, Y. *et al.* Heart Failure-Inducible Gene Therapy Targeting Protein Phosphatase 1 Prevents Progressive Left Ventricular Remodeling. *Plos One* **7**, e35875 (2012).
29. Grimm, D. *et al.* Fatality in mice due to oversaturation of cellular microRNA/short hairpin RNA pathways. *Nature* **441**, 537–541 (2006).
30. Giering, J. C., Grimm, D., Storm, T. A. & Kay, M. A. Expression of shRNA From a Tissue-specific pol II Promoter Is an Effective and Safe RNAi Therapeutic. *Mol. Ther.* **16**, 1630–1636 (2008).
31. Schaefer, B. C., Schaefer, M. L., Kappler, J. W., Marrack, P. & Kedl, R. M. Observation of Antigen-Dependent CD8+ T-Cell/ Dendritic Cell Interactions in Vivo. *Cell. Immunol.* **214**, 110–122 (2001).
32. McCarty, D. M., Monahan, P. E. & Samulski, R. J. Self-complementary recombinant adeno-associated virus (scAAV) vectors promote efficient transduction independently of DNA synthesis. *Gene Ther.* **8**, 1248–1254 (2001).
33. Tiscornia, G., Singer, O., Ikawa, M. & Verma, I. M. A general method for gene knockdown in mice by using lentiviral vectors expressing small interfering RNA. *Proc. Natl. Acad. Sci.* **100**, 1844–1848 (2003).

34. McCarty, D. M. *et al.* Adeno-associated virus terminal repeat (TR) mutant generates self-complementary vectors to overcome the rate-limiting step to transduction in vivo. *Gene Ther.* **10**, 2112–2118 (2003).
35. Graham, F. L., Smiley, J., Russell, W. C. & Nairn, R. Characteristics of a Human Cell Line Transformed by DNA from Human Adenovirus Type 5. *J. Gen. Virol.* **36**, 59–72 (1977).
36. Wu, J. C., Inubushi, M., Sundaresan, G., Schelbert, H. R. & Gambhir, S. S. Optical Imaging of Cardiac Reporter Gene Expression in Living Rats. *Circulation* **105**, 1631–1634 (2002).
37. Zincarelli, C., Soltys, S., Rengo, G. & Rabinowitz, J. E. Analysis of AAV Serotypes 1–9 Mediated Gene Expression and Tropism in Mice After Systemic Injection. *Mol. Ther.* **16**, 1073–1080 (2008).
38. Inagaki, K. *et al.* Robust Systemic Transduction with AAV9 Vectors in Mice: Efficient Global Cardiac Gene Transfer Superior to That of AAV8. *Mol. Ther.* **14**, 45–53 (2006).
39. Banerjee, I., Fuseler, J. W., Price, R. L., Borg, T. K. & Baudino, T. A. Determination of cell types and numbers during cardiac development in the neonatal and adult rat and mouse. *Am. J. Physiol. - Heart Circ. Physiol.* **293**, H1883–H1891 (2007).
40. Mayra, A. *et al.* Intraperitoneal AAV9-shRNA inhibits target expression in neonatal skeletal and cardiac muscles. *Biochem. Biophys. Res. Commun.* **405**, 204–209 (2011).
41. Bostick, B., Ghosh, A., Yue, Y., Long, C. & Duan, D. Systemic AAV-9 transduction in mice is influenced by animal age but not by the route of administration. *Gene Ther.* **14**, 1605–1609 (2007).
42. Cunningham, S. C., Dane, A. P., Spinoulas, A. & Alexander, I. E. Gene Delivery to the Juvenile Mouse Liver Using AAV2/8 Vectors. *Mol. Ther.* **16**, 1081–1088 (2008).
43. Flageul, M. *et al.* Transient expression of genes delivered to newborn rat liver using recombinant adeno-associated virus 2/8 vectors. *J. Gene Med.* **11**, 689–696 (2009).
44. Towne, C., Raoul, C., Schneider, B. L. & Aebischer, P. Systemic AAV6 Delivery Mediating RNA Interference Against SOD1: Neuromuscular Transduction Does Not Alter Disease Progression in fALS Mice. *Mol. Ther.* **16**, 1018–1025 (2008).
45. Fisher, K. J. *et al.* Transduction with recombinant adeno-associated virus for gene therapy is limited by leading-strand synthesis. *J. Virol.* **70**, 520–532 (1996).
46. Ferrari, F. K., Samulski, T., Shenk, T. & Samulski, R. J. Second-strand synthesis is a rate-limiting step for efficient transduction by recombinant adeno-associated virus vectors. *J. Virol.* **70**, 3227–3234 (1996).
47. Thomas, C. E., Storm, T. A., Huang, Z. & Kay, M. A. Rapid uncoating of vector genomes is the key to efficient liver transduction with pseudotyped adeno-associated virus vectors. *J. Virol.* **78**, 3110–3122 (2004).
48. McCarty, D. M. Self-complementary AAV Vectors; Advances and Applications. *Mol Ther* **16**, 1648–1656 (2008).
49. Yagi, H. *et al.* Complete restoration of phenylalanine oxidation in phenylketonuria mouse by a self-complementary adeno-associated virus vector. *J. Gene Med.* **13**, 114–122 (2011).

50. Lovric, J. *et al.* Terminal Differentiation of Cardiac and Skeletal Myocytes Induces Permissivity to AAV Transduction by Relieving Inhibition Imposed by DNA Damage Response Proteins. *Mol. Ther.* **20**, 2087–2097 (2012).
51. Go, A. S. *et al.* Heart Disease and Stroke Statistics—2013 Update A Report From the American Heart Association. *Circulation* **127**, e6–e245 (2013).
52. Pachori, A. S., Melo, L. G., Zhang, L., Solomon, S. D. & Dzau, V. J. Chronic Recurrent Myocardial Ischemic Injury Is Significantly Attenuated by Pre-Emptive Adeno-Associated Virus Heme Oxygenase-1 Gene Delivery. *J. Am. Coll. Cardiol.* **47**, 635–643 (2006).
53. Agrawal, R. S. *et al.* Pre-emptive gene therapy using recombinant adeno-associated virus delivery of extracellular superoxide dismutase protects heart against ischemic reperfusion injury, improves ventricular function and prolongs survival. *Gene Ther.* **11**, 962–969 (2004).
54. Prasad, K.-M. R., Smith, R. S., Xu, Y. & French, B. A. A single direct injection into the left ventricular wall of an adeno-associated virus 9 (AAV9) vector expressing extracellular superoxide dismutase from the cardiac troponin-T promoter protects mice against myocardial infarction. *J. Gene Med.* **13**, 333–341 (2011).
55. Konkalmatt, P. R. *et al.* Cardiac-Selective Expression of Extracellular Superoxide Dismutase After Systemic Injection of Adeno-Associated Virus 9 Protects the Heart Against Post-Myocardial Infarction Left Ventricular Remodeling. *Circ. Cardiovasc. Imaging* **6**, 478–486 (2013).
56. Svendsen, J. H., Bjerrum, P. J. & Haunsø, S. Myocardial capillary permeability after regional ischemia and reperfusion in the in vivo canine heart. Effect of superoxide dismutase. *Circ. Res.* **68**, 174–184 (1991).
57. Beyers, R. J. *et al.* T2-weighted MRI of post-infarct myocardial edema in mice. *Magn. Reson. Med.* **67**, 201–209 (2012).
58. Greelish, J. P. *et al.* Stable restoration of the sarcoglycan complex in dystrophic muscle perfused with histamine and a recombinant adeno-associated viral vector. *Nat. Med.* **5**, 439–443 (1999).
59. Arruda, V. R. *et al.* Regional intravascular delivery of AAV-2-F.IX to skeletal muscle achieves long-term correction of hemophilia B in a large animal model. *Blood* **105**, 3458–3464 (2005).
60. Bell, C. L. *et al.* The AAV9 receptor and its modification to improve in vivo lung gene transfer in mice. *J. Clin. Invest.* **121**, 2427–2435 (2011).
61. Yan, Z. *et al.* Distinct Classes of Proteasome-Modulating Agents Cooperatively Augment Recombinant Adeno-Associated Virus Type 2 and Type 5-Mediated Transduction from the Apical Surfaces of Human Airway Epithelia. *J. Virol.* **78**, 2863–2874 (2004).
62. Monahan, P. E. *et al.* Proteasome Inhibitors Enhance Gene Delivery by AAV Virus Vectors Expressing Large Genomes in Hemophilia Mouse and Dog Models: A Strategy for Broad Clinical Application. *Mol. Ther.* **18**, 1907–1916 (2010).
63. Johnson, J. S. *et al.* AAV Exploits Subcellular Stress Associated with Inflammation, Endoplasmic Reticulum Expansion, and Misfolded Proteins in Models of Cystic Fibrosis. *Plos Pathog.* **7**, e1002053 (2011).

64. Geisler, A. *et al.* microRNA122-regulated transgene expression increases specificity of cardiac gene transfer upon intravenous delivery of AAV9 vectors. *Gene Ther.* **18**, 199–209 (2010).
65. Qiao, C. *et al.* Liver-specific microRNA-122 target sequences incorporated in AAV vectors efficiently inhibits transgene expression in the liver. *Gene Ther.* **18**, 403–410 (2010).
66. Manthorpe, M. *et al.* Gene Therapy by Intramuscular Injection of Plasmid DNA: Studies on Firefly Luciferase Gene Expression in Mice. *Hum. Gene Ther.* **4**, 419–431 (1993).
67. Böhmer, M. R. *et al.* Focused Ultrasound and Microbubbles for Enhanced Extravasation. *J. Control. Release Off. J. Control. Release Soc.* **148**, 18–24 (2010).
68. Zavecz, J. H. & Levi, R. Separation of primary and secondary cardiovascular events in systemic anaphylaxis. *Circ. Res.* **40**, 15–19 (1977).
69. Kaspar, B. K. *et al.* Myocardial gene transfer and long-term expression following intracoronary delivery of adeno-associated virus. *J. Gene Med.* **7**, 316–324 (2005).
70. Bridges, C. R. *et al.* Global cardiac-specific transgene expression using cardiopulmonary bypass with cardiac isolation. *Ann. Thorac. Surg.* **73**, 1939–1946 (2002).
71. Katwal, A. B. *et al.* Adeno-associated virus serotype 9 efficiently targets ischemic skeletal muscle following systemic delivery. *Gene Ther.* (2013). doi:10.1038/gt.2013.16
72. Maser, R. S., Monsen, K. J., Nelms, B. E. & Petrini, J. H. hMre11 and hRad50 nuclear foci are induced during the normal cellular response to DNA double-strand breaks. *Mol. Cell. Biol.* **17**, 6087–6096 (1997).
73. Mirzoeva, O. K. & Petrini, J. H. J. DNA Damage-Dependent Nuclear Dynamics of the Mre11 Complex. *Mol. Cell. Biol.* **21**, 281–288 (2001).
74. Schwartz, R. A. *et al.* The Mre11/Rad50/Nbs1 Complex Limits Adeno-Associated Virus Transduction and Replication. *J. Virol.* **81**, 12936–12945 (2007).
75. Cervelli, T. *et al.* Processing of recombinant AAV genomes occurs in specific nuclear structures that overlap with foci of DNA-damage-response proteins. *J. Cell Sci.* **121**, 349–357 (2008).
76. Shen, S. *et al.* Glycan Binding Avidity Determines the Systemic Fate of Adeno-Associated Virus Type 9. *J. Virol.* **86**, 10408–10417 (2012).
77. Zincarelli, C., Soltys, S., Rengo, G., Koch, W. J. & Rabinowitz, J. E. Comparative Cardiac Gene Delivery of Adeno-Associated Virus Serotypes 1-9 reveals that AAV6 Mediates the Most Efficient Transduction in Mouse Heart. *Clin. Transl. Sci.* **3**, 81–89 (2010).
78. Zak, R. Development and proliferative capacity of cardiac muscle cells. *Circ. Res.* **35**, suppl II:17–26 (1974).
79. Nag, A. Study of non-muscle cells of the adult mammalian heart: a fine structural analysis and distribution. *Cytobios* **28**, 41–61 (1980).
80. Snider, P. *et al.* Origin of Cardiac Fibroblasts and the Role of Periostin. *Circ. Res.* **105**, 934–947 (2009).

81. Lindsley, A. *et al.* Identification and characterization of a novel Schwann and outflow tract endocardial cushion lineage-restricted periostin enhancer. *Dev. Biol.* **307**, 340–355 (2007).
82. Shimshek, D. R. *et al.* Codon-improved Cre recombinase (iCre) expression in the mouse. *genesis* **32**, 19–26 (2002).
83. Madisen, L. *et al.* A robust and high-throughput Cre reporting and characterization system for the whole mouse brain. *Nat. Neurosci.* **13**, 133–140 (2010).
84. Safran, M. *et al.* Mouse reporter strain for noninvasive bioluminescent imaging of cells that have undergone Cre-mediated recombination. *Mol. Imaging* **2**, 297–302 (2003).
85. Shimazaki, M. *et al.* Periostin is essential for cardiac healing after acute myocardial infarction. *J. Exp. Med.* **205**, 295–303 (2008).
86. French, B. A. & Kramer, C. M. Mechanisms of postinfarct left ventricular remodeling. *Drug Discov. Today Dis. Mech.* **4**, 185–196 (2007).
87. Frangogiannis, N. G. Targeting the inflammatory response in healing myocardial infarcts. *Curr. Med. Chem.* **13**, 1877–1893 (2006).
88. Ieda, M. *et al.* Direct Reprogramming of Fibroblasts into Functional Cardiomyocytes by Defined Factors. *Cell* **142**, 375–386 (2010).
89. Inagawa, K. *et al.* Induction of Cardiomyocyte-like Cells in Infarct Hearts by Gene Transfer of Gata4, Mef2c, and Tbx5. *Circ. Res.* (2012). doi:10.1161/CIRCRESAHA.112.271148
90. Qian, L. *et al.* In vivo reprogramming of murine cardiac fibroblasts into induced cardiomyocytes. *Nature* **485**, 593–598 (2012).
91. Jayawardena, T. M. *et al.* MicroRNA-Mediated In Vitro and In Vivo Direct Reprogramming of Cardiac Fibroblasts to Cardiomyocytes. *Circ. Res.* **110**, 1465–1473 (2012).
92. Islas, J. F. *et al.* Transcription factors ETS2 and MESP1 transdifferentiate human dermal fibroblasts into cardiac progenitors. *Proc. Natl. Acad. Sci.* **109**, 13016–13021 (2012).
93. Chen, C., Krohn, J., Bhattacharya, S. & Davies, B. A Comparison of Exogenous Promoter Activity at the ROSA26 Locus Using a PhiC31 Integrase Mediated Cassette Exchange Approach in Mouse ES Cells. *Plos One* **6**, e23376 (2011).
94. Norris, R. A. *et al.* Neonatal and Adult Cardiovascular Pathophysiological Remodeling and Repair. *Ann. N. Y. Acad. Sci.* **1123**, 30–40 (2008).
95. Oka, T. *et al.* Genetic Manipulation of Periostin Expression Reveals a Role in Cardiac Hypertrophy and Ventricular Remodeling. *Circ. Res.* **101**, 313–321 (2007).
96. Kühn, B. *et al.* Periostin induces proliferation of differentiated cardiomyocytes and promotes cardiac repair. *Nat. Med.* **13**, 962–969 (2007).
97. Hajdu, Z. *et al.* Recruitment of bone marrow-derived valve interstitial cells is a normal homeostatic process. *J. Mol. Cell. Cardiol.* **51**, 955–965 (2011).
98. Visconti, R. P. & Markwald, R. R. Recruitment of New Cells into the Postnatal Heart: Potential Modification of Phenotype by Periostin. *Ann. N. Y. Acad. Sci.* **1080**, 19–33 (2006).



99. Mollmann, H. *et al.* Bone marrow-derived cells contribute to infarct remodelling. *Cardiovasc. Res.* **71**, 661–671 (2006).
100. Strieter, R. M., Keeley, E. C., Hughes, M. A., Burdick, M. D. & Mehrad, B. The role of circulating mesenchymal progenitor cells (fibrocytes) in the pathogenesis of pulmonary fibrosis. *J. Leukoc. Biol.* **86**, 1111–1118 (2009).
101. Ziegler, B. L. *et al.* KDR Receptor: A Key Marker Defining Hematopoietic Stem Cells. *Science* **285**, 1553–1558 (1999).
102. Shao, R. *et al.* Acquired Expression of Periostin by Human Breast Cancers Promotes Tumor Angiogenesis through Up-Regulation of Vascular Endothelial Growth Factor Receptor 2 Expression. *Mol. Cell. Biol.* **24**, 3992–4003 (2004).
103. Puglisi, F. *et al.* Expression of periostin in human breast cancer. *J. Clin. Pathol.* **61**, 494–498 (2008).
104. Nolan, D. J. *et al.* Bone marrow-derived endothelial progenitor cells are a major determinant of nascent tumor neovascularization. *Genes Dev.* **21**, 1546–1558 (2007).
105. Maltais, S., Perrault, L. P. & Ly, H. Q. The bone marrow–cardiac axis: role of endothelial progenitor cells in heart failure☆. *Eur. J. Cardiothorac. Surg.* **39**, 368–374 (2011).
106. Shintani, S. *et al.* Mobilization of Endothelial Progenitor Cells in Patients With Acute Myocardial Infarction. *Circulation* **103**, 2776–2779 (2001).
107. Kocher, A. A. *et al.* Neovascularization of ischemic myocardium by human bone-marrow–derived angioblasts prevents cardiomyocyte apoptosis, reduces remodeling and improves cardiac function. *Nat. Med.* **7**, 430–436 (2001).
108. Urbich, C. & Dimmeler, S. Endothelial Progenitor Cells Characterization and Role in Vascular Biology. *Circ. Res.* **95**, 343–353 (2004).
109. Yoder, M. C. *et al.* Redefining endothelial progenitor cells via clonal analysis and hematopoietic stem/progenitor cell principals. *Blood* **109**, 1801–1809 (2007).
110. Fadini, G. P., Losordo, D. & Dimmeler, S. Critical Reevaluation of Endothelial Progenitor Cell Phenotypes for Therapeutic and Diagnostic Use. *Circ. Res.* **110**, 624–637 (2012).
111. Zhong, L. *et al.* Evaluation of Primitive Murine Hematopoietic Stem and Progenitor Cell Transduction In Vitro and In Vivo by Recombinant Adeno-Associated Virus Vector Serotypes 1 Through 5. *Hum. Gene Ther.* **17**, 321–333 (2006).
112. Maina, N. *et al.* Optimization of Recombinant Adeno-Associated Viral Vectors for Human  $\beta$ -Globin Gene Transfer and Transgene Expression. *Hum. Gene Ther.* **19**, 365–375 (2008).
113. Song, L. *et al.* High-Efficiency Transduction of Primary Human Hematopoietic Stem Cells and Erythroid Lineage-Restricted Expression by Optimized AAV6 Serotype Vectors In Vitro and in a Murine Xenograft Model In Vivo. *Plos One* **8**, e58757 (2013).
114. Orlic, D. *et al.* Bone marrow cells regenerate infarcted myocardium. *Nature* **410**, 701–705 (2001).

115. Nygren, J. M. *et al.* Bone marrow–derived hematopoietic cells generate cardiomyocytes at a low frequency through cell fusion, but not transdifferentiation. *Nat. Med.* **10**, 494–501 (2004).
116. Murry, C. E. *et al.* Haematopoietic stem cells do not transdifferentiate into cardiac myocytes in myocardial infarcts. *Nature* **428**, 664–668 (2004).
117. Boyle, M. P. & Weisman, H. F. Limitation of infarct expansion and ventricular remodeling by late reperfusion. Study of time course and mechanism in a rat model. *Circulation* **88**, 2872–2883 (1993).
118. Segers, V. F. M. & Lee, R. T. Protein Therapeutics for Cardiac Regeneration after Myocardial Infarction. *J Cardiovasc. Transl. Res.* **3**, 469–477 (2010).
119. Loffredo, F. S., Steinhauser, M. L., Gannon, J. & Lee, R. T. Bone Marrow-Derived Cell Therapy Stimulates Endogenous Cardiomyocyte Progenitors and Promotes Cardiac Repair. *Cell Stem Cell* **8**, 389–398 (2011).
120. Stegmeier, F., Hu, G., Rickles, R. J., Hannon, G. J. & Elledge, S. J. A lentiviral microRNA-based system for single-copy polymerase II-regulated RNA interference in mammalian cells. *Proc. Natl. Acad. Sci. U. S. A.* **102**, 13212–13217 (2005).
121. Boudreau, R. L., Martins, I. & Davidson, B. L. Artificial MicroRNAs as siRNA Shuttles: Improved Safety as Compared to shRNAs In vitro and In vivo. *Mol Ther* **17**, 169–175 (2008).
122. Snyder, L. L., Ahmed, I. & Steel, L. F. RNA polymerase III can drive polycistronic expression of functional interfering RNAs designed to resemble microRNAs. *Nucleic Acids Res.* **37**, e127 (2009).